

EVALUATION OF SALT STRUCTURES FOR UNDERGROUND GAS STORAGE IN  
THE TUZGÖLÜ AND THE ÇANKIRI BASINS, TÜRKİYE

A THESIS SUBMITTED TO  
THE GRADUATE SCHOOL OF NATURAL AND APPLIED SCIENCES  
OF  
MIDDLE EAST TECHNICAL UNIVERSITY

BY  
AYŞE GÜNGÖR

IN PARTIAL FULFILLMENT OF THE REQUIREMENTS  
FOR  
THE DEGREE OF DOCTOR OF PHILOSOPHY  
IN  
GEOLOGICAL ENGINEERING

JANUARY 2023

Approval of the thesis:

**EVALUATION OF SALT STRUCTURES FOR UNDERGROUND GAS  
STORAGE IN THE TUZGÖLÜ AND THE ÇANKIRI BASINS, TÜRKİYE**

submitted by **AYŞE GÜNGÖR** in partial fulfillment of the requirements for the degree of **Doctor of Philosophy in Geological Engineering, Middle East Technical University** by,

Prof. Dr. Halil Kalıpçılar  
Dean, Graduate School of **Natural and Applied Sciences**

\_\_\_\_\_

Prof. Dr. Erdin Bozkurt  
Head of the Department, **Geological Engineering**

\_\_\_\_\_

Prof. Dr. Nuretdin Kaymakcı  
Supervisor, **Geological Engineering Dept, METU**

\_\_\_\_\_

**Examining Committee Members:**

Prof. Dr. Erdin Bozkurt  
Geological Engineering Dept, METU

\_\_\_\_\_

Prof. Dr. Nuretdin Kaymakcı  
Geological Engineering Dept, METU

\_\_\_\_\_

Prof. Dr. Fuat Bora Rojay  
Geological Engineering Dept, METU.,

\_\_\_\_\_

Assoc. Prof. Dr. Bora Uzel  
Geological Engineering Dept, Dokuz Eylül Uni.

\_\_\_\_\_

Assoc. Prof. Dr. Erhan Gülyüz  
Geological Engineering Dept, Van Yüzüncü Yıl Uni.

\_\_\_\_\_

Date: 25.01.2023



**I hereby declare that all information in this document has been obtained and presented in accordance with academic rules and ethical conduct. I also declare that, as required by these rules and conduct, I have fully cited and referenced all material and results that are not original to this work.**

Ayşe Güngör

Signature:

## **ABSTRACT**

### **EVALUATION OF SALT STRUCTURES FOR UNDERGROUND GAS STORAGE IN THE TUZGÖLÜ AND THE ÇANKIRI BASINS, TÜRKİYE**

Güngör, Ayşe  
Doctor of Philosophy, Geological Engineering  
Supervisor: Prof. Dr. Nuretdin Kaymakcı

January 2023, 113 pages

Natural gas is a fossil fuel that is present in every step of our daily life, in terms of commercial, domestic, and industrial areas. It has wide low and high demand periods which necessitates its storage during low periods to be used during the high periods. One of the widely used storage methods is underground natural gas storage (UGS) facilities that have been used since 1915. They are economically important in long-term usage in the marketing area. Therefore, finding new suitable underground storage locations in Türkiye is getting strategically important. Apart from depleted oil or gas fields, salt domes and other salt bodies are widely used for this purpose. In this context, this study aims at mapping and evaluating the salt bodies in various parts of Türkiye using potential field data and seismic data sets and to design proper cavern patterns suitable for efficient underground storage facilities. For this purpose, two candidate sites are selected in Tuzgölü and Çankırı basins, which contain thick salt deposits and bodies suitable for constructing underground salt caverns for gas storage. The location of the salt bodies was determined by potential field data then they are mapped out using 2D seismic data sets. The 2D seismic interpretations are modeled in the Leapfrog Geo software for generating 3D static (solid) volumes. Then, the underground salt cavern is designed based on the analytical solution

method that takes the shape of the salt body and geomechanical properties into consideration.

**Keywords:** Underground Natural Gas Storage, Salt Domes, Potential Field Data, Seismic Reflection Data, Salt Cavern

## ÖZ

### **TUZ GÖLÜ VE ÇANKIRI HAVZALARINDAKİ TUZ YAPILARININ YERALTINDA GAZ DEPOLAMAK İÇİN DEĞERLENDİRİLMESİ, TÜRKİYE**

Güngör, Ayşe  
Doktora, Jeoloji Mühendisliği  
Tez Yöneticisi: Prof. Dr. Nuretdin Kaymakçı

Ocak 2023, 113 sayfa

Doğal gaz, ticari, evsel ve endüstriyel alanlarda günlük hayatımızın her adımında yer alan bir fosil yakıttır. Günlük hayatta geniş düşük ve yüksek talep dönemlerine sahiptir ve bu nedenle düşük dönemlerde depolanması, yüksek dönemlerde kullanılması gerekir. Yaygın olarak kullanılan depolama yöntemlerinden biri de 1915 yılından beri kullanılmakta olan yeraltı doğalgaz depolama (UGS) tesisleridir. Pazarlama alanında uzun süreli kullanımda ekonomik açıdan önemlidir. Bu nedenle Türkiye'de yeni uygun yeraltı depolama yerleri bulmak stratejik olarak önem kazanmaktadır. Tükenmiş petrol veya gaz sahalarının yanı sıra, tuz kubbeleri ve diğer tuz kütleleri bu amaç için yaygın olarak kullanılmaktadır. Bu bağlamda, bu çalışma, potansiyel saha verileri ve sismik veri setleri kullanılarak Türkiye'nin çeşitli bölgelerindeki tuz kütlelerinin haritalanması, değerlendirilmesi ve verimli yeraltı depolama tesisi için uygun bir mağara deseninin tasarlanmasını amaçlamaktadır. Bu amaçla, gaz depolama için yeraltı tuz mağarası inşa etmeye uygun kalın tuz yatakları ve gövdeleri içeren Tuzgölü ve Çankırı havzalarında iki aday saha seçilmiştir. Tuz kütlelerinin konumu, potansiyel alan verileriyle belirlendi ve ardından 2B sismik veri setleri kullanılarak haritalandı. 2B sismik yorumlar, 3B statik (katı) hacimler

oluřturmak iin Leapfrog Geo yazılımında modellenmiřtir. Daha sonra tuz kütlesinin řeklini ve jeomekanik özellikleri dikkate alan analitik özüm yöntemi kullanılarak yeraltı tuz mağarası tasarlanmıştır.

**Anahtar Kelimeler:** Yer altı doğal gaz depolaması, Tuz yapısı, Potansiyel Saha Verileri, Sismik Yansıma Verileri, Tuz Mağarası

To My Family

## ACKNOWLEDGEMENTS

I would like to express my gratitude to all those who allowed me to complete this thesis. I am deeply thankful to my super advisor, Professor Dr. Nuretdin Kaymakcı, whose encouragement, guidance, and suggestions helped me during the time I was researching and writing this thesis.

I would like to thank the professors that enlighten me with their knowledge and kindness in the Department of Geological Engineering of Middle East Technical University. I am also grateful to be a partition of the ‘Energy storage and energy supplies’ project that is supported by the ‘Council of higher education’ (YÖK). I also thank Seequent Company for their support and for giving access to the software license to the Leap Frog software to develop 3D model salt structures and cavern designing.

Briefly, I am so thankful for whom had excitement about keeping a light on my way whenever I needed it.

Ultimately, I offer my regards and blessings to my family who supported me in many respects during the completion of my thesis, and whole my life. Especially, I would like to give my special thanks to my mother Naciye Güngör, and my father Muammer Güngör whose love enabled me to complete this study.

## TABLE OF CONTENTS

ABSTRACT.....	v
ÖZ .....	vii
ACKNOWLEDGEMENTS .....	x
TABLE OF CONTENTS.....	xi
LIST OF TABLES .....	xiii
LIST OF FIGURES .....	xiv
LIST OF ABBREVIATION .....	xvii
LIST OF SYMBOLS .....	xviii
CHAPTERS	
1. INTRODUCTION .....	1
1.1. Purpose and Scope .....	1
1.2. Motivation.....	2
1.3. Background .....	3
1.3.1. Gravity and Magnetism .....	3
1.3.2. Seismic Data .....	6
1.3.3. Salt Properties .....	7
1.3.4. Salt Structures .....	10
1.3.5. Solution Mining .....	11
1.3.6. Salt Caverns .....	11
1.3.7. Cavern Designing.....	12
1.4. The Tectonic Outline of Türkiye .....	16
1.5. The Geology Outline of the Study Areas.....	19
1.5.1. Tuzgölü Basin .....	19
1.5.2. Çankırı Basin.....	24
1.6. Data and Methodology.....	30
2. THE UNDERGROUND STORAGEES .....	37

2.1.	Background.....	37
2.2.	The Underground Storage Background in Türkiye .....	39
2.3.	The Fundamentals of the Cavern Design .....	43
2.3.1.	Site selection.....	44
2.3.2.	Cavern shape and dimension .....	44
2.3.3.	Geomechanical properties .....	45
2.3.4.	Salt creep .....	50
2.3.5.	Surface Subsidence.....	53
2.3.6.	Thermal Conditions .....	55
3.	RESULTS OF THE STUDY.....	57
3.1.	The Seismic Data Interpretation .....	57
3.1.1.	Tuzgölü Basin Interpretation.....	57
3.1.2.	Çankırı Basin Interpretation .....	68
3.2.	3D Salt Volume .....	74
3.2.1.	Tuzgölü Basin 3D Volume .....	74
3.2.2.	Çankırı Basin 3D Volume .....	77
3.3.	Designing of the Cavern .....	80
3.3.1.	Assumptions .....	80
3.3.2.	Cavern Scenarios .....	81
3.3.3.	Parameters .....	86
4.	DISCUSSION.....	93
4.1.	The Seismic Data Interpretation .....	93
4.2.	3D Salt Volume .....	94
4.3.	Salt cavern design.....	95
5.	CONCLUSION .....	101
	REFERENCES .....	103
	CURRICULUM VITAE .....	113

## LIST OF TABLES

### TABLES

Table 1. 1 The borehole list used in this study.....	31
Table 2. 1 Comparison of differences between UGS types (modified from EIA 2022) .....	39
Table 2. 2 Information on the Tuzgölü Underground Natural Gas Storage Project Planned Capacity (Botas 2022).....	43
Table 2. 3 Mechanical parameters values of the rock salt around the world (Düzyol 2004) .....	48
Table 3. 1 The Tuzgölü Basin's Salt body information.....	74
Table 3. 2 The Çankırı Basin's Salt body information .....	77
Table 3. 3 The cavern design calculation with the temperature.....	81
Table 3. 4 Salt bulk depth information chart for study areas. ....	82
Table 3. 5 The design parameter of the cavern .....	82
Table 3. 6 Initial vertical Stress ( $P_v$ ) and Vertical Total Stress gradient ( $S_v$ ) of the Cavern, Salt, base (cushion) Gas, and Roof Cavern individually.....	87
Table 3. 7 The depth relationship with total vertical stress, with geological and technical tightness (Yellow columns are representing the salt strata, and grey columns are representing the cavern).....	88
Table 3. 8 Characteristic values used for the creep and elastic material properties of rock salt. (Modified from Ozarslan 2012 and Susan 2019) .....	91
Table 3. 9 Average Internal Pressure ( $V_i$ ) is listed with the Convergence Rate and Volume convergence calculation results of the Çankırı Basin .....	92

## LIST OF FIGURES

### FIGURES

Figure 1. 1 Variation of the density of salt and clastic sediments with depth to (Jackson, 1986).....	9
Figure 1. 2 Graph showing the strength of salt with depth compared to other sedimentary rocks (Weijermars et al. (1993), Jackson & Vendeville (1994)) .....	10
Figure 1. 3 Diagram of different types of salt structures, their names, and geometries. (Jackson, 2017).....	11
Figure 1. 4 A schematic diagram of a simplified fundamental environment for a salt cavern. (Modified from CAES, 2022) .....	15
Figure 1. 5 An illustration of various types of underground storage in salt structures. (Modified from BGS, 2022) .....	15
Figure 1. 6 Depth versus shapes, and relative volumes of typical salt cavern gas storage facilities in salt domes around the world except for Salies de Bean and Regina south cavern which are in a salt bed and designed horizontally (modified from Warren, 2006). .....	16
Figure 1. 7 a) Simplified Paleotectonic map of Türkiye, b) Main successor foreland basins of Central Anatolia. c) Simplified geological map of central Anatolia showing the localities of the Çankırı and Tuzgölü basins (Gülyüz et al. 2020). .....	18
Figure 1. 8 Generalized stratigraphical column of Tuzgölü Basin (Görür et al. 1998 .....	21
Figure 1. 9 Correlation the stratigraphy of the Tuzgölü Basin from west to east (adopted from Dirik & Erol, 2000).....	22
Figure 1. 10 Bezirci-1 borehole (TPAO, 1977).....	23
Figure 1. 11 Geological map of the Çankırı Basin. Sağpazar-1 Borehole data are located on the map (Kaymakci et al. 2010) .....	27
Figure 1. 12 Generalized tectonostratigraphic column of the Çankırı Basin (modified from Kaymakci et al. 2009).....	28
Figure 1.13. Borehole section of Sağpazar-1 well. (TPAO, 1996) .....	29
Figure 1. 14 Layout of Seismic profiles and wells in Tuzgölü Basin overlaid on 1/500K geological map of Türkiye. Bezirci-1, Sultanhanı 1, and Aksaray-1 Borehole data are located on the map (Şenel, 2002). .....	33
Figure 1. 15 Layout of the 2D Seismic profiles and location of the wells in the Çankırı Basin overlaid on 1/500K geological map of Türkiye Sağpazar-1 Borehole data are located on the map (Uğuz et al. 2002).....	34
Figure 1. 16 Interpretation of gravity image of Çankırı basin (Kaymakcı et al. 2009). .....	35
Figure 2. 1 Schematic illustration of underground storage types (API 2022).....	39

Figure 2. 2 Water Supply and discharge Planned Within the Scope of Gas Storage Expansion Project (Botaş 2022, WorldBank, n.d).....	41
Figure 2. 3 Tuzgözü Underground Natural Gas Storage Project, and the facilities (Botaş 2017, WorldBank, n.d) .....	42
Figure 2. 4 Four different shapes of salt caverns: ellipsoid-shape, irregular-shape, cylinder-shape, and cuboid-shape (h is for the effective volume of the cavern, which is called base gas, upper-part stands for the sediments in the bottom of the cavern (modified from Liu 2020))......	48
Figure 2. 5 General demands for the geomechanical design of caverns in salt (modified from (Heusermann, Rolfs, & Schmidt 2003) after (Lux, 1984, Lux, 2009) .....	49
Figure 2. 6 Typical creep test result (Modified from H. Wang et al. 2017) .....	52
Figure 2. 7 Simplified diagram showing salt creep and surface of subsidence is affecting the cavern to shrink and getting more squeeze from the original size of the cavern (Modified after Warren, 2006) .....	55
Figure 3. 1 The original TG7-ext line.....	59
Figure 3. 2 The interpreted TG7 ext. line involves the time depth conversion and the salt structure depicted in a yellow color salt view drawn on the defined seismic profile. The Bezirci-1 borehole has been placed above the seismic section to identify the roof of the salt formation. (Shot point interval:50m).....	60
Figure 3. 3 The original TG15 seismic profile.....	62
Figure 3. 4 The interpreted TG15 seismic profile. The negative. residual gravity is representing the salt boundary the salt structure is remarked by yellow on the unmigrated seismic section. The diffractions are remarked by red color. (Shot point interval:50m).....	63
Figure 3. 5 The original view of the south-eastern seismic profile. (Shot point interval:50m).....	65
Figure 3. 6 The interpreted version of the south-eastern seismic profile. (Shot point interval:50m).....	66
Figure 3. 7 The interpreted reference seismic profile TG24 (Figure 3. 6) (a) and a simplified cross-section along the Sultanhanı-1 well (b) that is generated via (a). 67	
Figure 3. 8 Display of the original section of the COV95306. ....	70
Figure 3. 9 Display of the interpreted section of the COV95306 that is correlated with Sağpazar-1 based on the salt top. ....	71
Figure 3. 10 Cross-section view of the parallel seismic profiles A and B from the Çankırı Basin.....	72
Figure 3.11 The interpreted reference seismic profile COV95306 (Figure 3. 9) (a) and a simplified cross-section (b) along the Sağpazar-1 well that is generated via (a). .....	73

Figure 3. 12. Seismic profiles, Bezirci-1 borehole, Sultanhanı-1 borehole, and top view of salt bodies in the Tuzgölü Basin. Three pieces of the salt body are seen clearly on the base map. (Generated by Leapfrog Geo). .....	75
Figure 3. 13. 3D model of the Tuzgölü salt structure view to NE.....	76
Figure 3. 14 Displaying the top view of the 3D salt body of the Çankırı Basin that is overlapping with the seismic database map. Three pieces of the salt body are seen clearly on the base map. (Blue and red color lines determine the seismic profile locations on the base map, the interpretation had been completed with the red color lines) (Generated by Leapfrog Geo). .....	78
Figure 3. 15 The 3D volume of the Çankırı Basin salt structure view (Generated by Leapfrog Geo).....	79
Figure 3. 16 The view of the ellipsoidal cavern mesh file and the information chart (Generated by Leapfrog Geo).....	84
Figure 3. 17 The schematic view of the base gas and a rooftop view of the cavern. ....	85
Figure 3. 18 The schematic view of the two-cavern scenario in the salt structure.	85
Figure 3. 19 Display the vertical total stress graph. ....	89
Figure 3. 20 Graphical display of the convergence rate versus average internal pressure in a year .....	92

## **LIST OF ABBREVIATION**

### **ABBREVIATIONS**

UGS: Underground Gas Storage

2D: Two Dimension

3D: Three Dimension

bcm: Billion Cubic Meter

mcm: Million Cubic Meter

MPa: MegaPascal

## LIST OF SYMBOLS

### SYMBOLS

$\acute{e}$ (GPa)	: Elastic module
G(GPa)	: Rigidity rate
$\nu$	: Poison Rate
$\sigma_c$ (MPa)	: Compressive Strength
$\sigma_t$ (MPa)	: Tensile Strength
$P_v$	: Vertical Initial Stress
Q	: Energy of Activation
R	: The Universal Gas Constant.
T	: Temperature
$\acute{e}_{ss}$	: Steady-State Creep Strain Rate
k	: Total Stress Ratio
$V_p$	: Production Rate
Vk	: Volume Convergence
A	: Creep Material Model Parameter

## CHAPTER 1

### INTRODUCTION

#### 1.1. Purpose and Scope

The main aim of this study is to design a salt cavern for underground gas storage by delineating the 3D volume of salt bodies in the Çankırı and the Tuzgözü Basins.

The salt body geometries are determined by magnetic and gravity methods which have specific magnetic susceptibility and density information. In addition, available well log data correlated with the seismic 2D data set which is also used for to-time-depth conversion of seismic velocity to define the depth and bulk thickness of the salt. The generated 3D salt volume is used as a constraint to design underground salt caverns to be used as gas storage during low demand of gas.

The salt cavern design is performed with an analytical approach method that is based on the fundamentals of geomechanical properties. It is not the main aim of this study where to build underground storage precisely since it requires a thorough analysis of in-situ stress, seismic hazard risk assessment, environmental impact assessment, etc. which are outside the scope of this study.

This simple analytical model is applied here to provide constraints on the design of caverns for future projects.

Single cavern and multi-cavern scenarios are applied for both basins assuming that the salt properties and the geological conditions are similar. The Çankırı basin cavern design is determined as a recommendation. However, the Tuzgözü Basin cavern design is compared with the existing Tuzgözü Underground gas storage facility that is constructed in 2017 by the BOTAS Company.

## 1.2. Motivation

Natural gas is a nonrenewable fossil fuel that has a broad range of uses. Rapid industrialization and urbanization in developing countries have significantly increased the global demand for natural gas. Also, the latest events in Europe, the invasion of Ukraine by Russia created a considerable risk of a possible energy crisis and household heating problems under cold winter circumstances (Zachmann et al. 2021). Therefore, underground gas storage (UGS) is becoming an essential part of the energy supply chain. It is crucial for the seasonal demand, and it is concerned about geopolitics uncertainty, especially for European countries.

Natural gas can safely be stored underground to be able to meet the broad range of use in the period of low- and high-demand periods of energy. There are three types of storage. These include depleted oil/gas fields, salt caverns, and aquifers. Each storage type is unique in its physical properties, such as its porosity, permeability, stability, etc., and economic factors such as the delivery rate and the injection period. (US Energy Information Agency, 2015).

The storage of aquifers is not preferable because of economic constraints, and there is a potential risk to the environment. The other question is the stability of the long term, the uncontrolled permeability of natural gas can be escaped from storage by the storage system.

In contrast, depleted oil and gas reservoirs are the most preferred ones due to their wide availability in the world and already-known subsurface conditions that reduces the risk factor to build an underground facility (API, 2022).

The unique physical properties of the salt structure give the advantage to be used as underground storage, even though they have much smaller volumes than other storage types. The high deliverability rate is meeting short-term changes in demand and supply. While the injection period is less than other types, the working volume is the smallest among other storage types (Daneshvar, 2011).

Based on the domestic production of natural gas Türkiye is a net importer of natural gas. The imported amount of gas is 46.6 billion cubic meters (bcm) in 2022 (TUIK, 2022).

Natural gas provides a significant amount of power generation and heating. 150-170 million cubic meters (mcm) per day of natural gas is consumed in Türkiye. This consumption increases in wintertime and expectedly falls in summer. In other words, the energy demand changes seasonally. Türkiye's total natural gas consumption exceeded 50 billion cubic meters (bcm) in 2022, and ranks the 4th natural gas consumer in Europe, while, it is holding the 3rd place in imports. To mitigate fluctuations in the energy demand of Türkiye, underground storage is under consideration in energy politics since the beginning of the 21st century. In Türkiye, there are two facilities for underground storage, one is in Silivri where gas is stored in depleted gas fields, and the second one is in the Tuzgölü Basin where gas is stored in artificially formed salt caverns in a salt formation (Botaş, 2022).

The Tuzgölü storage capacity increased from 1.2 bcm to 5.4 bcm, however, the storage capacity of the Silivri facility is 2.8 bcm and will increase to 4.6 bcm. In other words, the total storage capacity will reach 10 bcm by 2023. Türkiye is planning on increasing the gas storage capacity to secure the supply-demand balance (Botaş, 2022). Therefore, thick salt formations in the Tuzgölü and the Çankırı basins make these basins excellent places for future underground gas storage sites.

### **1.3. Background**

#### **1.3.1. Gravity and Magnetism**

Salt structures have unique physical properties, which are different from the sediments surrounding them. The depositional conditions and the shape of the salt are affected by the creep and flow under adequate pressure (Ode, 1968).

Gravity and magnetism are the potential field methods among the geophysical survey methods, providing information about the unique physical properties of the rocks on

a plan view and at depth (Lichoro, 2016). While the gravity method measures the strength of the gravitational attraction of the Earth based on the density of the rocks below, the magnetic field measures the strength of the magnetic field and magnetic susceptibility of the rocks.

The salt is incompressible like fluids when it is completely compacted and has a density of about  $2.2 \text{ g/cm}^3$ . These properties make the density change insignificant with increasing depth in contrast to the surrounding deposits. When the density of surrounding rocks exceeds the density of the salt due to overburden and compaction, the lower-density salt becomes unstable due to buoyancy forces and tends to move upwards to lower density levels, resulting in the development of very complex salt structures and salt domes (Ode, 1968). Measurement of gravity variation over the land provides locating the geometries and depths of salt bodies. To assess differences between actual gravity and computed gravity as well as remove the topographical effects, various techniques have been developed, such as Free-air gravity, Bouguer gravity, and Isostatic reduction methods (William, 2004). The Bouguer gravity anomaly is a kind of gravity anomaly, which contains planar terrain correction different than free air gravity correction to reduce the difference between the computed and actual gravity. The vertical component is subtracted from the sea level datum (Wilcox, 1990). The Bouguer gravity anomaly is different from the conceptual models of spherical and planar Bouguer anomalies. It is corrected for the height at which it is measured and the attraction of terrain (William, 2004). In other words, it is a planar correction application to reduce the effect of the topography. The Bouguer anomaly provides the most accurate information on the gravity distribution below the surface as a result of the removal of the topographic and geoid effect (Vaníček et al. 2004).

The magnetic method is categorized as a passive method and is based on measuring the current magnetic field value which is the magnetic susceptibility of the subsurface rock (Haldar, 2018). Magnetic properties provide important information to locate and map salt bodies (Heinrich et al. 2017). Since, the magnetic susceptibility of the salt rocks is very weak due to being composed of diamagnetic

minerals, such as halite, sylvite, gypsum, and anhydrite, and they are characterized by negative magnetic anomaly while surrounding sediments are positive (Heinrich et al. 2017). The gravity data is used in combination with magnetic data to determine the location and geometries of salt bodies more accurately which can also be used to aid the interpretation of salt bodies on seismic profiles.

In nature, the sediment compaction leads to an increase in the density of the accumulated sediments with depth. Nevertheless, at shallower depths and when the density of the surrounding rocks is not large enough to create density anomaly, hence no gravity anomaly, between the salt and surrounding rocks. However, magnetic susceptibility differences between the salts and surrounding sedimentary rocks become useful to delineate their boundaries. This is mainly because the magnetic susceptibility of the sediments is generally positive, whereas most of the evaporites including the salt rocks (halite, anhydrite, gypsum, etc.) are negative and it is not affected by the increasing depth (Fichler et al. 2007). Therefore, magnetic methods are very useful to determine the thickness and depth of the base of a salt body, which is very difficult to determine by gravity methods alone.

To gain a comprehensive understanding of the purpose of this research, the Bouguer gravity and aeromagnetic field map of Türkiye is first assessed. This provided locating gravity and magnetic anomalies or major basins in central Anatolia. Also, a residual gravity map is used to determine the salt boundary from a regional perspective by correlation with seismic sections.

After obtaining the residual gravity values, they are plotted as a graph, indicating a connection between the seismic shot points and gravity values and the location of the negative gravity value relative to the salt boundary. Unfortunately, the Bouguer and magnetic data maps could be obtained as printed images with a very limited resolution. Nevertheless, they were adequate to locate suitable areas for further study.

### 1.3.2. Seismic Data

In addition to gravity and magnetic methods, the seismic reflection method is also used in this study. The seismic reflection method is based on the acoustic energy that is spreading in the subsurface and reflected from the interfaces of the different layers back to the receiver on the surface.

2D seismic data is a kind of cross-section of 3D seismic, although 2D seismic data is inadequate subsurface information rather than 3D seismic response, it supplied the fundamental idea for interpretation starting. On the other side, 3D data provides an adequate and specified 3D volume image of the subsurface for a more reliable seismic interpretation (Yılmaz, 2007).

The seismic reflection data is provided generally in the time domain; however, results of seismic interpretation are required to be in the depth domain. Therefore, the time domain is converted into the depth domain by three different methods using available seismic velocities, sonic logs from well data, and check shots (Sheriff, R.E., & L.P.Geldart, 1995). In regards to the time-to-depth conversion, seismic velocities are employed in the simple relationship that  $\text{Depth} = \text{Velocity} \times \text{Time}$ .

Understanding the salt geometry is an essential part of the seismic interpretation, the unique qualities of the salt cause complications while interpreting of seismic section. Salt velocity is one of the important factors and can travel faster or slower than surrounding sedimentary rocks, which generally have slower velocities than most salts. Thus, the seismic reflection at the top surface of a salt layer is typically strong due to the large impedance (density x velocity) contrast, known as hard-kick in seismic interpretation jargon.

The seismic velocity is leading the understanding of the subsurface precisely by conversion from travel time to depth, correlation with borehole, creating migration section, lithological interpretation, and understanding of geological interpretation (Brouwer & Helbig, 1998), (Yordkayhun, 2008). The discriminative of the unique property of salt is the velocity. The density of evaporate is  $2.2 \text{ kg/m}^3$ , though the pure halite has a  $2.165 \text{ kg/m}^3$  density, and the velocity of the halite is about 4500 m/s.

The velocity could be changed if the salt layer contains other evaporitic rocks in addition to halite (Jackson & Hudec, 2017).

Salt bodies are critical for subsurface in the industry, due to the physical qualifications of salt make unique and easily determine from the surrounding rocks. In this case, the interpretation of salt is getting more interesting and supported by the development of the interpretation techniques of the seismic sections.

The salt geometry is unpredictable due to its subsurface is not homogenous and deposition is not regular. In such cases, 2D seismic data is not precise enough for the interpretation of salt bodies compared to 3D seismic data which generally provides a relatively better image of the salt to interpret. This makes salt bodies, e.g., salt domes, readily imaged in seismic reflection data, although steep walls cannot properly be imaged in conventional 2-D seismic data (Jackson & Hudec, 2017). Seismic resolution plays an important role while extracting the salt geometry that is controlled by the acquisition parameters, which are receiver interval, shot point interval, and the number of channels.

Seismic migration is an imaging procedure, that aims to re-placement the layers in their proper position and remove the diffraction effect from the dataset to have a better image for interpretation. Otherwise, diffraction seems on the stack section as a remaining noise type dominantly. Seismic processing is the only way to suppress that kind of noise from the data set. The low resolution and the signal/noise ratio of the seismic section must have been increased before interpretation to get better salt imaging in 3D volume. This is necessarily the ultimate procedure due to the stack section is not proper for the interpretation.

### **1.3.3. Salt Properties**

Rock salt is a crystalline form of the mineral halite (NaCl). In the literature, the word salt is mostly used for halite even if the salt includes other evaporites like anhydrite or gypsum (Hudec & Jackson, 2007). Evaporitic salt deposits consist of halite, gypsum, and anhydrite, which can be deposited in marine or nonmarine depositional

environments (Schwab, 2003). The mechanical behavior of salt consists of thermal expansion, elastic deformation, plastic deformation, and failure (Senseny et al. 1992).

Salt has unique physical properties when compared to the surrounding formation types. The first significant parameter is the density which is measured as 2.0 to 2.2 g/cm<sup>3</sup>. Salt is less dense than any other carbonate rock though the density of salt is higher than unconsolidated clastic sediments (Figure 1. 1). The density value is a distinguishing factor for the salt structure and insignificantly changes even when subject to pressure and temperature. During the deposition, salt is denser than clastic and carbonate sediments though after burial salt becomes less dense than the environment due to the compaction of the surrounding sediments. In addition, the salt becomes mechanically weaker as the temperature increases with depth. Salt has no porosity, practically even at very shallow burial depths. It is almost incompressible and so does not become much denser even if the depth increases (Hudec & Jackson, 2007). Salt becomes ductile and deformable under high pressure and temperature. It has high thermal conductivity and it is almost none magnetic but depending on the impurities it may be very weakly diamagnetic.

The salt strength against depth is depicted in Figure 1. 2 (Weijermars, Jackson, & Vendeville, 1993). Salt is more sensitive to extensional stress than to compressional stress for low mean stresses but not for high mean stresses (Fossum & Fredrich 2002). Compressive strength is related to the temperature and pressure of the environment in a direct way. On the other hand, the strain rate also controls the deformation of the salt in the opposite way (Senseny et al. 1992).

Salt flows like a fluid with depth among other deposits like carbonates and siliciclastic rocks. Plastic or ductile deformation of salt takes place only when the applied stress reached the yield point. In other words, after the yield stress is reached the deformation is the function of time, strain rate, and viscosity. Therefore, the high viscosity property of the salt facilitates its fluid-like behavior, which means that it can be mobilized beneath the overburden. Viscosity depends strongly on temperature, but if the temperature is constant and the rock is perfectly viscous,

viscosity does not vary with the strain rate and remains constant with time. (Hudec & Jackson, 2007)

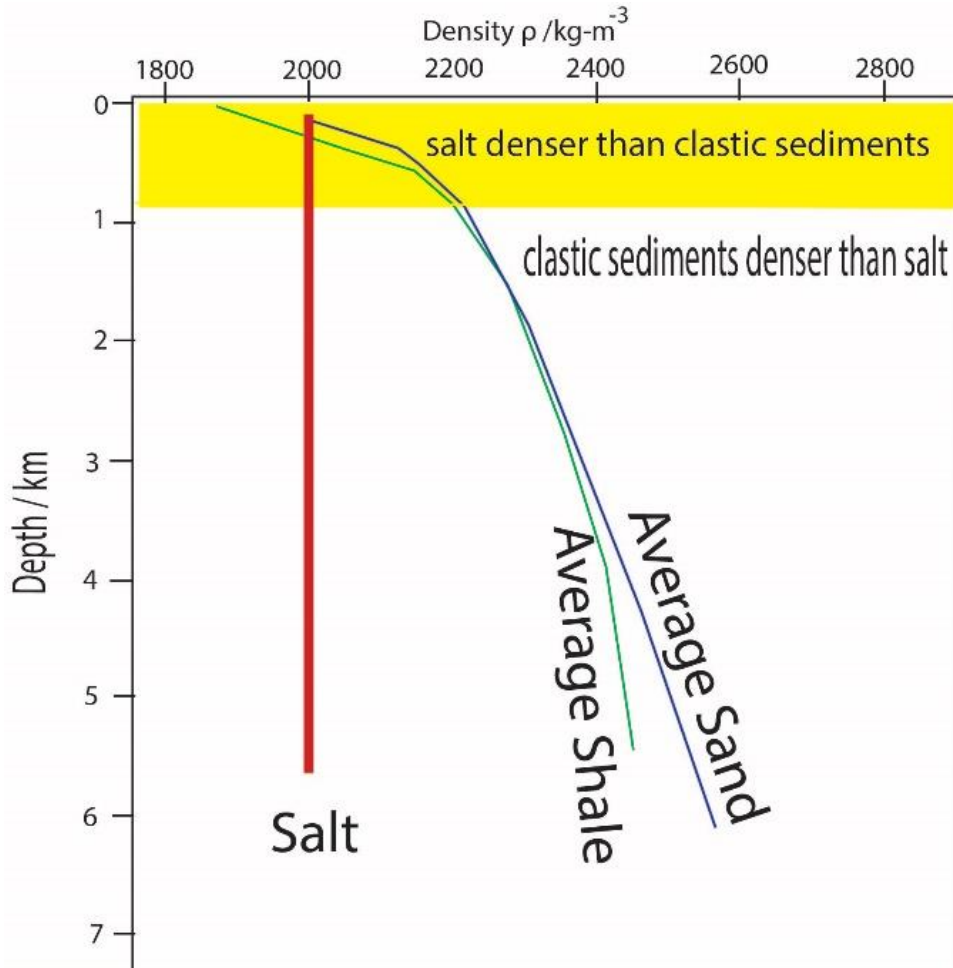


Figure 1. 1 Variation of the density of salt and clastic sediments with depth to (Jackson, 1986)

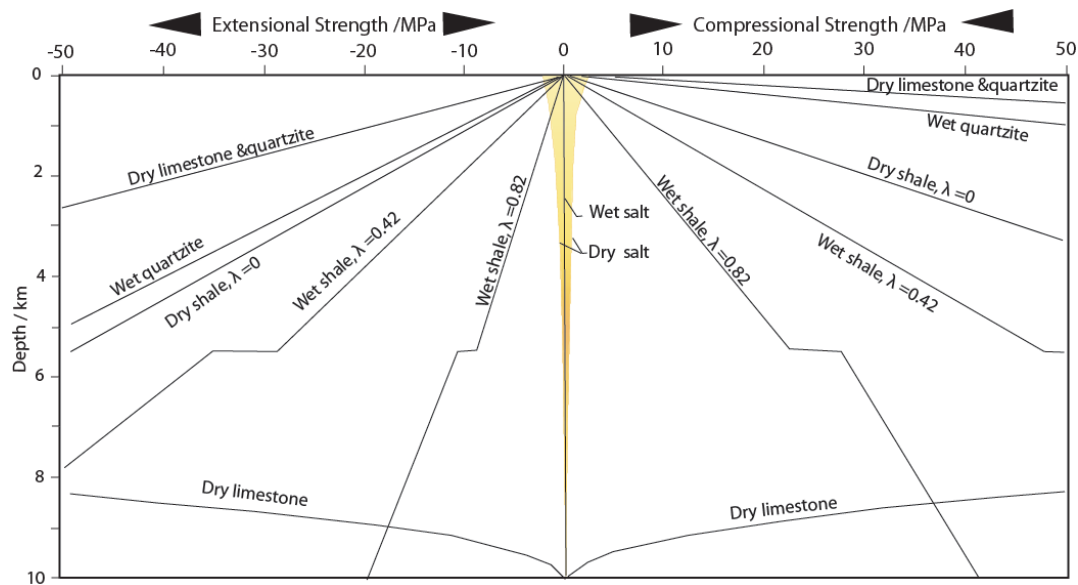


Figure 1. 2 Graph showing the strength of salt with depth compared to other sedimentary rocks (Weijermars et al. (1993), Jackson & Vendeville (1994))

### 1.3.4. Salt Structures

These extraordinary properties of salt result in complex geometrical structures. Salt ridges, pillows, diapirs, and even salt glaciers are special structures that are of importance in many settings. They can be developed in all kinds of tectonic settings from extensional to contractional tectonics settings (Martin & Jackson, 2017). The geometries of a salt structure are classified based on their geometry and relationship concerning surrounding rocks, such as salt dome, salt anticlinal, diapiric folds, salt canopy, etc. The salt diapirs and domes generally provide suitable geometries for underground storage buildings (Fossen, 2010). The geometry of the cavern is affected by the geometry and size of the salt domes and diapirs. The salt bed structures are shallower, wider, and thinner than the salt domes. They are also suitable as underground storage facilities; however, they require different cavern designs (Figure 1. 3).

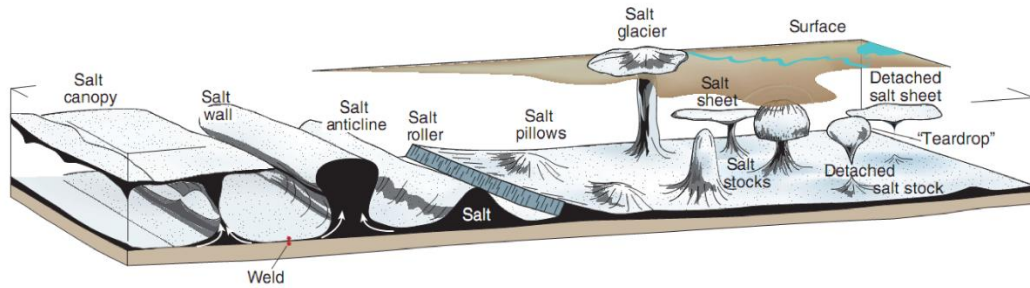


Figure 1. 3 Diagram of different types of salt structures, their names, and geometries. (Jackson, 2017)

### 1.3.5. Solution Mining

Solution mining is one of the processing methods, an alternative to mechanical digging in salt mines (Richner et al. (1992), Warren, (2006)). Despite its safety advantages over the traditional mining process, there is still a risk attached to it such as collapsing and environmental degeneration (Warren, 2006).

Solution mining processing generates huge advantages for underground storage. The salt caverns provide the most suitable advantages due to their ductility, tightness, and ability to self-cure in case of any damage could happen (Xing, et al. 2015). The geomechanical characteristics of salt structures are susceptible to temperature and humidity, which are important factors to be considered in terms of stress and strain conditions in time.

### 1.3.6. Salt Caverns

A salt cavern is a type of underground storage that is a method of leaching to create an artificial shape in the salt structure (Muhammed et al. 2021) why is to collect a variety of hydrocarbon products including natural gas, liquid hydrocarbons, compressed air, hydrogen, etc. Salt structures commonly used as underground storage since the 1940s, to supply energy demand regularly and reliably (Jirik, C. J.,

Weaver, L. K., 1976). The salt cavern is created by solution mining that uses technology to develop storage in salt domes, and salt beds (Figure 1. 4). The cavern structure is usually wider at the bottom and narrower at the top. (Onal, 2013). The depth of the cavern has a wide range from a few hundred to a thousand meters in the world. The key aspects of UGS are including threshold pressure, rock mechanical properties, in-situ stress, and faults (BGS, 2008) (Figure 1. 5).

Figure 1.6 is an illustration of the summary of the various salt caverns all around the world. The shallowest one is from Sallie's de Bean and is designed in a salt-bedded horizontal shape. The first deepest cavern leached in a salt dome at Eminence, Mississippi including a design purpose at the depth of 1,740-2,040 m. This cavern has lost 40% of its purpose volume in 2 years due to the creep of the salt that built in the cavern. The internal pressure is not provided to protect the cavern from surface subsidence and the size of the cavern is squeezed (Warren, 2016).

Nowadays, salt caverns for underground gas storage are drilled deeper than 1500 m., for example, the deepest salt cavern in the world was drilled in the Netherlands with a depth of 2,900 m with an ellipsoid shape (Zhang et al. 2001).

### **1.3.7. Cavern Designing**

Designing methods had been changed during the history of underground storage facilities. Different approaches are tested and proposed to apply to get the best solution with the most suitable cavern stability. At the beginning of the design history empirical approaches are common though, to reduce the possible problems numerical approaches had been becoming the most popular and reliable method. After the experimental method is not giving satisfying knowledge based on the stability of the cavern so analytical approach method moved forward with simple geometry. While the assumptions have been changed to find a solution for new challenges such as dilation, salt creep, thermal conductivity, etc., the numerical approaches method is helping to predict those kinds of problems with a simulation model. This numerical approach requires some parameters to be constant though desired parameters

obtained by in-situ laboratory tests are recommended to get more reliable models before construction (Habibi, 2019).

However, an analytical model is a kind of basic approach, only giving the volume of a single cavern, capacity, and convergence, it is also beneficial to determine the possible deformation of the surface by this method. The most useful advantage of this method is to enable simplifying the cavern design with the fundamentals. However, it also has disadvantages due to the nonhomogeneous nature of the subsurface, and hard to describe the method with a single parameter (Tajdus et al. 2021).

The geomechanical parameters of the salt are the most important issue while designing the salt cavern for underground gas storage, due to it is necessary to carry out the risk management, and financing of the project, and to determine the long-term stability. Geomechanical parameters are only determined by the in-situ laboratory tests and the results are utilized for designing the cavern concerning the fundamentals of the design.

The salt cavern design is the first aim of this study after unraveling the 3D salt volume of the candidate study sites. Building a cavern in a salt structure is easily accomplished with a solution mining method by which the salt structure (cavern) is obtained by controlled salt leaching. This method is the most common way due to its low cost, and providing technical aspects such as cavern geometry, size, the stress-strain factor of the surrounding rocks, overburden thickness, pressure, temperature conditions within the salt, etc. (Allen et al. 1982).

The first essential for designing of cavern starts with the appropriate site selection and continues with cavern shape and dimension, geomechanical properties related to salt creep, surface subsidence, and thermal conditions (Habibi, 2019).

The modeling methods in the history of cavern design consist of empirical, analytical, and numerical solution methods (Habibi, 2019). The analytical approach method only requires a single cavern shape to investigate the relationship between the salt and cavern by convergence rate, depth, and thickness of the cavern (Tajdus

et al. 2021). Due to the lack of geomechanical information related to the salt bodies in this study, an analytical approach is followed.

The design of the cavern depends on the geometry and thickness of the salt structures. For example, thick and pure salt deposits are very common in Europe, mainly in the south Permian basin (Gerling et al. 1999) thinner and impure rock salt structures are observed in China (Wang et. al. 2015, Xing, et.al. 2015).

Since there is no standard cavern design available, the shape and dimension of each cavern could be unique and are controlled by three factors to be considered during building a cavern in a salt structure. These include 1) the thickness of the salt should be sufficient in a proper depth. 2) Sufficient static stability and reliable tightness that may yield acceptable surface subsidence. 3) Availability of sufficient fresh water supply for dissolving the salt. In addition to these factors, the environmental hazard potential of the structure should be considered after removing the brine outside the cavern. (Allen, 1982, Lux, 2009).

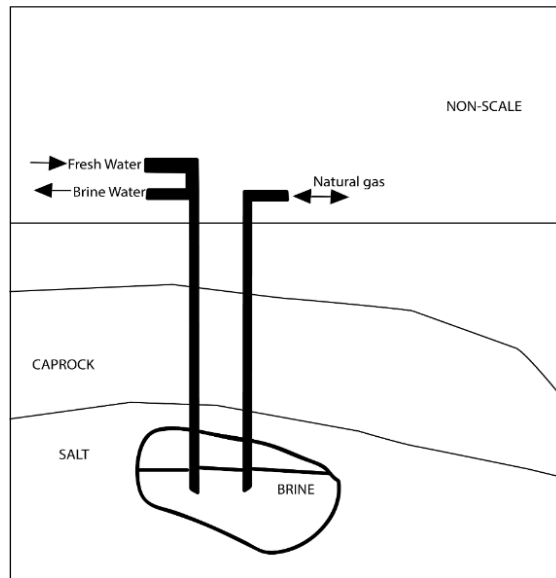


Figure 1. 4 A schematic diagram of a simplified fundamental environment for a salt cavern. (Modified from CAES, 2022)

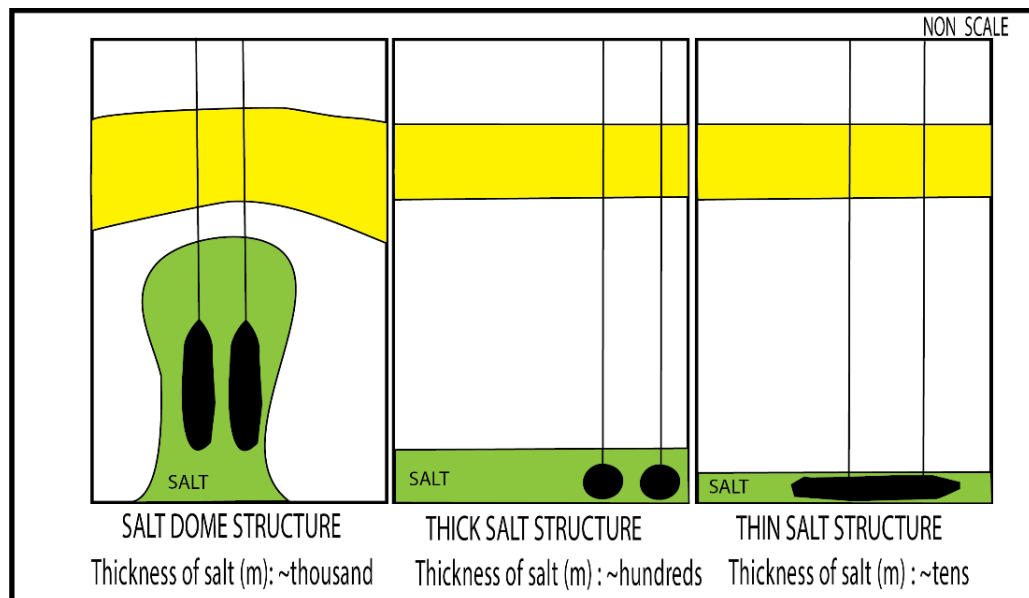


Figure 1. 5 An illustration of various types of underground storage in salt structures. (Modified from BGS, 2022)

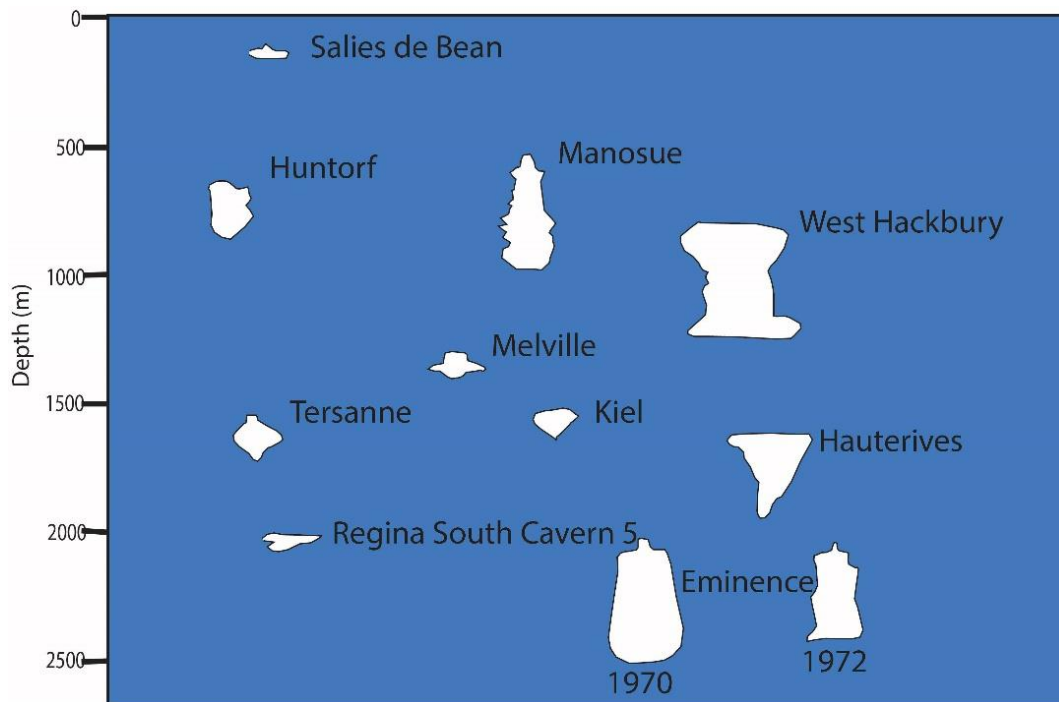


Figure 1. 6 Depth versus shapes, and relative volumes of typical salt cavern gas storage facilities in salt domes around the world except for Salies de Bean and Regina south cavern which are in a salt bed and designed horizontally (modified from Warren, 2006).

#### 1.4. The Tectonic Outline of Türkiye

The present tectonic scheme of Türkiye is related to the evolution of Paleo- and Neotethys oceans since the Late Palaeozoic. During its evolution, various pieces of continental blocks or microcontinents detached from the northern margin of the Gondwana and collided with the southern margin of Eurasia diachronously mainly during the Mesozoic (Cimmerian orogeny) and the Late Cretaceous to the Early Cenozoic (Alpine orogeny). Paleo-Tethyan evolution of Türkiye is relatively less

known due to overprinting of successive tectonic events that related to the opening and closure of the Neotethys, which is also referred to as Mesozoic Tethys.

The Neotethys opened along several branches separated by various continental fragments from the northern margin of the Gondwana and later they are closed and the continental fragments amalgamated to form the present tectonic scheme of Turkey and surrounding regions, as the Neotethys obliterated and closed completely. Among these, Türkiye. Izmir-Ankara-Erzincan and (IAESZ) demarcate the former position of the Northern Branch in Türkiye (Figure 1. 7). Along the IAESZ, the Pontides with Eurasian Affinity in the north and Taurides with Gondwana affinity in the south collided and amalgamated as the Northern Branch of Neotethys subducted below the Pontides. The Inner-Tauride Suture, however, was developed within the Taurides, and it separated the Kırşehir Block from the Taurides during the Mesozoic. During the Late Cretaceous Kırşehir Block amalgamated with Taurides as the intervening oceanic lithosphere completely subducted, below Kırşehir Block, and obliterated. The subduction and collision processes resulted in the development of fore-arc to foreland basin complexes and successor basins, such as Çankırı, Tuzgölü, Haymana, Ulukışla, Çiçekdağı, Ayhan, Sivas accumulated a very thick marine to continental clastics and carbonates, as well, very remarkable evaporitic sequences which are the main concern of this study (Kaymakcı et al. 2009, Kergaravat et al. 2016, Clark & Roberson 2002, Gülyüz et al. 2020). These evaporitic sequences resulted in various holokinetic structures of different sizes, shapes, and depths. Salts are mostly developed within the late Eocene to Oligocene and Miocene strata, as well as Messinian in the continental lacustrine environments (Kaymakcı et al. 2010).

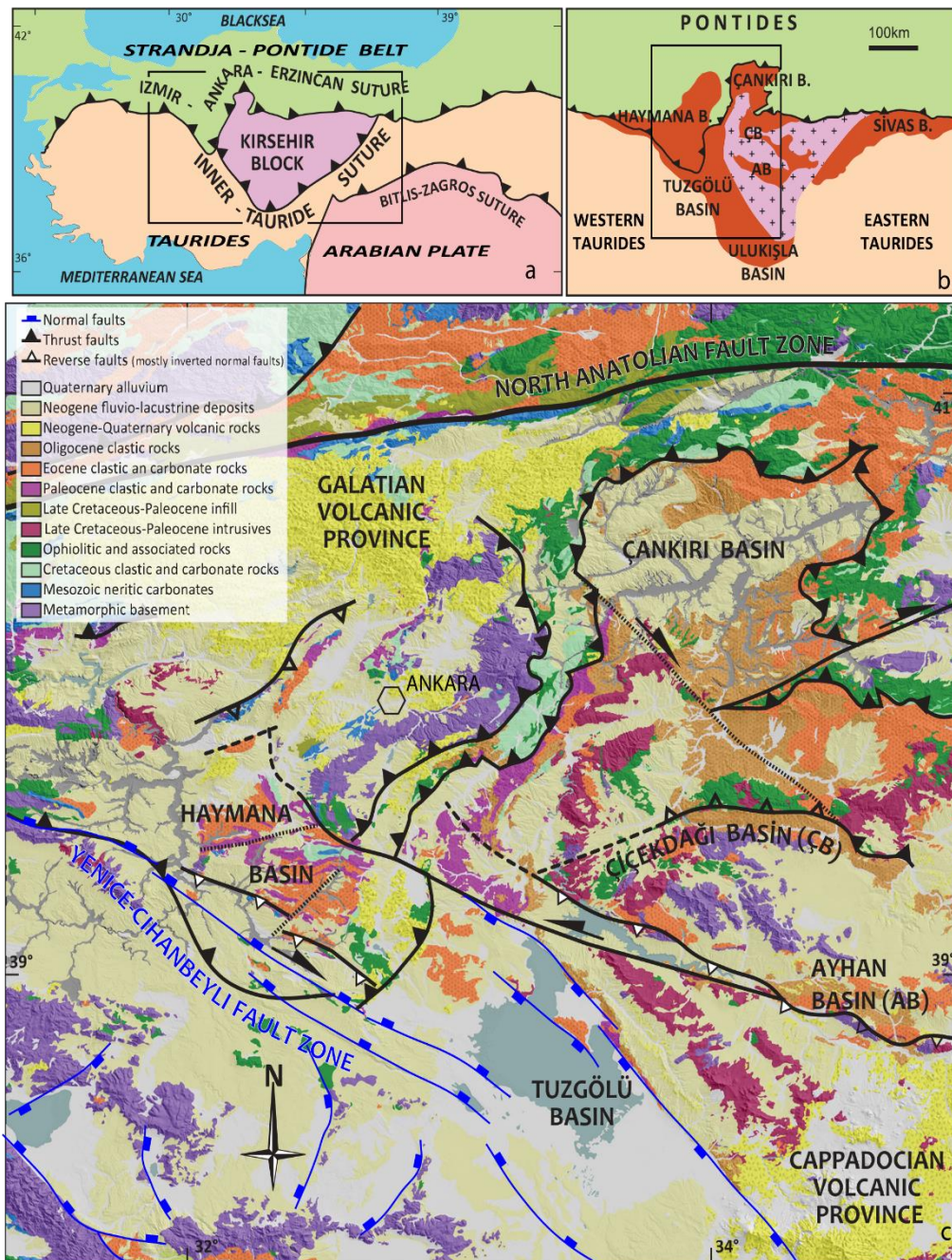


Figure 1. 7 a) Simplified Paleotectonic map of Türkiye, b) Main successor foreland basins of Central Anatolia. c) Simplified geological map of central Anatolia showing the localities of the Çankırı and Tuğçölü basins (Gülyüz et al. 2020).

## **1.5. The Geology Outline of the Study Areas**

### **1.5.1. Tuzgölü Basin**

The Tuzgölü Basin is one of the successor foreland basins (Gülyüz et al. 2020) in Central Anatolia such as the Haymana and Tuzgölü basins. Bounded in the north by the Izmir-Ankara Suture Zone, Ulukışla basin to the South, Tuzgölü fault to the east side, and Yeniceoba, Cihanbeyli fault to the West (Figure 1. 7). These basins are also interconnected to each other during certain periods of geologic times (Rojay, 2013).

The Tuzgölü Basin straddles the Inner-Tauride suture and developed both on the Taurides in the west and the Kırşehir Block in the east. The stratigraphy, origin, and tectonic characteristics of the Tuzgölü Basin has been the topic of various controversy some suggested that is a fault-controlled intermontane basin (Uğurtaş, 1975, Arıkan 1975), syn-collisional extensional basin (Çemen et al. 1999), forearc basin (Görür et al. 1984 ,Yılmaz et. al. 1987, Göncüoğlu et. al. 1991).

The large axis of the Tuzgölü Basin trends NW-SE trending and is dominated by Paleogene salt deposits, and related structures (Arıkan 1975, Ugurtas, 1975, Dirik, 2000). It covers around 20,000 km<sup>2</sup> area and about 10 km basin fill thickness. It evolved from Late Cretaceous to Oligocene as a marine to continental flysch to molasse basin (Arıkan, 1975, Ugurtas, 1975, Dirik, 2000), and during the Neogene, it became a part of Central Anatolian fluvio-lacustrine basin system (Özsayın et al. 2013). The true infill of the basin is composed of various marine to continental deposits composed of mainly clastics and carbonates. They are overlain by a few hundred meters thick fluvio-lacustrine sediments extending beyond the boundaries of the basin. In the west, the basement of the basin is constituted by various meta-carbonates, marbles, and high-pressure metamorphic rock remnants belonging to the northern edge of the Tauride Block, whereas, granitoid and roof pendants of ophiolitic rocks belonging to Kırşehir Block constitute the basement in the east (Çemen et al. 1999). The Tuzgölü Basin contains Maastrichtian to Tertiary units during the deposition, and the regression and transgression are interrupted sedimentary succession. The Late Eocene evaporites occurred during the closure regime of the basin (Çemen et. al., 1999). The

sedimentary infill of the Tuzgölü Basin started with the terrestrial clastics in the Upper Cretaceous – the Paleocene and continued with the Eocene marine sediments deposition. The Eocene strata are overlain by the Oligocene evaporites with an angular unconformity. (Ozsayın et. al, 2013). The controversy between stratigraphy units is divided the basin into two parts, the eastern and the western (Arıkan & Dirik, 2000, Dirik & Erol, 2000, Ozsayın et. al, 2013). The generalized stratigraphical column of the lithological units around the basin and the correlation of the sedimentary units are modified and depicted in Figure 1. 8 and Figure 1. 9.

The Tuzgölü Basin is fault-controlling (Uğurtaş, 1975, Arıkan, 1975), and the complex sedimentary deposition has seemed due to the tectonic activity. The evaporite samples appeared in the Paleocene strata overlining above the Haymana Formation in Kırkkavak Formation. The salt is deposited in the Paleocene strata at 1,332m in the southwestern part and the Eocene strata at 1,450m depth in the northeastern. The two boreholes are 42 km away and hardly correlate them.

The regional shortening dominantly controlled the sediment succession in NNW-SSE to NE-SW compression in the bedrock units of the basin (Ozsayın et al. 2013).

Bezirci-1 borehole is located in the southern part of the Tuzgölü Basin (Figure 1. 14) and is used to tie the formation tops and the age relationship with the thickness and depth information for the seismic sections. According to the relinquishment reports, the salt is 1270m thick and deposited by the end of the Cretaceous and mainly during the Paleocene (Figure 1. 10) In the well, the salt penetrated below the Upper Eocene-Miocene Mezgit Formation at 1,332 m and continued up to the Haymana Formation at 2,632 m. The thickness of the salt structure reaches up to 1300 within the borehole 1,300 m (Figure 1. 10).

Aksaray-1 borehole data is located in the eastern part of the study area (Figure 1. 14). The salt is penetrated in the Eocene Eski Polatlı Formation within the 1,450m and 1,600 m depths along the borehole. The absence of the seismic profile of this borehole caused it to keep out of the interpretation of the survey area.

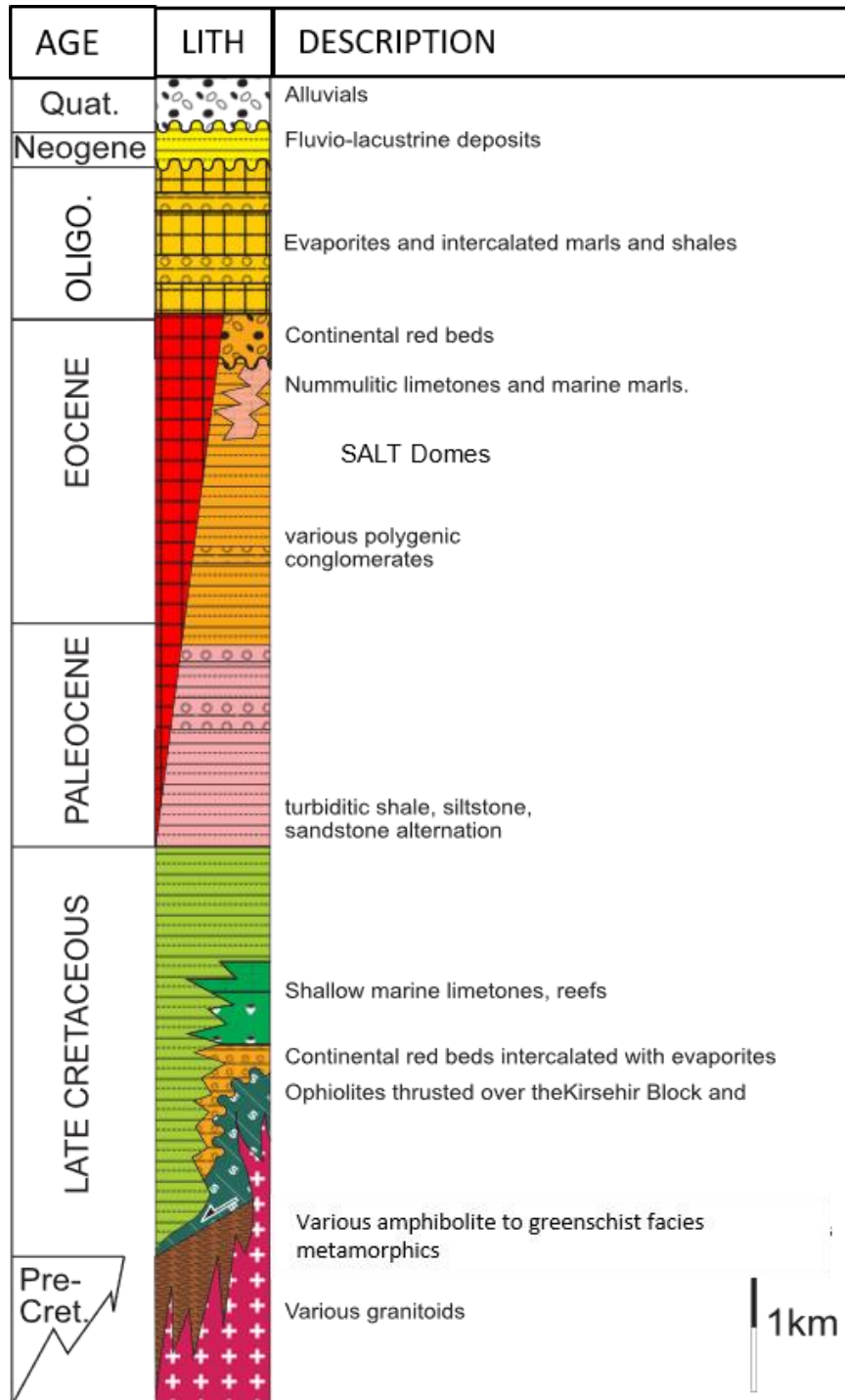


Figure 1. 8 Generalized stratigraphical column of Tuzgözü Basin (Görür et al. 1998 Dirik & Erol, 2000, Ozsayın et al. 2013)

AGE	WESTERN PART	LITHOLOGY	EASTERN PART	
TERTIARY	QUATERNARY			
	PALEOCENE	ÇİHANBEYLİ FM	Aluvium Lacustrine & Limestone Continental Clastic & Tuff	ÇİHANBEYLİ FM
		GÖKDAĞ FM	Gypsum-shales Continental Clastic & Tuff Evaporites	KOÇHISAR FM
	EOCENE	ESKİPOLATLI FM	Shale & Turbiditic Sandstone	YASSIPUR FM
KIRKKAVAK FM			ASMABOĞAZI FM	
CRETACEOUS	KARTAL FM	Continental Clastics Ophiolitic Melange	KARTAL FM	
		Kütahya-Bolkardağı Metamorphics	Central Anatolian Crystalline Complex	

Figure 1. 9 Correlation the stratigraphy of the Tuzgölü Basin from west to east (adopted from Dirik & Erol, 2000)

BEZIRCI -1 BOREHOLE			
AGE	PLIOCENE	OLIGO-MIOCENE	U.CRETACEOUS-PALEOCENE?
FORMATION	CHANBEYLİ	MEZGİT	SALT
THICKNESS (m)	584	748	1270
DEPTH (m)	584	1332	2602
			3800
			4607
U. CRETACEOUS (MAASTRICTIAN)			HAYMANA

Figure 1. 10 Bezirci-1 borehole (TPAO, 1977).

### 1.5.2. Çankırı Basin

Çankırı Basin is located in the NW part of the Central Anatolia, it is one of the largest interior basins developed during the late Cretaceous to Recent. It straddles the Izmir-Ankara-Erzincan Suture Zone and developed on the upper Cretaceous subduction complex of the IAESZ that intruded partially by the granitoids of the Kırşehir Block (Figure 1. 11). It was a fore-arc basin during the Late Cretaceous and converted into a foreland basin after the collision of the Kırşehir Block into the southern margin of Eurasia by the end of Cretaceous. The Upper Cretaceous Paleogene sequences deposited diachronously over the upper Cretaceous ophiolitic melanges and exhumed granitoid of the Kırşehir block (Kaymakçı et al. 2009) (Figure 1. 12).

The infill of the Çankırı Basin is divided into two sequences based on their tectonostratigraphy. The first sequence includes Upper Cretaceous to Early Miocene fore-arc to foreland deposits marking the timing of subduction and collision. The second sequence is related to post-collisional events during post-lower Miocene times. Between the Late Eocene to the Oligocene strata, thick evaporite units are been located (Kaymakçı, 2009) (Figure 1. 12).

Çankırı Basin comprises 9 distinct stratigraphical sequences. These include from older to younger; 1) the Upper Cretaceous units, 2) Paleocene to Middle Eocene marine clastics and carbonates, 3) Middle Eocene Nummulitic limestone, Kocaçay Formation, which is the youngest marine unit in the basin, 4) Upper Eocene to Middle Oligocene continental red coarse clastics, Incik formation, which is the thickest (2,000m) units in the basin, 5) Middle Oligocene evaporites of Güvendik Formation, 6) Salt Domes, 7) uppermost Oligocene to lower Miocene clastics, Kılçak Formation, marking the end of collision-related deformation. 8) Middle Miocene to Pliocene fluvio-lacustrine deposits, Çandır and Süleymanlı formations, and evaporites; Tuğlu and Bozkır formations, which are dominantly gypsum, and 9) Plio-Quaternary alluvial units (Kaymakçı et al. 2010). So far two oil wells have been

drilled in the basin and only Sağpazar-1(TPAO-1996) penetrated the salts in the basin (Kaymakcı et al. 2010) (Figure 1.13).

The closing phase of the northern part of the Çankırı Basin occurred under compressional deformation though the strike-slip fault system generally affected the basin infill at the NE-SW orientation. Also, Middle Miocene normal faults dominate the basin center (Kaymakci et al. 2010).

The structural development of the basin consists of four phases, (1) pre-Late Paleocene deformation occurred only in the southern part, (2) compressional deformation, (3) extensional deformation in the Middle Miocene (4) regional transcurrent tectonics since the Late Miocene (Kaymakci et al. 2003a).

The tectonic development of the Çankırı Basin was affected by three different fault types such as compressional, strike-slip, and normal faults. The compressional faults are observed in the rim of the basin. The closing phase of the northern part of the Çankırı Basin has occurred under compressional deformation though the strike-slip fault system is generally affected by the basin infill at the NE-SW orientation. Also, the normal faults dominate the center of the basin (Kaymakci et al. 2009)(Kaymakci et al. 2010). Two depositional sequences are significantly divided by a local unconformity in the Çankırı Basin. The northern part of the basin is mainly evaluated by the local unconformities through the Cretaceous to Paleocene units without no major hiatuses in the basin center (Kaymakci et al. 2009).

The salt domes possibly originated between Middle Eocene to mid-Oligocene (Kaymakcı et al. 2010) and they are locally deformed and pierced into the younger units up to Late Miocene Bozkır Formation (Kaymakcı et al. 2010). On the surface, they are easily delineated in the gravity images due to low gravity anomaly corresponding to the thick basin infill and salt structure, while high values correspond to the surrounding ophiolitic mélangé and the granitoids.

According to the Sağpazar-1 (Figure 1. 15) borehole report, anhydrite halite is recorded between 1,630m and 1,660 m depth. Also, various salts are penetrated from 1,765m to 3,700 m depth, which is around 2000m in thickness. The Sağpazar-1 borehole (Figure 1.13) ended up at 3,700 m depth. In the well, the Mid-Oligocene

Güvendik Formation is 480 m thick and between 0-166 m depth including white beige, anhydrite, and gypsum alternated with red and green shales. Between 166m and - 380 m, anhydrite with shale intercalations intersected. Halite (NaCl) is intersected between 380 - 480 m.

The Late Eocene-Oligocene İncik Formation underlies the Güvendik Formation and is intersected between 480 meters and 3,700 meters depth, reaching up to 3,220 m thickness at the Sağpazar-1 well. Within the İncik Formation, anhydrite-halite interlayers are encountered between 1,630 m and 1,660 m depth, and evaporites are encountered between 1,765 meters to 3,700 meters depth various, which means that approximately 2000 meters thick salt exist in the basin.

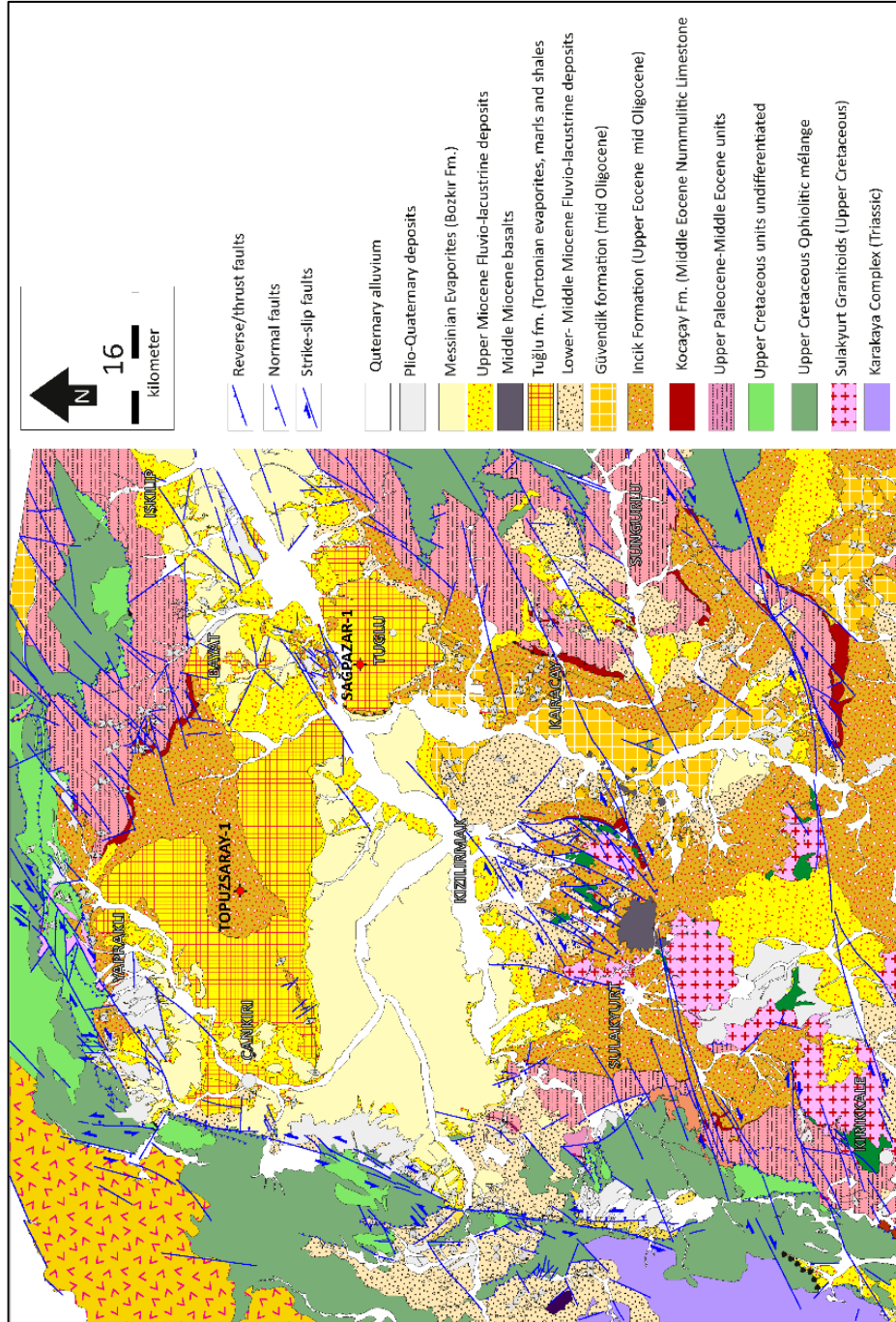


Figure 1. 11 Geological map of the Çankırı Basin. Sağpazar-1 Borehole data are located on the map (Kaymakci et al. 2010)

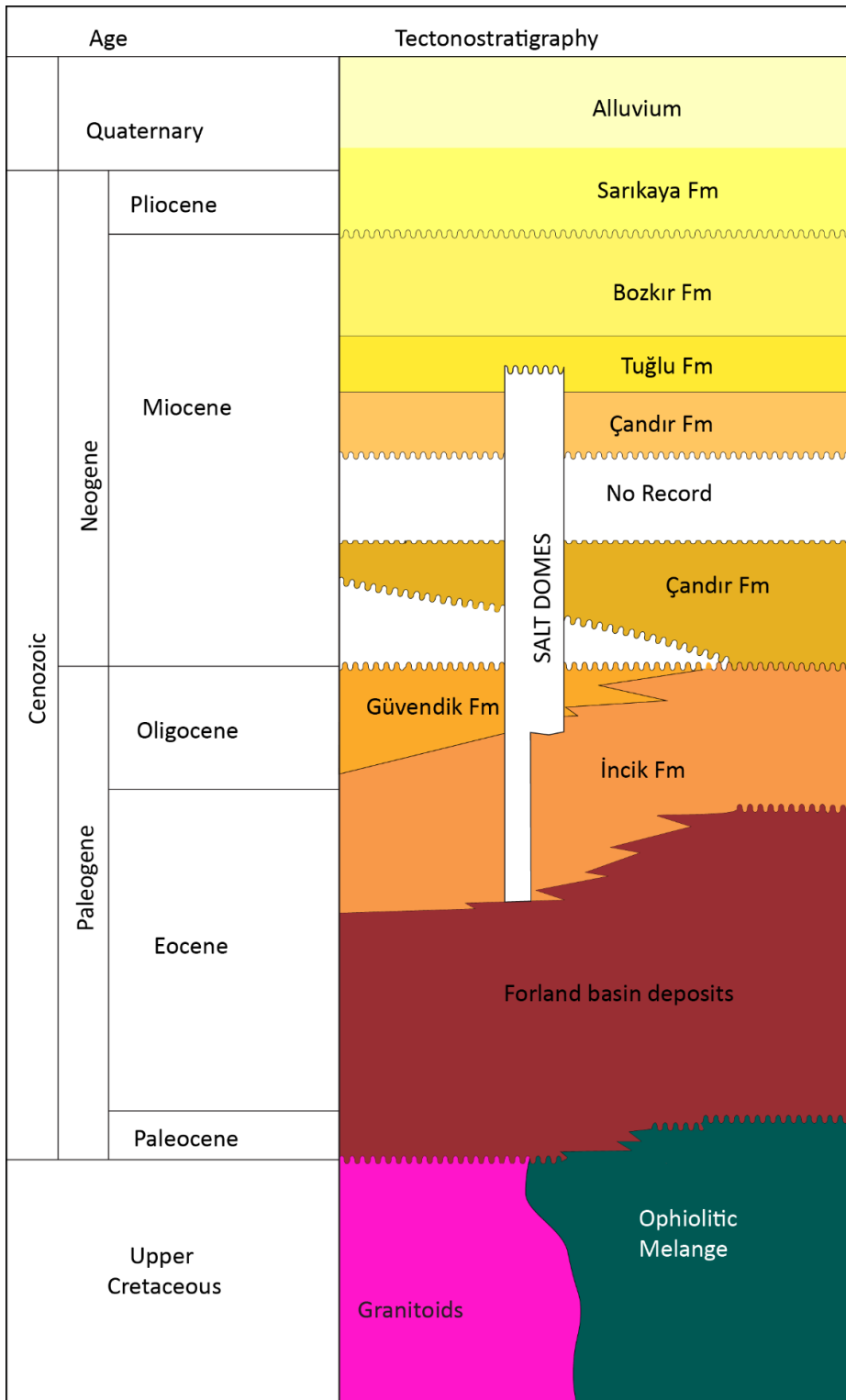


Figure 1. 12 Generalized tectonostratigraphic column of the Çankırı Basin (modified from Kaymakci et al. 2009)

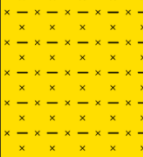
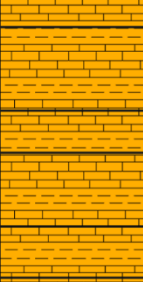
AGE	FORMATION	THICKNESS (meter)	DEPTH (meter)	LITHOLOGY	DESCRIPTION
OLIGOCENE	BAYINDIR	480			Buff to white gypsum and anhydrite intercalated with yellowish to beige marl
LATE EOCENE - OLIGOCENE		3700	1000		Brick red color mudstone, shale and sandstone
			2000		Red to green to buff mudstone and shale intercalated with dolomites
					Greenish gray paper shale
			3000		Anhydrite intercalated with shale

Figure 1.13. Borehole section of Sağpazar-1 well. (TPAO, 1996)

## 1.6. Data and Methodology

Potential field data and seismic reflection profiles are used in this study. The potential field data sets are obtained from the MTA website. The seismic data is obtained as hard copies from Turkish Petroleum Affairs (MAPEG). Obtained printed 2D seismic profiles and they are scanned to interpret in graphic drawing software. The gravity Bouguer map of Türkiye changes between the -169 and 83 mGal values which means the lower gravity values belong to less dense rocks, however, the higher gravity values belong to the denser rocks. The negative gravity values are much more extended across Türkiye, possibly due to an increase in the topography eastwards resulting from the deep-seated isostatic compensation. The residual gravity of the Tuzgölü Basin is gridded in 0.5 contour interval within third order polynomial surface. The gravity image of the Çankırı Basin is gridded to 2\*2 km by the conventional Kriging method (Kaymakcı, 2010) (Figure 1. 16).

In the Tuzgölü Basin, 28 seismic 2D unmigrated seismic data were used making up a total 402,650 km line length and covering approximately 4.200 km<sup>2</sup> area (Figure 1. 14). The 2D seismic data set of the Tuzgölü Basin is the stack version, and the resolution is 6-fold, resulting in a chaotic image on the seismic section. The seismic profiles are also unmigrated, and the issue of arranging the unmigrated seismic profile is here appearing as a diffraction (Figure 3. 3 and Figure 3. 4). Therefore, the quality of seismic interpretation is impaired by diffraction. The diffraction present in the unmigrated seismic profiles was only identified dominantly in three or fewer of them, which restricted their interpretation. Therefore, the salt interpretation was committed through correlation with the salt orientation on the adjacent seismic profile and residual gravity chart on those diffracted profiles in terms of unraveling the salt boundary.

Diffraction alters the whole of the data set, in normal conditions, re-processing of the data set is preferable. Unfortunately, the seismic data set is not available to re-process. Therefore, the 2D unmigrated seismic sections are assumed to be admissible for interpretation.

As opposed to the Tuzgölü Basin, seismic sections of the Çankırı Basin are migrated and have a higher seismic resolution of 60-fold, which is ten times greater than the Tuzgölü Basin. Thus, the seismic sections of the Çankırı Basin are of good quality with a high Signal/Noise ratio. In the Çankırı Basin, 15 seismic lines make up 700 km line length and cover a 4.122 km<sup>2</sup> area are obtained from Türkiye Petroleum Affairs (MAPEG) that were acquired by Turkish Petroleum Company in various vintages (Figure 1. 15).

The depth imaging of the salt is an essential part of underground gas storage projects. The seismic method is aimed at a visualization of salt bodies based on density and speed information from the subsurface. The contrast in velocity at the sediment and evaporite interfaces is a valuable feature. The seismic velocity increases with the depth, but the structure of salt causes an inversion of the information about the seismic velocity, and the reflection coefficient is notable because the salt density is a significant item. During the seismic interpretation, borehole data is used as a reference for formation tops and time/depth conversion. Table 1. 1 depicts the list of boreholes used in this study.

Table 1. 1 The borehole list used in this study.

<b>Borehole Name</b>	<b>Area</b>
Bezirci_1 Sultanhanı-1 Aksaray-1	Tuzgölü Basin
Sağpazar-1	Çankırı Basin

The seismic energy is absorbed while traveling through the media. The energy transmission decreases with increased depth. Here, the seismic energy is absorbed below around 3,000 ms in time, 5,000 meters in depth, therefore the salt bottom hardly was interpreted precisely for a few of the seismic profiles. This is solved by carrying the salt bottom interpretation from the adjacent seismic profiles if the energy absorption caused energy missing on the profile.

After completing the interpretation, the seismic sections were digitized and geocoded using the Leapfrog Geo software and the 3D volumes of the salt bodies were

generated. The outline of the salt formations was defined as a diapir in the Tuzgölü Basin and as a dome in the Çankırı Basin. Subsequently, these 3D volumes have been employed for the depth and thickness of the salt bodies.

The distance of the seismic profiles is irregular and for the generation of the volume view, a more frequent data set is requested. The irregular 2D seismic gridding size, which is the nature of the 2D seismic survey, had a paramount effect on the interpolation of salt in this study. Therefore, 3D volume composition involves several distinct units; three components in the Çankırı Basin and four components in the Tuzgölü Basin. Utilizing the spheroidal approach does not eliminate the repercussions of this several pieces view by extrapolation even if the interpolation parameters are maintained at an ideal level. The interpolation may present an unfavorable consequence. The 2D mesh files were converted into the 3D volume by interpolation, even if the parameters were not wider, the 3D salt volume was constructed possibly overestimated. In the coming times, provided a project is acquired from the 3D seismic data set in the Çankırı Basin, the volume of salt would be calculated more accurately. There is plenty of advantages of the 3D seismic data set in terms of the underground facility location, the number of salt caverns that plan to build in the 3D salt body, and prevent from possible damage conditions, and calculating the safety factor of the cavern stability. Like, Botaş firm had obtained the 3D volume of salt before building the facility.

This study does not involve laboratory tests or numerical databases; therefore, a cavern was developed by utilizing analytical modeling. The analytical model approach could be considered an inversion technique. Firstly, the shape of the cavern is decided based on the depth and thickness of the 3D salt structure volume. Subsequently, the fundamental features were employed in the design that involves six terms from shape to thermal conditions. In this study, the Leapfrog software was employed to create the cavern in the form of a mesh record.

The salt cavern was constructed to propose the finest shape, size, and physical specifications concerning the 3D volume of the salt structure.

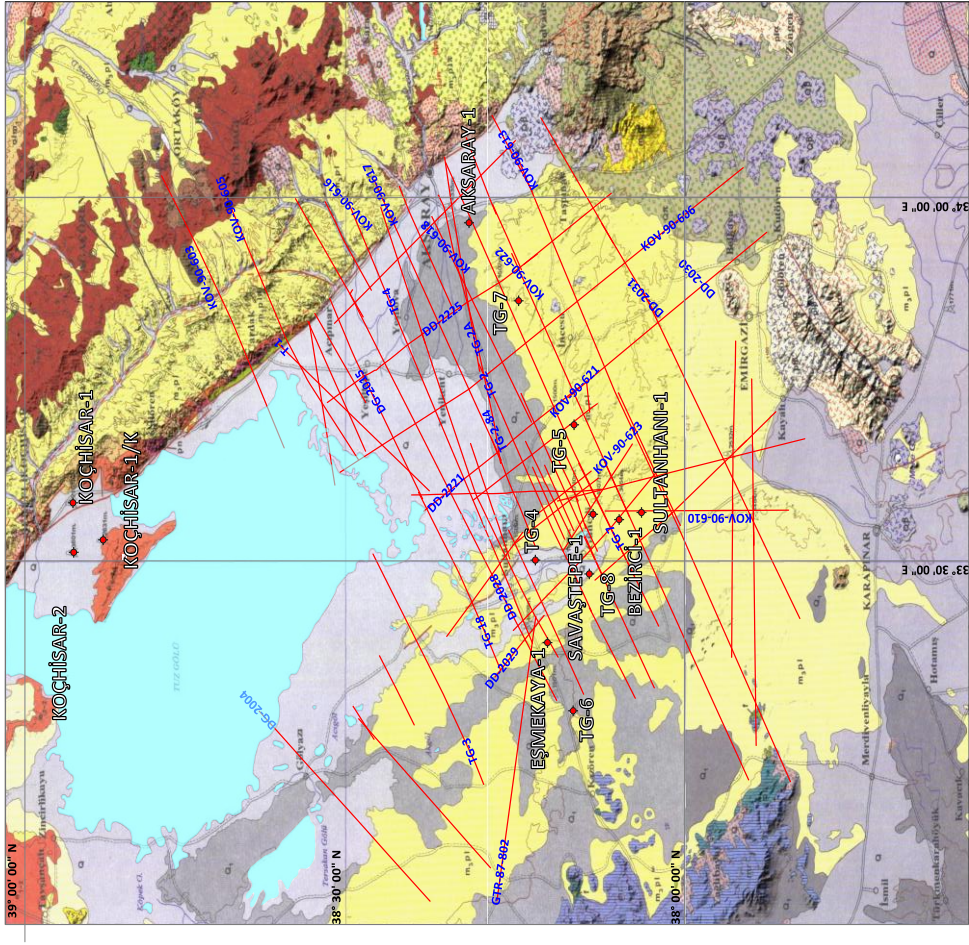


Figure 1. 14 Layout of Seismic profiles and wells in Tuzgözü Basin overlaid on 1/500K geological map of Türkiye. Bezirci-1, Sultanhanı 1, and Aksaray-1 Borehole data are located on the map (Şenel, 2002).

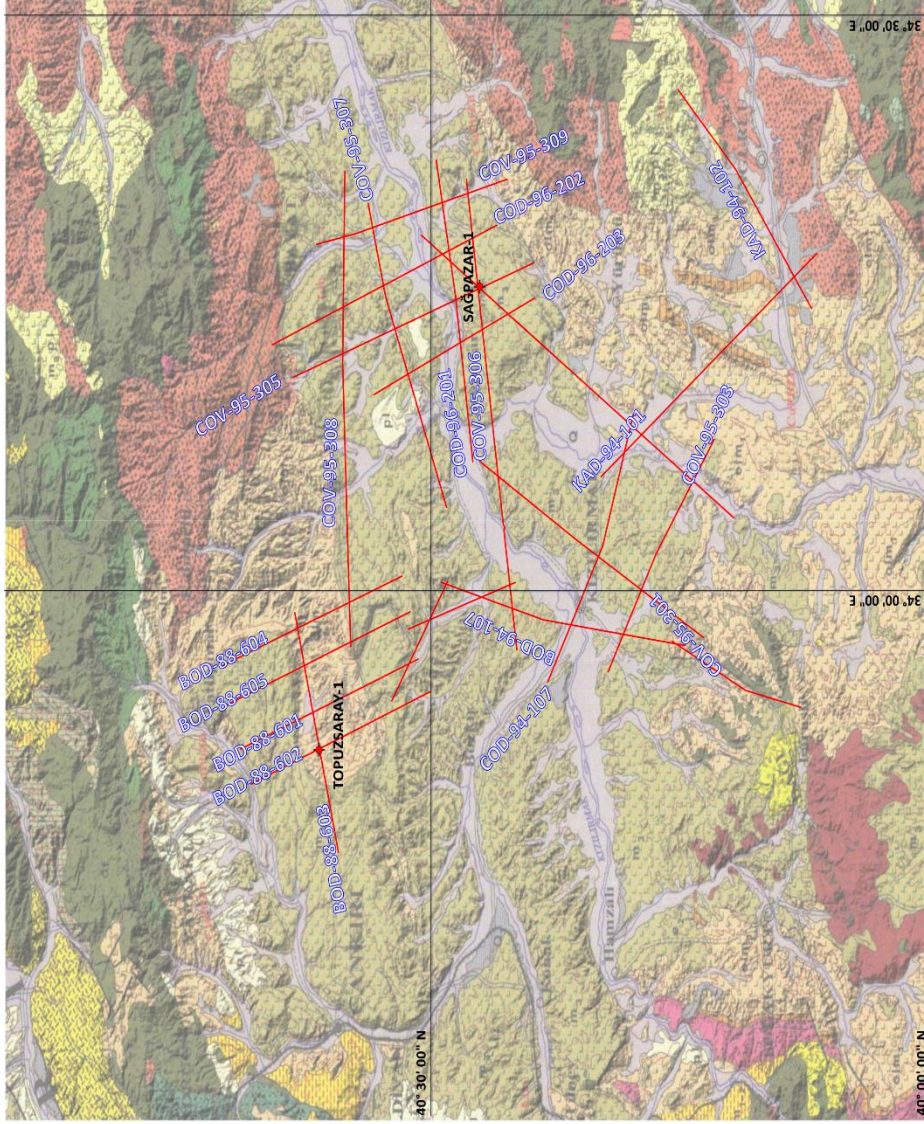


Figure 1. 15 Layout of the 2D Seismic profiles and location of the wells in the Çankırı Basin overlaid on 1/500K geological map of Türkiye Sağpazar-1 Borehole data are located on the map (Uğuz et al. 2002).

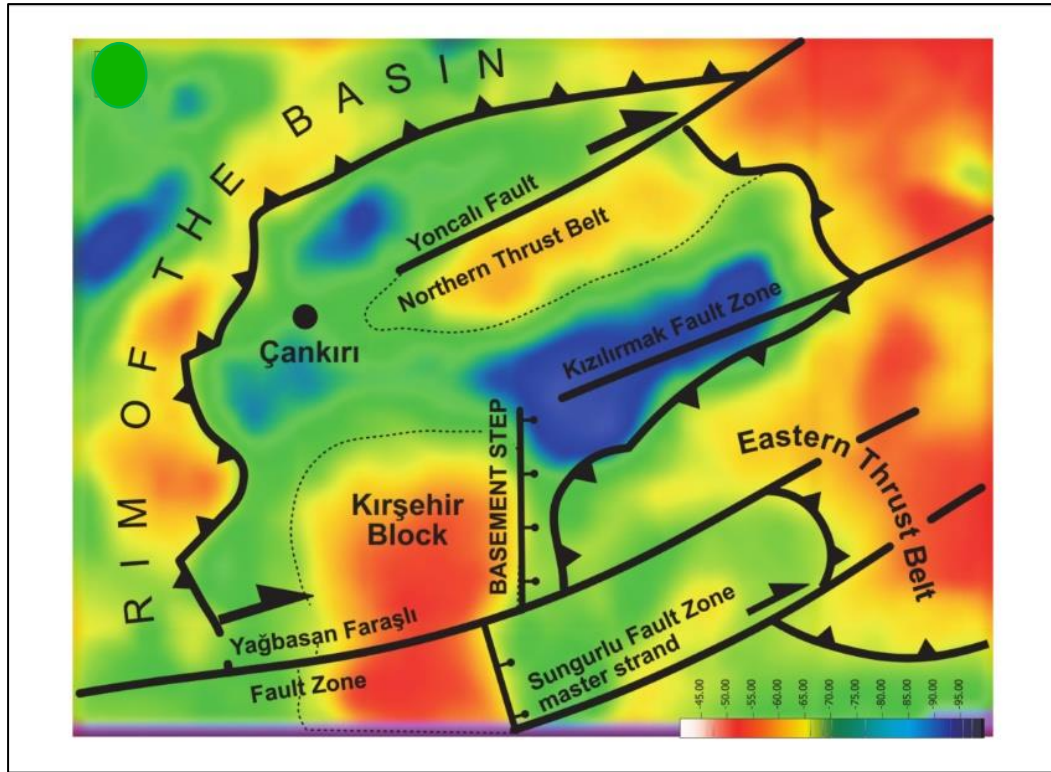


Figure 1. 16 Interpretation of gravity image of Çankırı basin (Kaymakçı et al. 2009).



## CHAPTER 2

### THE UNDERGROUND STORAGE

In this chapter, the underground storages are evaluated for their technical concerns to the cavern design.

#### 1.7. Background

Natural gas is known since ancient times, though it was not used commercially until recently. To reciprocate the increase in demand and consumption of natural gas worldwide necessitates its storage when demand is low to be used when the demand increases. Therefore, storing natural gas is one way of keeping the balance in seasonal changes.

The first underground storage was established in Canada in a partially depleted Ontario gas field, in 1915 (Muhammed et al. 2022). After that, the underground storage of natural gas has become a more interesting subject at the beginning of the 21st century. As the energy demand has increased globally, while the capacity of the gas reserves could not keep pace with the demand underground natural gas storage brought a solution to correspond to the gas demand by injection of the gas into the storage facilities by appropriate techniques.

Various types of storage measurements quantify the gas volume in the storage. Those storage measures are also effective to quantify the capacity of the facility which are; total gas, base gas (cushion gas), and working gas (deliverability) capacity. Those are variable and change over time. Total gas is equivalent to the volume of the storage which could be decided at the storage design step. Base or cushion gas is the volume that is maintained in the underground storage to provide the required pressure and keep the deliverability at optimum rates. Working gas is representing the circulation of the injection and withdrawal of the gas. Working gas or deliverability is the amount of gas in a daily process that can be extracted from

storage. (Kappa 2022). Working gas is the total amount of the injected gas that is to be withdrawn. The injection and withdrawal rate of the gas is belonging to the deliverability part of the process. The cushion gas guarantee to keep the safety and maintenance of the cavern that necessarily stays in the cavern under any circumstances (Muhammed et al. 2022). These volumetric properties are affected by the storage design parameters and demand different things. Cushion gas is affected by the depth due to the pressure, the relationship between cushion gas and depth is inversely related. While lower caverns desire less cushion gas, deeper caverns desire more cushion gas, which means the operational cost has directly affected the depth of the cavern (Lord, Kobos, & Borns 2014)(Zivar, Kumar, & Foroozesh 2021) (Muhammed et al. 2022).

Underground storages have to be under hydrocarbon geological conditions, such as cap rock to get safety and stability (Molíková et al. 2022). The depleted oil/gas fields are the most common among these methods due to not being necessary to build a storage cavern, create a pipeline connection, or drill a well to inject and withdraw, however, slow rate of injection and withdrawal rates are their main disadvantage. Aquifers are only preferred as a last choice due to their durability is weak to build a cavern due to their physical properties (EIA, 2016). As mentioned previously, there are three different types of storage, 1. depleted oil/gas fields, 2. aquifers, and 3. salt structures (Figure 2. 1). Each storage has its pros and cons, physical characteristics such as porosity and permeability, economic constraints as well as installation costs, rate of deliverability, and duration (life cycle) (EIA, 2015). As shown in Table 2. 1 the salt cavern working volume is smaller than other underground gas storage (UGS) facilities, though the injection rate and withdrawal rate are much higher, which results in relatively very quick injection and withdrawal periods. As a result, more than 660 UGS facilities exist in the entire world and 68 more storage projects are underway all of which provide 48bcm of working gas capacity.

Table 2. 1 Comparison of differences between UGS types (modified from EIA 2022)

	Depleted Fields	Aquifers	Salt Formations
Working volume	Medium to Large	Large	Small
Withdrawal Flow Rate	Medium	Medium	High
Injection Period	~200 days	~200 days	~ 30 days
Withdrawal Period	100 to 150 days	100 to 150 days	10 to 20 days
Development Duration	5 to 8 years	10 to 12 years	5 to 10 years

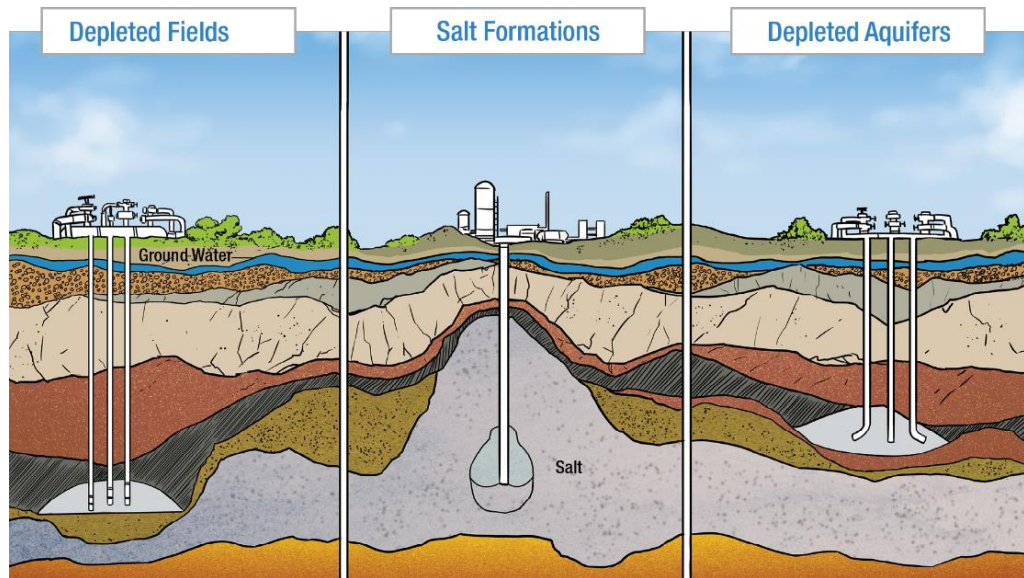


Figure 2. 1 Schematic illustration of underground storage types (API 2022)

### 1.8. The Underground Storage Background in Türkiye

The underground storage subject is one of the main issues in Türkiye over the last two decades due to increased energy demand, which is mostly based on imported

natural gas. So far, there are two facilities for underground storage, one is in Silivri (İstanbul), and the other one is in the Tuzgölü area (Botaş 2022).

a. **Silivri Facility:** This facility is installed by Botaş in 2007 and it provides the storage of natural gas transported to the depleted hydrocarbon wells in the Marmara region from the transmission network and has already reached a 2.8-billion m<sup>3</sup> storage capacity which is planned to increase to 4.6 billion m<sup>3</sup>.

b. **Tuzgölü Facility:** Turkey's national gas company Botaş has invested and started a UGS facility project in the Tuzgölü area in 2017. Botaş had been launched the facility after ensuring the 3D imaging of the salt body of the Tuzgölü Basin has been done by a 3D seismic survey. The project is kept as an ongoing project and step by step extends the capacity of the facility. It is located in Aksaray Province which is 40 km away from Tuzgölü and is centered what the necessities for an underground gas storage facility. Concerning the Botaş report (storage expansion project) the number of caverns is increasing step by step. The depth of caverns is not located at the same depth due to the subsurface geology and some technical necessities. The cavern is located 600-700 meters of starting depths within a 1500 m thick salt column. depth is between 1,100-1,450 m and the volume of the capacity is reported 630.000<sup>3</sup> -750.000m<sup>3</sup>.

Table 2.2 is containing the phases of the project. The 1<sup>st</sup> phase is completed with 12 caverns with 630.000 m<sup>3</sup> -750.000 m<sup>3</sup> volume capacity. The 2<sup>nd</sup> phase commenced with a 1 billion cubic meters (bcm) capacity and is planned to be increased to 5.4 billion cubic meters (bcm) by 2023. The planned salt caverns will have similar geometry to the existing caverns. By the end of the project, the facility will reach 60 caverns. The caverns have been produced by dissolving the salt using freshwater provided by the Hirfanlı Dam Lake (Figure 2. 2). The dissolved brines are discharged into the Tuzgölü area (Figure 2. 3). The storage facility is built nearby the energy transmission corridor. In other words, the storage facility is almost on the main route of the natural gas pipelines. It is located 23 km away from the Eastern Anatolia Natural Gas Main Transmission Line. Such as short distance provides high

punctuality in terms of withdrawing and injection periods to meet fluctuating energy demands.

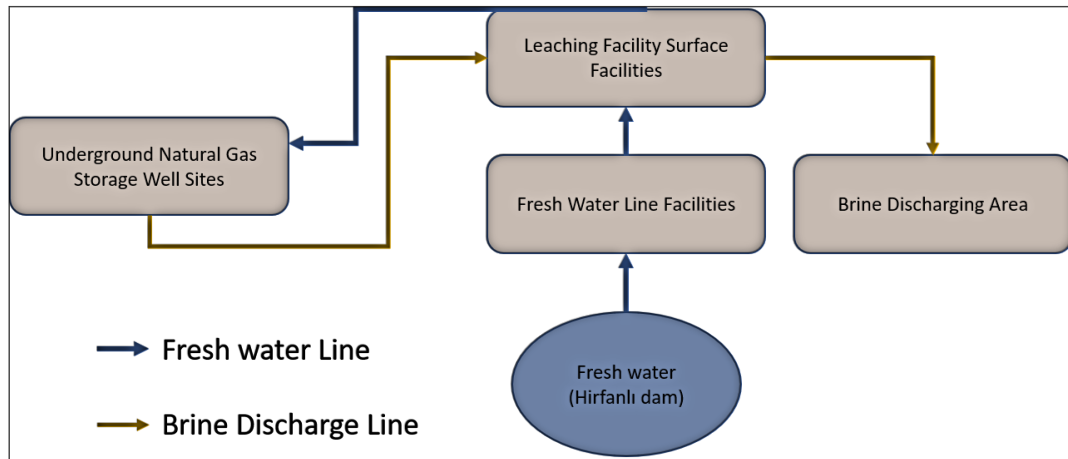


Figure 2. 2 Water Supply and discharge Planned Within the Scope of Gas Storage Expansion Project (Botaş 2022, WorldBank, n.d).

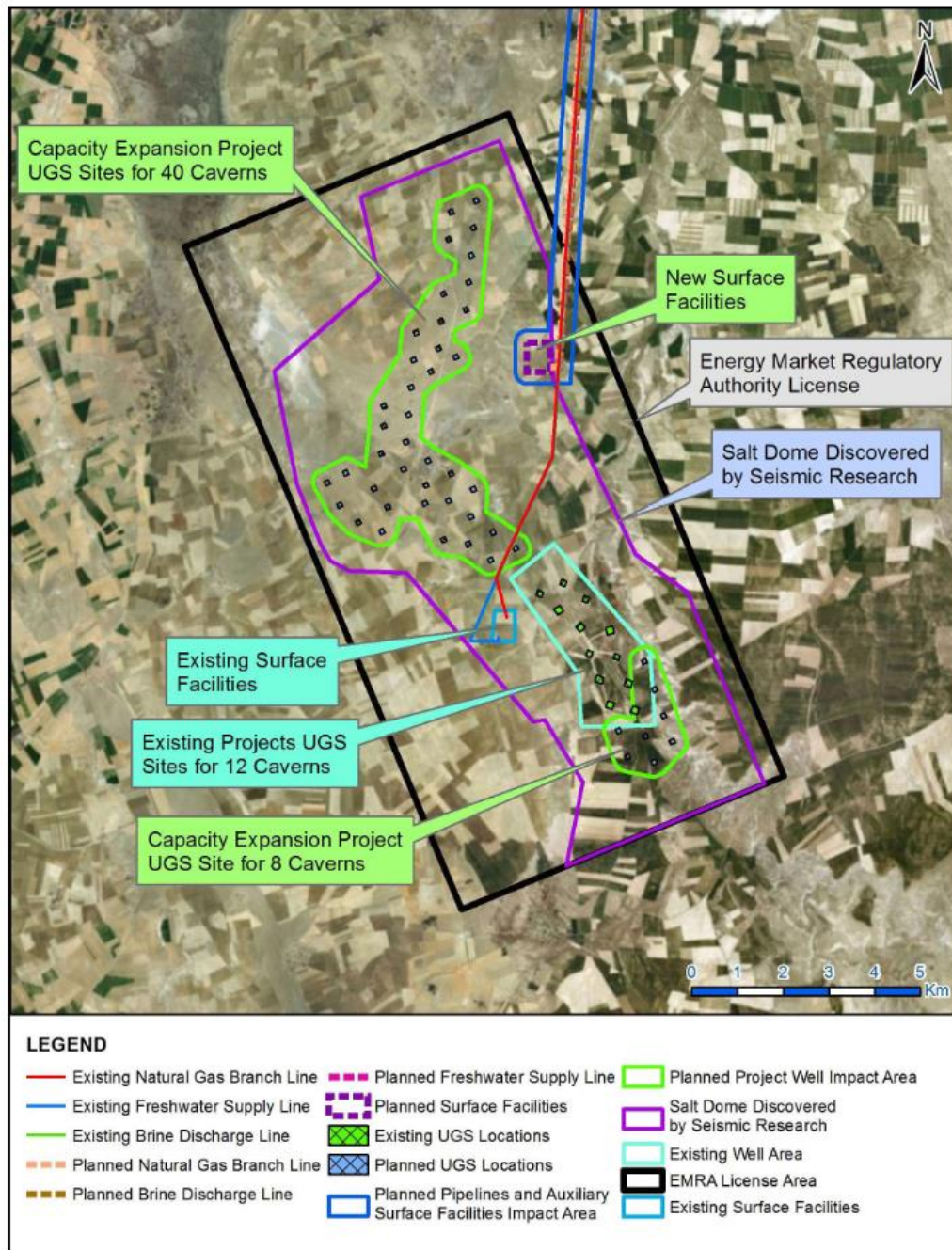


Figure 2. 3 Tuzgözü Underground Natural Gas Storage Project, and the facilities (Botaş 2017, WorldBank, n.d)

Table 2. 2 Information on the Tuzgözü Underground Natural Gas Storage Project Planned Capacity (Botas 2022)

Items	1 <sup>st</sup> Phase	2 <sup>nd</sup> Phase
Storage type	Salt formation/Salt Cavern	Salt formation/Salt Cavern
Depth of Entry Salt	500m -860m	500m -860m
Salt Dome depth	>1,500m(Drilling), 1500m-2000m (seismic)	>1,500m(Drilling), 1500m-2000m (seismic)
Number of UGS/Caverns	12 Caverns	48 Caverns
Cavern Volume	630,000 m <sup>3</sup>	630,000m <sup>3</sup> -750,000m <sup>3</sup>
Situation	Completed	Planning phase

### 1.9. The Fundamentals of the Cavern Design

The salt deposits request to have sufficient enough thickness of the cavern wall even if it designs as a single one but in general underground storages are designed with multiple caverns to get the ability of the long-term stability of salt deposits. So, the solution mining method in the salt deposits requires sufficient diameter and thickness to accommodate one or more solution-mined openings at substantial distances from the top, bottom, and sides of the formation (Allen, Doherty, & Thoms 1982b).

The other major requirements to be considered for solution mining include the water to be injected and the brine to be removed outside of the cavern. Water injection refers to pumping water into the salt structure. After finishing pumping the brine is withdrawn outside of the cavern. Every 7-8 m<sup>3</sup> fresh water could dissolve 1m<sup>3</sup> halite. The suitable depth of the salt is more than 400-500 m and shallower than 2,000m (Warren, 2016).

The fundamental parameters of designing require a few conditions that typically consist of physical effects (Heusermann, Rolfs, & Schmidt 2003). Bruno 2005 stated

that while the elastic deformation and thermal expansion behaviors could be determined by physical condition parameters and not expected to change everywhere, in contrast, the inelastic deformation, creep properties, and damage behaviors could be different and play an important role.

### **1.9.1. Site selection**

Successful development of a UGS must include an appropriate site selection based on subsurface information, suitable performance analysis based on geological, fluid dynamics, and geomechanically approaches, and eventually an adequate monitoring program (Verga, 2018).

### **1.9.2. Cavern shape and dimension**

The shape and dimension of the salt cavern directly reduce the negative effect of long-term usage of the storage and give a release on safety. The safety factor, volume shrinkage, overburden pressure, and plastic volume are the most effective parameters that should be considered while deciding the cavern shape. In the literature, there is no one-way solution through different media causing different problems which may lead to different solutions. (Wang, et al. 2013).

There are several types of cavern shapes, which are ellipsoidal, irregular, cylindrical, and cuboid respectively (Figure 2. 4). Ellipsoidal shape is much more reliable in terms of stability. The irregular shape of the cavern type is giving a good solution to the shallower structures, such as salt pillows and salt beds. The cylindrical shape and cuboid shape do not have good stability in terms of deformation (Liu et al. 2020).

While an ellipsoid shape cavern type seems much preferable due to it giving more stable characteristic behaviors when compared to the other shapes (Wang et. al. 2011). The ellipsoid model is much better based on long-term processing. Moreover,

some researchers have suggested a rectangular cavern type according to the corner radius and stability (Cristescu & Paraschiv, 1995) ( Wang et al. 2013).

The complex structure and the homogeneity of the subsurface are unordinary giving the challenge to design salt cavern types, so irregular type caverns are suggested no matter what type of salt structure is dealing with (Liu et al. 2020). The current solution mining methods are also not allowed to design a regular shape cavern due to the heterogeneity of the subsurface.

### **1.9.3. Geomechanical properties**

The geomechanical parameters supply the fundamental criteria to design a cavern to be sure the stability of the facility and increase the safety factors. These fundamentals consist of physical effects (pressure, temperature), stress, strength, and geological anomalies. Those are giving insurance for safety factors before, during, and after the cavern design is completed. (Heusermann, Rolfs, & Schmidt 2003).

Cavern depth, cavern geometry, the distance between caverns depending on the case of a cavern field, the distance of cavern to neighboring, geological, pressure regimes during a storage operation, and constitutive behaviors of the host rock (short and long term) are the most important parameters while constructing the cavern (Heusermann, Rolfs, & Schmidt 2003).

The salt cavern design is allowing reducing the stress risk by using the geomechanical characteristics of the salt and surrounding area. Stress/strain ratios are not important just for construction time, also important for production time. Geometrical parameters are including salt roof thickness (s), cavern roof depth (z), cavern height (h), cavern diameter (d), Pillar width (b), and distance to the edge of the salt dome (a) (Figure 2. 5).

The mechanical behaviors are observed by so many authors and approached to the if a constant mechanical stress load into the system the steady-state strain rate of the rock salt is approached to the point of a non-linear function of the applied stress, the

volume has not been changed and the system is sensitive to the temperature (Berest et al. 2013).

In general, the mechanical behavior of the salt which is affecting the deformation rate is influenced by thermal conditions and stress issues. The inside stress is determined by the overburden weight and the inside pressure is represented by the operating gas pressure (Onal, 2013). Stress-strain rate is controlled by three fundamental parameters, which are the elastic behaviors of salt, thermal expansion of salt, and salt creeps (Brouard, 1997). When the leaching process starts the pressure value is causing initial stress ( $P_v$ ) (Ozarslan, 2012). The pressure regime is the first consideration to avoid surface subsidence during the gas injection and withdrawal period (Susan, 2019). The internal gas pressure is the key factor in the safety and stability of the cavern. The priority for the underground gas storage is initial stress and the vertical component can be estimated for flat ground surface and deep salt deposit either; in MegaPascal (MPa) unit (Ozarslan, 2012).

$$P_v = 0,022 H \quad (1)$$

Here  $P_v$  is the vertical initial stress component and  $H$  is the starting depth of the cavern. The maximum pressure of the cavern is generally close to the vertical initial stress component (Ozarslan, 2012).

Susan 2019; stated that; cavern pressure is the most effective to protect the cavern in long-term stability to keep this in balance. In this case, the cavern pressure and lithostatic pressure have to be in balance, and cavern pressure couldn't exceed the lithostatic pressure. Also, the cavern pressure could affect the neighboring caverns and cause collapse. It could be kept in a safety zone with the pillow width. The sealing of the cavern is ensured by the thickness selection of the top of the cavern, which is measured by the salt top and cavern distance. To avoid surface subsidence, the cavern pressure has to keep in balance with the lithostatic pressure during the process.

The geological tightness and technical tightness are providing the sealing of the cavern and keep the cavern safe. The geological tightness must be thick enough against the storage pressure. The technical tightness is including the casing system. The geological tightness and technical tightness can provide optimum limitations by keeping the pressure rates in balance. The maximum cavern pressure  $P_{max}$  should be 10% lower than the minimum pressure value ( $\sigma_{min} \geq 1.1 P_{max}$ ). On the other side, the technical tightness could be at most 15% of the maximum pressure rate. Compressive stress  $\sigma_{xx} = 0,85 P_{max}$  (Susan, 2019).

The lithostatic pressure gradient is related to the density of the rock material and transmitted through the layers. The overburden pressure is equal to the total value of the lithostatic pressure and fluid pressure (Tiab & Donaldson, 2016). The total vertical stress gradient is compressive stress and equal to the lithostatic stress gradient  $S_v$ . Typical lithostatic pressure is around 23 Mpa, pore pressure is around 10 Mpa, and formalized as (Dnicolasespinoza, 2022);

$$\int_0^{S_v(z)} dS_v = \int_0^z \rho_{bulk}(z) g dz \quad (2)$$

$$S_v(z) = \rho_{bulk} g z \quad (3)$$

$$P_p = \rho_w g z \quad (4)$$

Here;  $s_v$  is the total stress,  $\rho_{bulk}(z) g$  is the lithostatic stress gradient,  $z$  is the depth,  $g$  is the gravitational acceleration, and  $P_p$  pore pressure, respectively. The effective vertical stress ( $\sigma_v$ ) is the difference between total stress ( $s_v$ ) and pore pressure ( $P_p$ ) and can be estimated with a given depth:

$$\sigma_v = S_v - P_p \quad (5)$$

Table 2. 3 is generated by Düzyol (2004) to summarize the mechanical properties of rock salt around the world based on the laboratory test results.

Table 2. 3 Mechanical parameters values of the rock salt around the world (Düzyol, 2004)

Location	Density	Elastic module $\hat{\epsilon}$ (GPa)	Rigidity rate G(GPa)	Poison Rate $\nu$	Compressive Strength $\sigma_c$ (MPa)	Tensile Strength $\sigma_t$ (MPa)
Germany	-	31	-	0,23	-	0,5-3,5
Russian	-	-	-	-	35,4	1,56
France	-	16	-	0,2	-	2
Türkiye	2,18	0,14	-	-	28,3	1,96

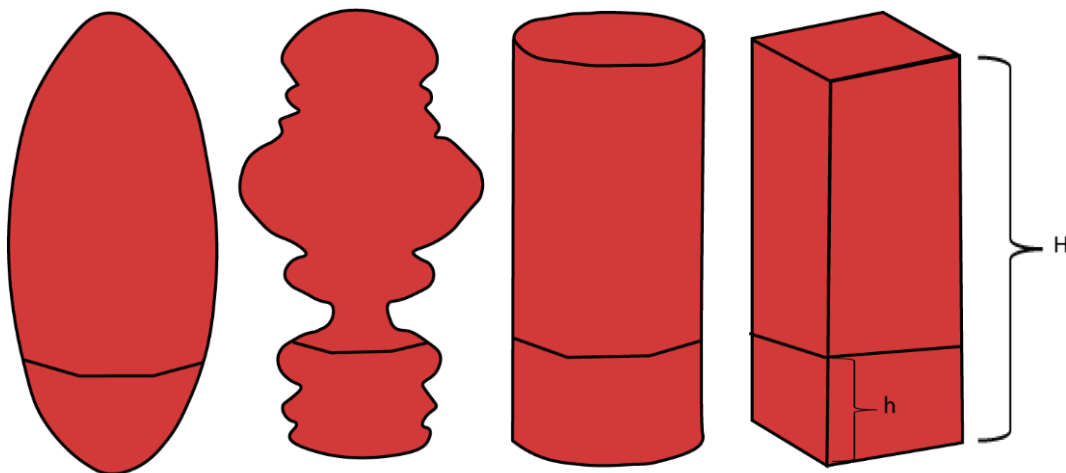


Figure 2. 4 Four different shapes of salt caverns: ellipsoid-shape, irregular-shape, cylinder-shape, and cuboid-shape (h is for the effective volume of the cavern, which is called base gas, upper-part stands for the sediments in the bottom of the cavern (modified from Liu 2020)).



#### 1.9.4. Salt creep

When the salt rock is subject to stress under pressure at a certain depth behaves like a visco-plastic material and tendency to creep (H. Wang et al. 2017).

Figure 2. 6 represents the typical creep test results that consist of two or three stages; transient, steady-state, and accelerative respectively. Transient and steady-state creep phases are following each other starting from the high-rate strain rate and, becoming normalized and stabilized. When the temperature and differential stress add to the system accelerative creep phase is occurring. This third creep stage is known also as the tertiary creep stage and governs the failure of the specimen (H. Wang et al. 2017).

Rock salts are affecting long-term non-linear creep deformation due to the subsurface overburden. Salt creep occurs in the range of 20–200°C temperature and as low as 0.2 MPa stress for long-term and short-term periods. (Kumar, 2021)

Several fundamental properties that are effective on salt creep are overburden pressure, internal pressure, salt type, cavern shape, cavern depth, and geothermal gradient. The salt cavern stability is effective between hundred meters and thousand meters depth which changed into an unstable form below a thousand-meter depth, which is at the elastic-plastic transition zone. The internal cavern pressures are not sufficient at this point and salt behaves unstable. This instability is causing subsidence and salt creeping so cavern size squeezing (Warren, 2006) (Figure 2. 7). There is a good salt creep example, which is seen in the Eminence cavern in Mississippi that occurred by shrinking of the cavern built at 1700 - 2000 m depth. This means 40% of the cavern volume loss (Warren, 2006). Salt creep occurs by the lithostatic pressure and cavern pressure differences (Warren, 2006) (Susan, 2019) (Li et al. 2021). To reduce the rate of the salt creep cavern pressure should be kept at high values to gain against the lithospheric pressure (Warren, 2006).

The creep rate of the rock salt under different circumstances during the operation a valid creep deformation model needs to be proposed to avoid possible damages (H.

Wang et al. 2017). Rock salt creep behavior occurs anytime even under small stress and is measured by this equation (Ozarslan, 2012);

$$\dot{\epsilon}_{ss} = A \exp (-Q/RT) \sigma^n \quad (6)$$

Function (6) is also known as Norton-Hoff law. Here, A is the creep material model that depends on the stress. Q is the energy of activation and is determined by the serial laboratory test with constant stress, and different temperature levels. Exponent n is the serial laboratory creep test at various stress with a constant temperature. R is the universal gas constant. T is the rock temperature at a certain depth. A steady-state creep strain rate is symbolized by  $\dot{\epsilon}_{ss}$ .

Generally, typical values are given during the tests, as constant for the components of n and Q/R, which are in the range of 3 to 6 and from 3,000 to 10,000 K, respectively. The steady-state strain rate ( $\dot{\epsilon}$ )<sub>ss</sub> is about  $10^{-10} \text{ s}^{-1}$  when given a 10 MPa for deviatoric stress ( $\sigma$ ) and 300 K for temperature (T) in the function. This rate is not representing the real world which is assumed as slower when compared with most laboratory tests, in which applied stress is larger than 10 MPa (Berest, et. al. 2013).

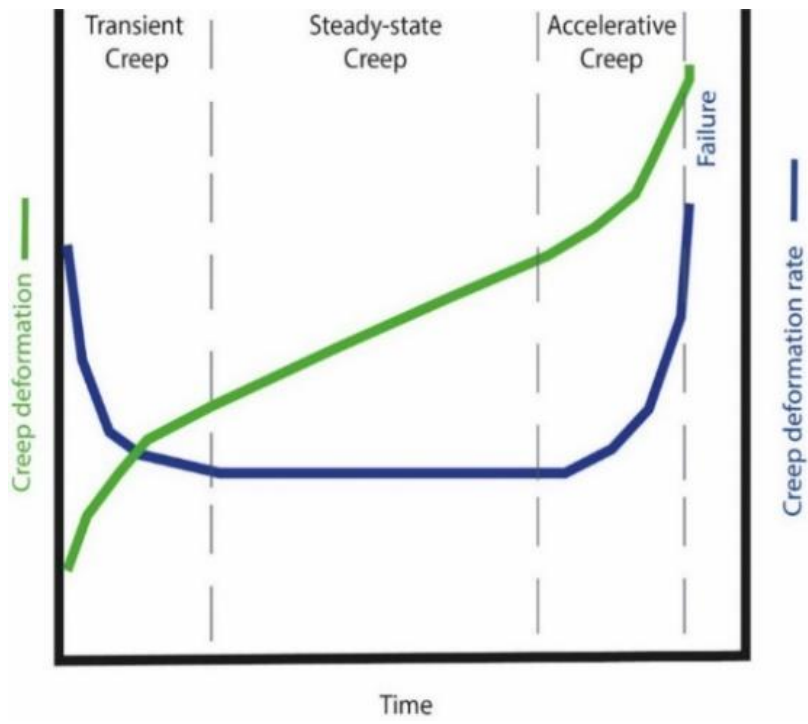


Figure 2. 6 Typical creep test result (Modified from H. Wang et al. 2017)

The Norton-Hoff law is a generalized formulation of;

$$d \varepsilon_{ij}^{SS} / dt = 3(A \exp (-Q/RT) \sigma^n) (J_2)^{(n-1)/2} S_{ij} / 2 \quad (7)$$

Here, the first invariant is  $S_{ij}$ , and formulize

$$S_{ij} = \sigma_{ij} - \sigma_{kk} \delta_{ij} \quad (8)$$

The second invariant is  $J_2$  is a deviatoric stress sensor that formulizes;

$$J_2 = S_{ij} S_{ji} / 2 \quad (9)$$

For an idealized cavern subjected to a constant pressure of geostatic lithospheric pressure of  $\rho_{lith}$  and cavern pressure  $\rho_c$ , the steady-state creep rate and second invariant formalized;

$$\sqrt{3J_2} = 3(\rho_{lith} - \rho_c) (a/r)^{3/n} / 2n \quad (10)$$

Here  $r$  is the distance to the cavern center and  $a$  is the radius of the cavern. In a conclusion, cavern tests are extrapolated in a stress range (Berest et al. 2012).

### 1.9.5. Surface Subsidence

Surface subsidence is a complicated procedure that occurs in dimensions of time and space (Han, Hu, and Zou 2020). Surface subsidence is happening during the construction period or injection period to the internal gas pressure limitation. To protect the cavern's stability the minimum gas pressure is ultimately kept in the

storage to avoid surface subsidence and volume shrinkage of the cavern (Li et al. 2021,) (Hardy, 1982) (Onal, 2013).

During the injection /withdrawal period, overburden would govern subsidence of the surface as a bowl shape or a depression (Figure 2. 7) (Warren, 2006). This could be more common in shallower storages than in deeper storages (Zhang et al. 2021). Surface subsidence is influenced by the depth, thickness, overburden pressure, leaching method, and most importantly the injection /withdrawal rate (Neal, 1991) (Warren, 2006).

Surface subsidence is a complex process and several methods are existing to prevent the storage from such damage by prediction. In generalized surface subsidence function is given (Susan, 2019);

$$S(x, y, t) = a f(x, y) V_k(t) \quad (11)$$

S is representing the subsidence in a certain time (t) at the x, y locations, a is the subsidence amount of the cavern volume of each cubic meter, the f(x, y) determines the shape of the subsidence bowl, and  $V_k$  is the volume convergence function in time (Susan, 2019).

Volume convergence can be estimated by the equation;

$$V_k(t) = V_p(t-1/k (1-\exp(-k.t))) \quad (12)$$

Here,  $V_p$  describes the rate of production, t is the time (day), and k convergence rate of the volume.

$$k = \sqrt{3} \left( \frac{\sqrt{3}(\rho_{litho} - \rho_i)^n}{n\rho^*} \right) . A. \exp\left(-\frac{Q}{RT}\right) \quad (13)$$

Here,  $\rho_{litho}$  represents the lithostatic pressure, while  $\rho_i$  represents the internal pressure with the exponential of n.  $\rho^*$  is the reference stress. Salt creep is represented

by A, Q is the activation energy, R is the universal gas constant, and T is the temperature (Susan, 2019).

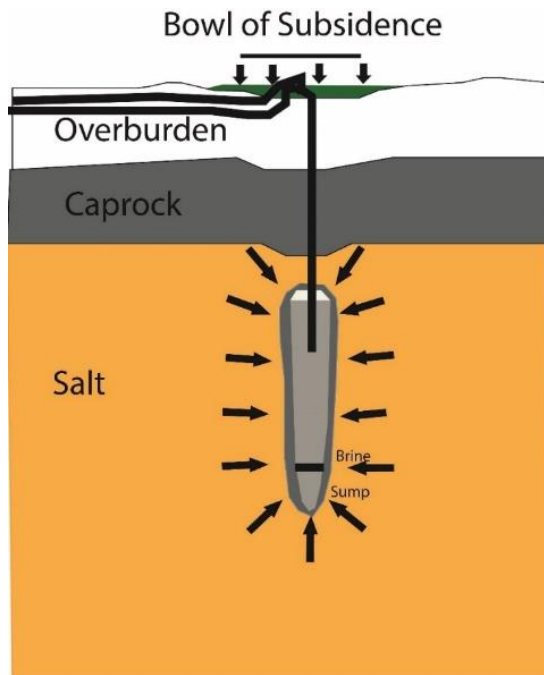


Figure 2. 7 Simplified diagram showing salt creep and surface of subsidence is affecting the cavern to shrink and getting more squeeze from the original size of the cavern (Modified after Warren, 2006)

#### 1.9.6. Thermal Conditions

If the rock salt material is pure halite, the leaching period is endothermic. In contrast, if the rock salt is involving anhydrite, gypsum, or calcium sulfate the leaching becomes less endothermic (Brouard, Bérest, & Couteau,1997), (Onal,2013). During the salt leaching period, the rock mass around the salt became cooler and caused a creep. During the solution mining period, the water is injected into the cavern and dissolved salt, which is brine withdrawn and this is causing temperature changes at a certain depth (Berest, 2001).

Salt dissolution is an endothermic activity and during the operation, heat transformation occurs between the surrounding rock and cavern turning into a cooler

when the leaching is completed. The injected cold water became a warmer brine (Bérest, Brouard, & Hévin, 2010) (Onal, 2013) (Jeannin, Myagkiy, & Vuddamalay 2022). The heat transfer is slower in a cavern though the temperature is changing faster due to the rapid injection and withdrawal are adiabatic(Bérest, 2019). The thermal exchange is not the most important parameter due to the slowness of the exchange processing. This is the first assumption from the beginning of salt leaching. The differences between the brine and fresh water are increased when the cavern is enlarged, for example, the brine water is 8 times bigger than water at the depth of 1000 m. On the other hand, thermal exchange between rock salt and the well tube is negligible when compared with fresh cold water and brine warm water (Brouard et al. 1997). The temperature can be estimated at the depth (Susan, 2019);

$$T= 290 + 0.023. H \quad (14)$$

Here, T is the temperature in Kelvin (K), and H is the depth of the cavern.

## CHAPTER 3

### RESULTS OF THE STUDY

This chapter involves the seismic data interpretation of the Tuzgölü Basin and the Çankırı Basin, as well as the 3D salt volume of the Tuzgölü Basin and the Çankırı Basin, and cavern design results.

#### 1.10. The Seismic Data Interpretation

The seismic data sets are in 2D at both study sites. Through the time-depth conversion method, the depth information is derived from the seismic velocity, generated during the processing of seismic data. They are correlated with the borehole data to interpret the formation tops. The top of the salt depth and the bottom of the salt depth in the seismic profiles were derived also from this correlation. The simplified cross-sections represent a summary of tectonic movement and sediment accumulation in the specific direction of the area. Their appearance does not aim at generalizing the geological circumstances of the regions.

##### 1.10.1. Tuzgölü Basin Interpretation

The Tuzgölü Basin seismic profiles are located in a certain area in the southern part of the basin. The interpretation of the Tuzgölü Basin began with a reference line close to the Bezirci-1 borehole, which was drilled by the TPAO firm in 1977. This study specified this borehole as a main well (Figure 1. 10). It was related to the adjacent seismic lines by utilizing the time–velocity relationship of the seismic sections. Bezirci-1 borehole has identified the presence of salt at a depth of 1,332 meters with a thickness of 1,270 meters (Figure 1. 10). The salt top was detectable on the reference seismic section at 900 ms and a depth of 1,305meters in the seismic

profile which is depicted in Figure 3. 1 and Figure 3. 2. Additionally, the depth of the salt bottom corresponds to 2,600 meters and 1,600 ms at accordance with time-depth conversion. The thickness of the salt is close to 1,300 meters thick. On the seismic sections, the Oligocene-Miocene Mezgit Formation and the Pliocene Cihanbeyli Formation were interpreted as a seal atop the salt layer (Table 3. 2).

In Figure 3. 3, NNW-SSE oriented seismic profile displayed with the residual gravity graph to mark the negative anomaly in gravity values is apparent. The gravity values show a negative anomaly that corresponds to the salt boundary. Here, the salt boundary was marked by the blue dashed line to correlate with the residual gravity graph and seismic profile (Figure 3. 4)

In Figure 3. 5 and Figure 3. 6, the seismic profile is depicted in its original and interpreted form. This seismic profile is located in the southeastern part of the study region. It was interpreted that the layering of salt is shaped like a diapir along this profile.

The seismic profile illustrated in Figure 3. 6 is inspired to generate a simplified cross-section (Figure 3. 7b). The interpreted seismic profile was displayed over the cross-section outlook by utilizing a diaphanous blue box to point out the cross-section-created area as shown in Figure 3. 7a). This simplified cross-section illustrates the salt in a diapir shape, with the Oligocene strata significantly pinched out in the survey area from north to south on the seismic profiles. The strata from the Oligocene-Miocene period cover the Paleocene strata. The salt layer extends to a depth of around 1,120 meters and is approximately 1,000 meters wide in the simplified cross-section, which is depicted in Figure 3. 7b. Moreover, the salt body is becoming wider towards the south. As a consequence of the salt analysis, the formation of the salt is finalizing in the stratigraphy of the Paleocene in the simplified cross-section. The salt concentration is divergent across the seismic profiles, which are two-dimensional and stretched out in different ways. Consequently, the range of the salt top is revealed between 800 meters and 1,400 meters in the seismic profiles.

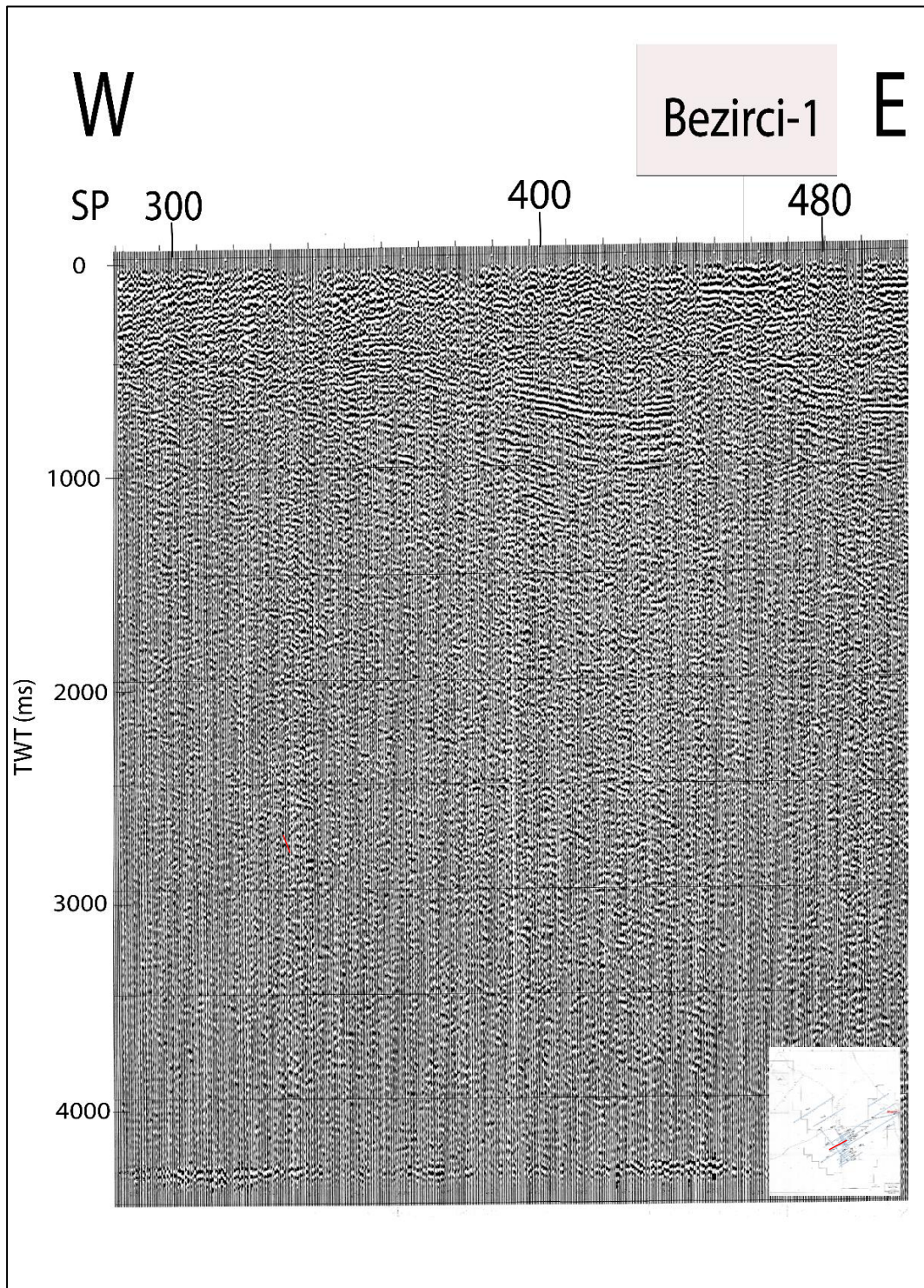


Figure 3. 1 The original TG7-ext line.

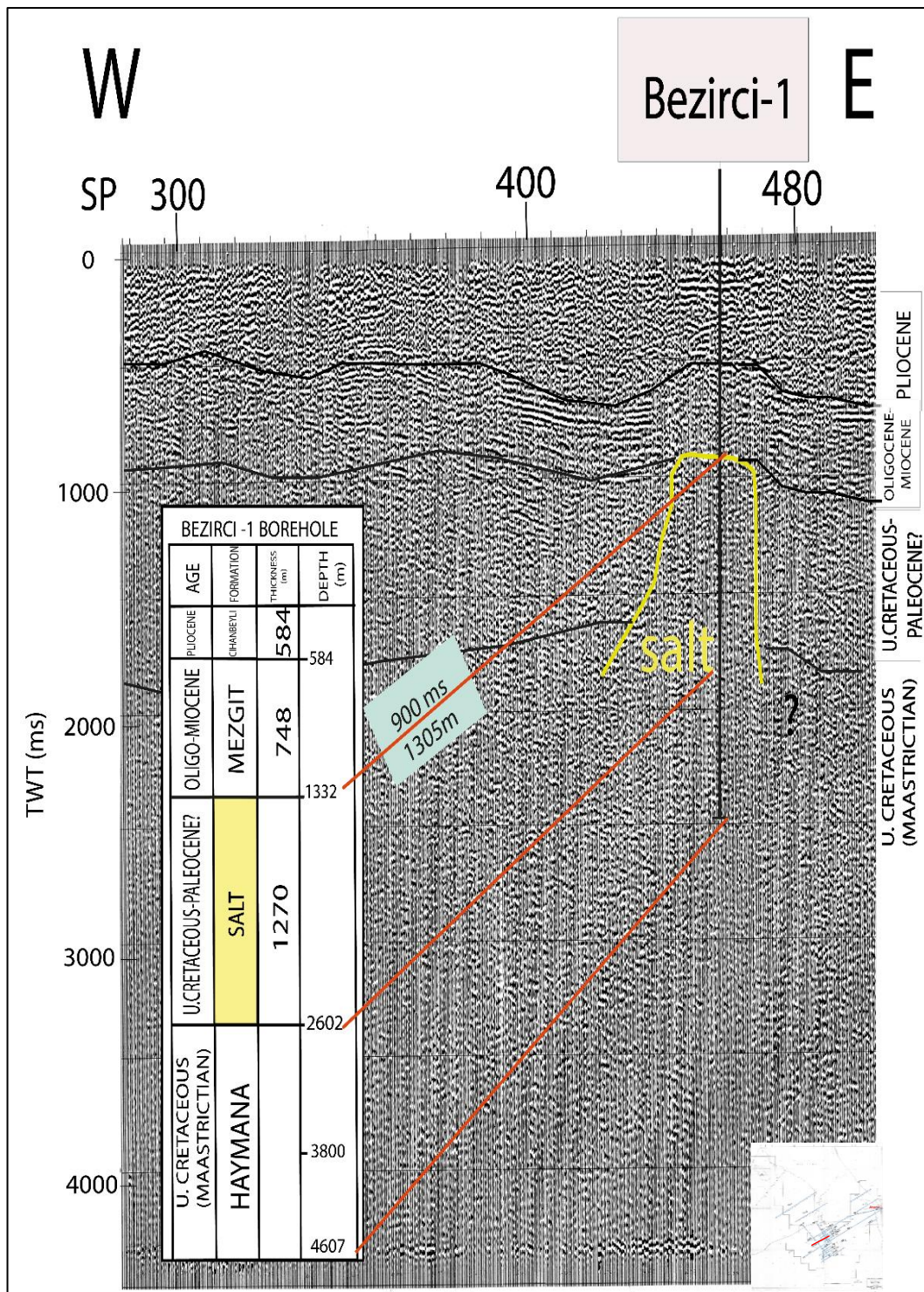


Figure 3. 2 The interpreted TG7 ext. line involves the time depth conversion and the salt structure depicted in a yellow color salt view drawn on the defined seismic

profile. The Bezirci-1 borehole has been placed above the seismic section to identify the roof of the salt formation. (Shot point interval:50m)

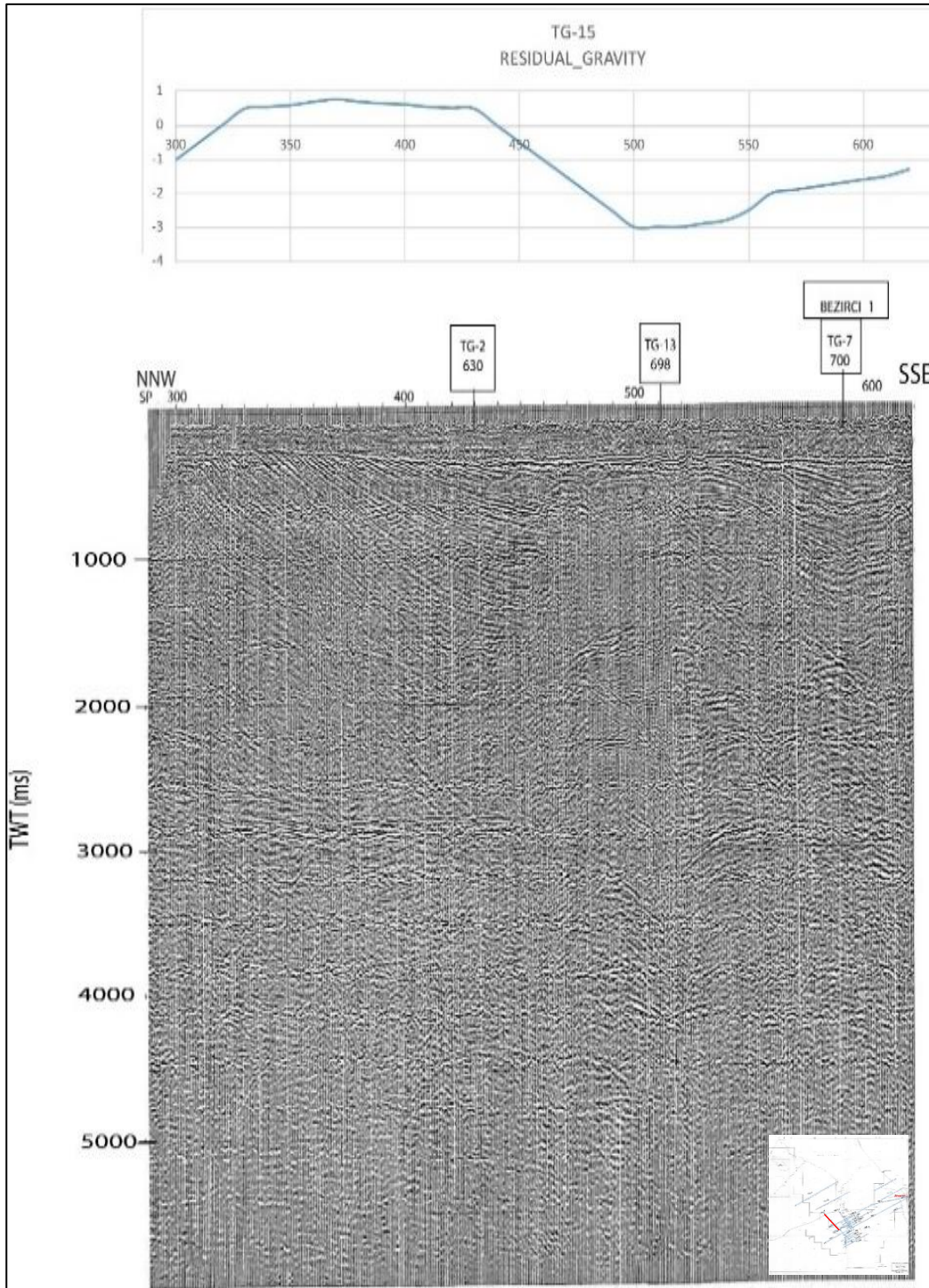


Figure 3. 3 The original TG15 seismic profile.



unmigrated seismic section. The diffractions are remarked by red color. (Shot point interval:50m)

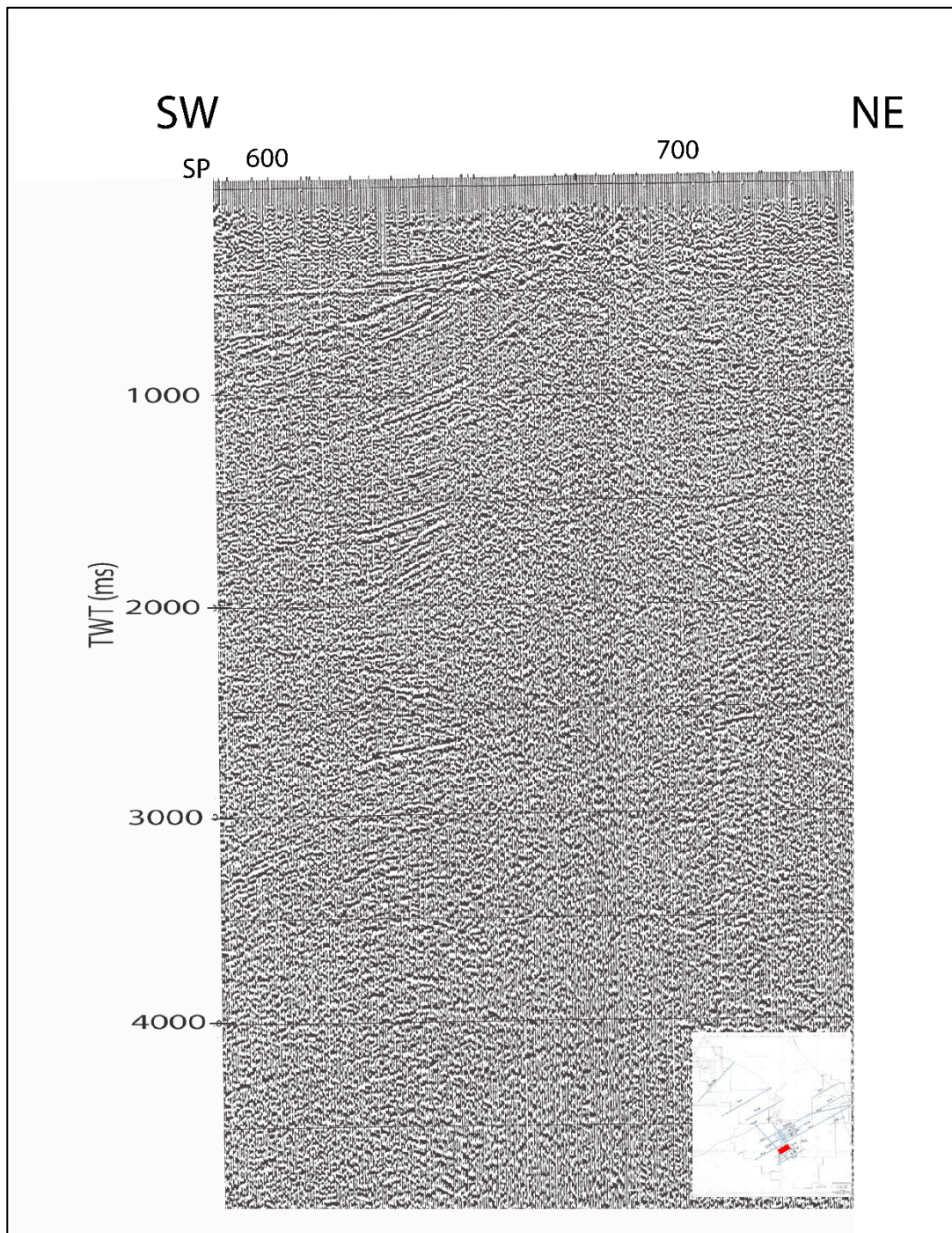


Figure 3. 5 The original view of the south-eastern seismic profile. (Shot point interval:50m)

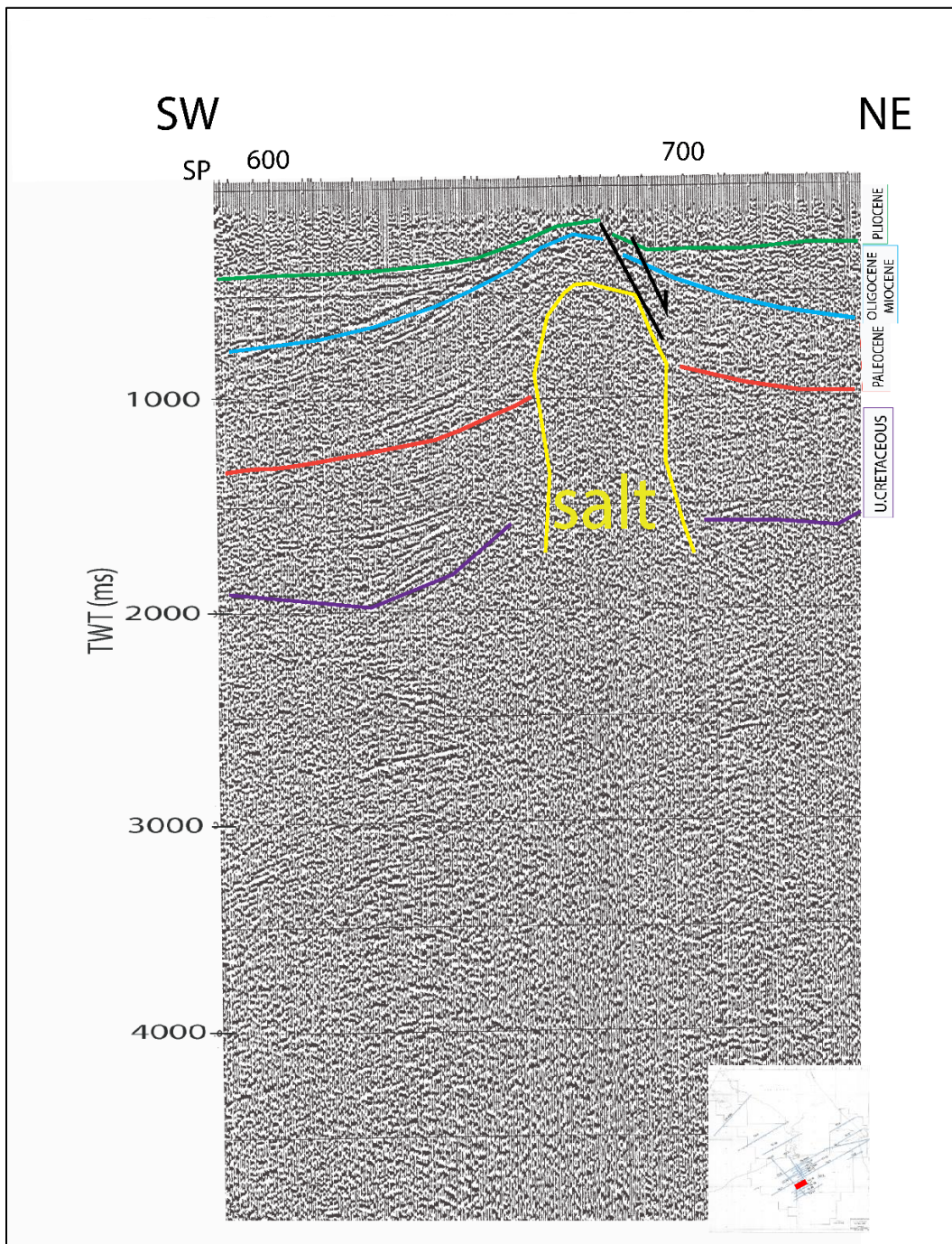


Figure 3. 6 The interpreted version of the south-eastern seismic profile. (Shot point interval:50m)

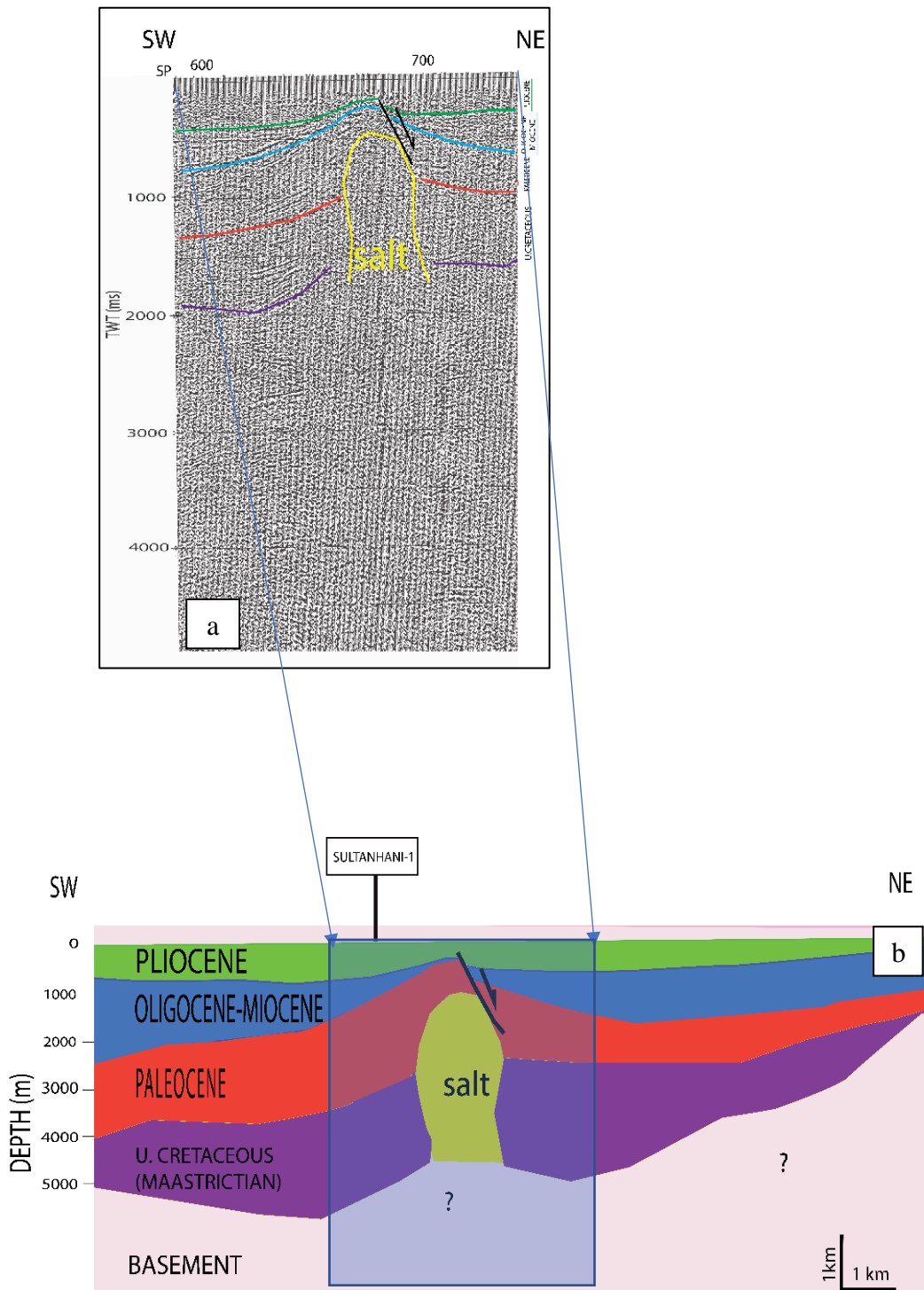


Figure 3. 7 The interpreted reference seismic profile TG24 (Figure 3. 6) (a) and a simplified cross-section along the Sultanhanı-1 well (b) that is generated via (a).

### 1.10.2. Çankırı Basin Interpretation

Analyzing the Çankırı Basin is commencing with a reference line, where is crossing over the Sağpazar-1, drilled by the TPAO firm in 1996, which is the main well used in this study (Figure 1. 12).

Utilizing the gravity image in Figure 1. 16, a low gravity area was identified in the northeastern section. The gravity image used to delineate the rim of the basin, the Kırşehir block, and thrust belts with positive anomaly values (50-55 mGal) in contrast to the negative anomaly values concerning the possible salt structure area ( $75\text{mGal}$ <).

The seismic profile presented in Figure 3. 8 and Figure 3. 9 are the original version as well as the interpreted version, respectively. The Sağpazarı-1 borehole is situated above this seismic section. Utilizing the time depth conversion, the depth of the salt deposit was derived which intersects the Sağpazar-1 borehole. The depicted salt structure was highlighted with yellow coloration on the seismic profile, from a starting point of 820 milliseconds, which corresponds to a depth of 1,450 meters (Figure 3. 9). It was determined that the Bayındır Formation has a thickness of 451 meters of sediment accumulation. The thickness of the Late Eocene-Oligocene Incik Formation is 1,000 meters and covers all around the salt structure as a cap rock. The width of the salt top is calculated at 550 meters at the 1,450 meters depth using the shot points provided on the seismic profile (Figure 3. 9).

The image in Figure 3. 10 is a cross-section of the parallel seismic profiles located in the northeast region of the basin. Those seismic profiles are oriented perpendicular to the reference seismic profile.

According to the salt interpretation, its size is progressively becoming smaller and more compressed in the northern region (Figure 3. 10). The salt structure is wider and shallower on the seismic profile B (Figure 3. 10), while the seismic profile A (Figure 3. 10) reveals the salt structure is narrow and plump as a result of the normal

fault compression. The distance between parallel seismic profiles is 2,5 km, and the salt structure changes rapidly, as a result of the salt surface being irregular.

An assessment of the seismic profile presented in Figure 3. 9 was conducted to create a simplified cross-sectional view in Figure 3.11b by correlating together the depths from the borehole. This cross-section view is summarized the tectonic movements and sediment deposition that surround the salt structure (Figure 3.11b).

The interpreted seismic profile was depicted above the cross-section image, showing the inspired area while drawing the cross-section as the transparent blue box in Figure 3.11a. The correlation of Sağpazar-1 (TPAO, 1996) borehole and seismic data points to the conclusion that a salt structure exists in the Late Eocene-Oligocene strata. In the simplified section, normal and reverse fault motion and compressional deformation occurring in the Early Eocene - Middle Oligocene are observed at the top of the salt structure. The Bayındır Formation and İncik Formation are placed above the salt body. On the right edge of the cross-section, a normal fault is directed to the northeastern part and had been active in the sediment deposition from the Late Eocene to the Oligocene. Along with this, the seismic profiles showed the depth of the salt layer to range from 800 to 1,500 meters. In the presented cross-section, the closure regime is delineated by the presence of normal and reverse faults. Analysis of this study has also revealed that the Çankırı Basin's salt structure has a distinct dome shape (Figure 3.11b).

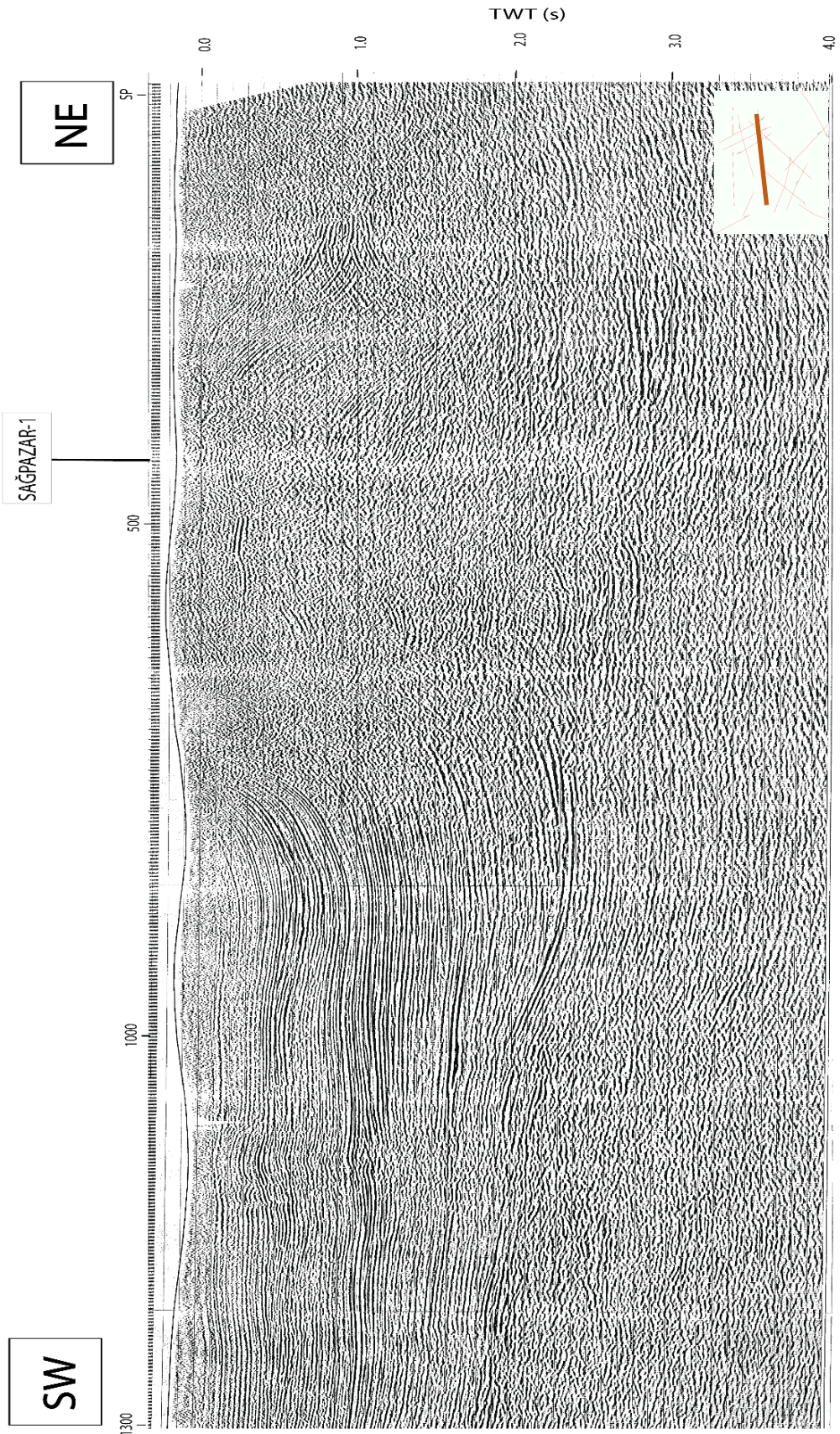


Figure 3. 8 Display of the original section of the COV95306.

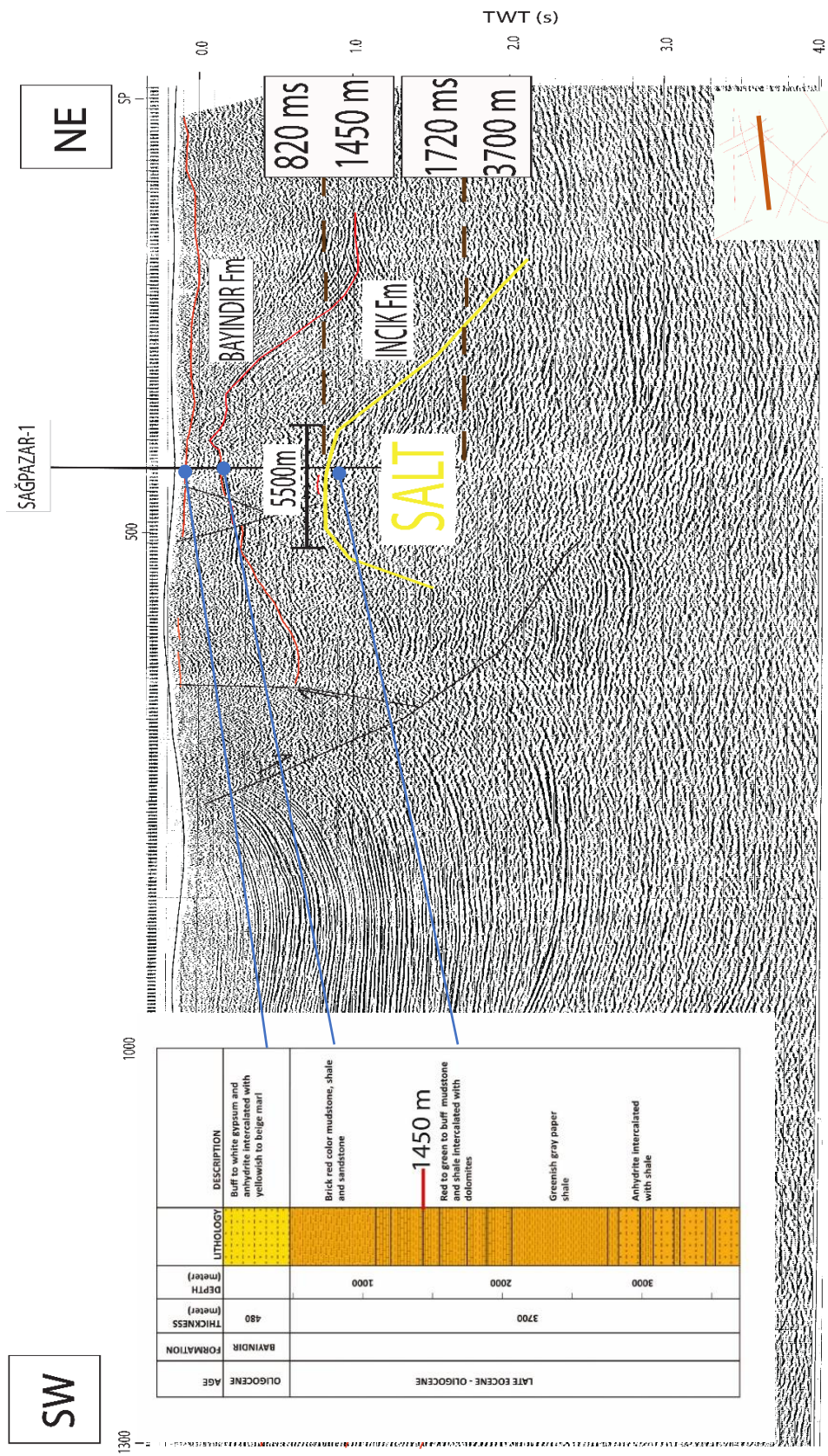


Figure 3. 9 Display of the interpreted section of the COV95306 that is correlated with Sağpazar-1 based on the salt top.

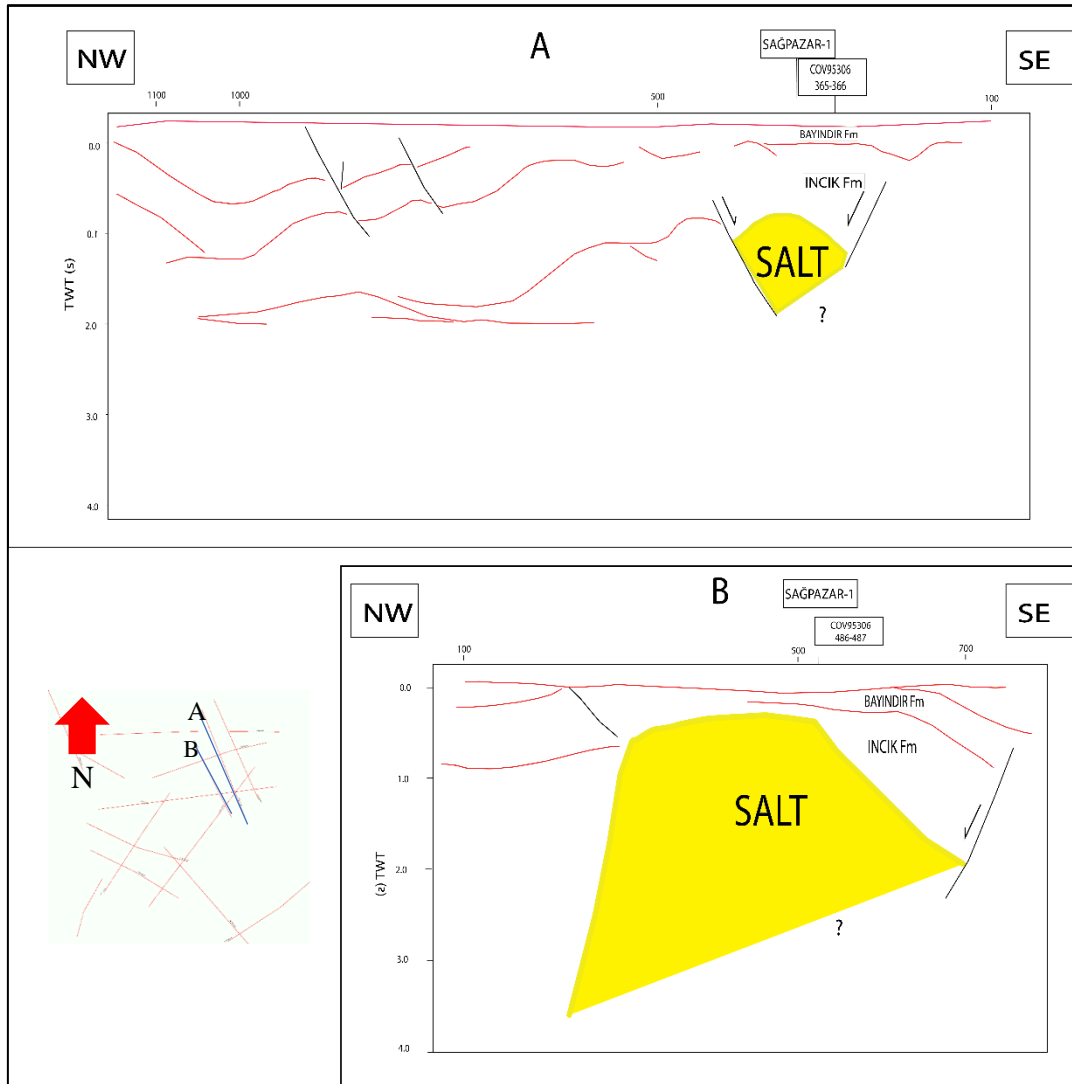


Figure 3. 10 Cross-section view of the parallel seismic profiles A and B from the Çankırı Basin.

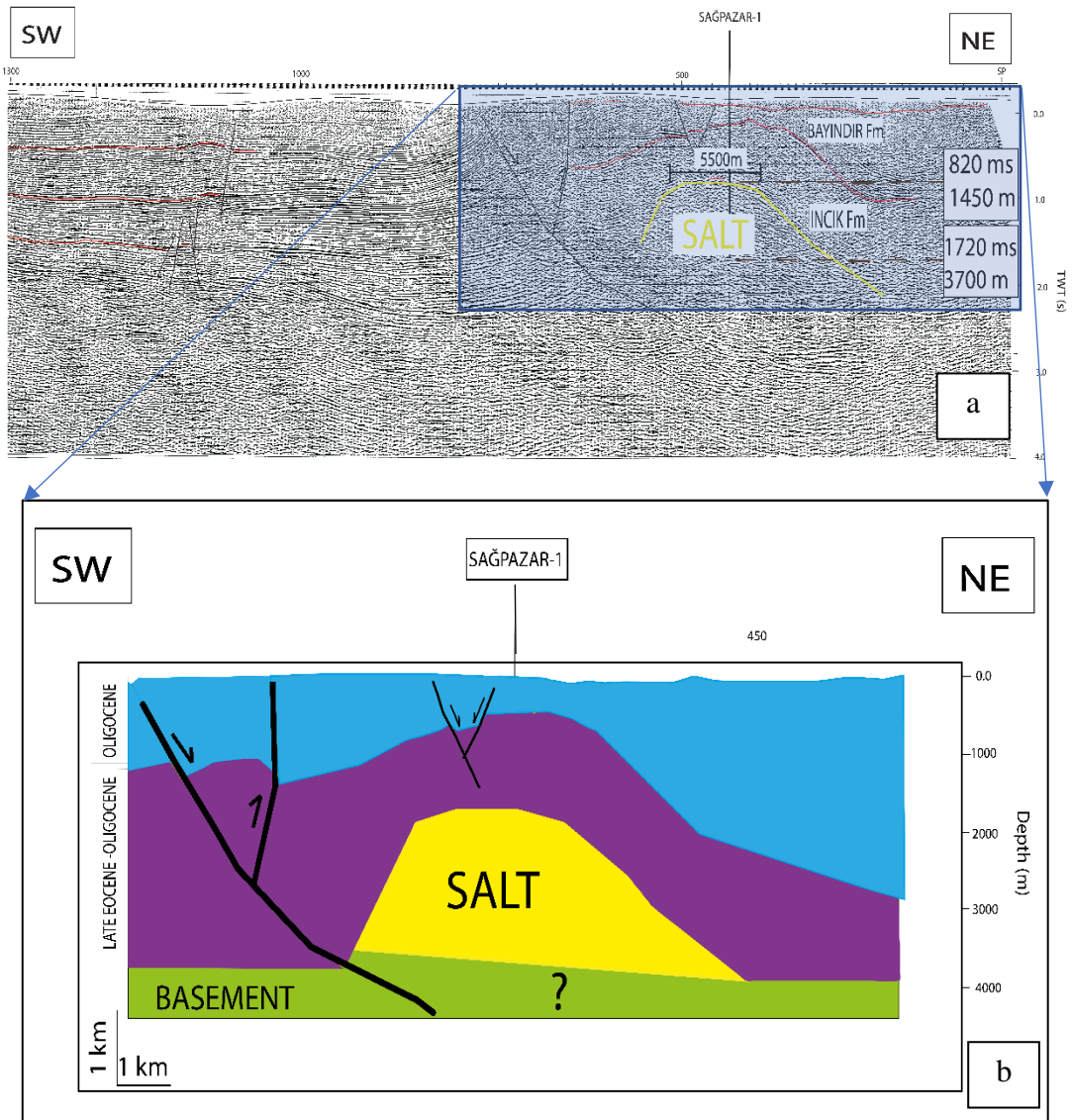


Figure 3.11 The interpreted reference seismic profile COV95306 (Figure 3. 9) (a) and a simplified cross-section (b) along the Sağpazar-1 well that is generated via (a).

## 1.11. 3D Salt Volume

### 1.11.1. Tuzgölü Basin 3D Volume

The majority of the salt body's 3D solid volume of the Tuzgölü Basin is depicted through the various salt diapirs running through the NNW-SSE direction (Figure 3. 12) and covering a 96 km<sup>2</sup> area.

The variant of the mass thickness of salt depth in the top and bottom portions of the 3D volume is notable (Figure 3. 13). The salt top range is between 800 meters and 1,650 meters. The bottom of the salt is between 3,500 meters and 4,500 meters range. In other words, the bulk thickness of the salt changes along the study area with the range of 2,700-2,850 meters. Therefore, its overall size is calculated as 219.03 bcm (Table 3. 1). Additionally, the salt begins at 1,305 meters and finishes at 3,455 meters on the top of the Bezirci-1 borehole location which is represented in the 3D volume of this study. The view of the 3D volume of salt consists of four pieces they also point out the diapir structures and the bulk depth thickness with displaying depth in the z domain (Figure 3. 13).

Table 3. 1 The Tuzgölü Basin's Salt body information

	Min	Max
Salt Top	800m	1650m
Salt Bottom	3500m	4500m
The Bulk Thickness of Salt	2700m	2850m

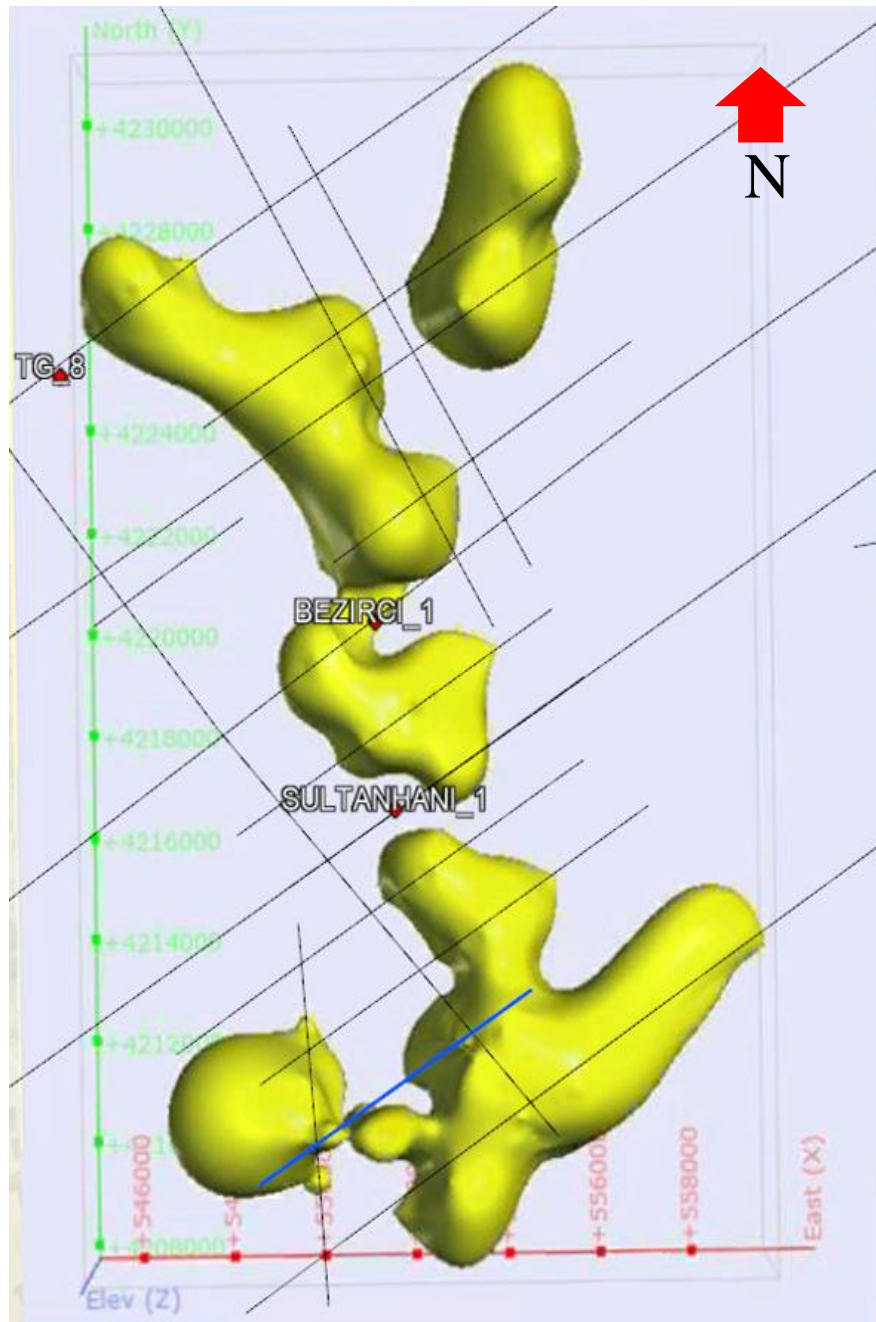


Figure 3. 12. Seismic profiles, Bezirci-1 borehole, Sultanhanı-1 borehole, and top view of salt bodies in the Tuzgözü Basin. Three pieces of the salt body are seen clearly on the base map. (Generated by Leapfrog Geo).

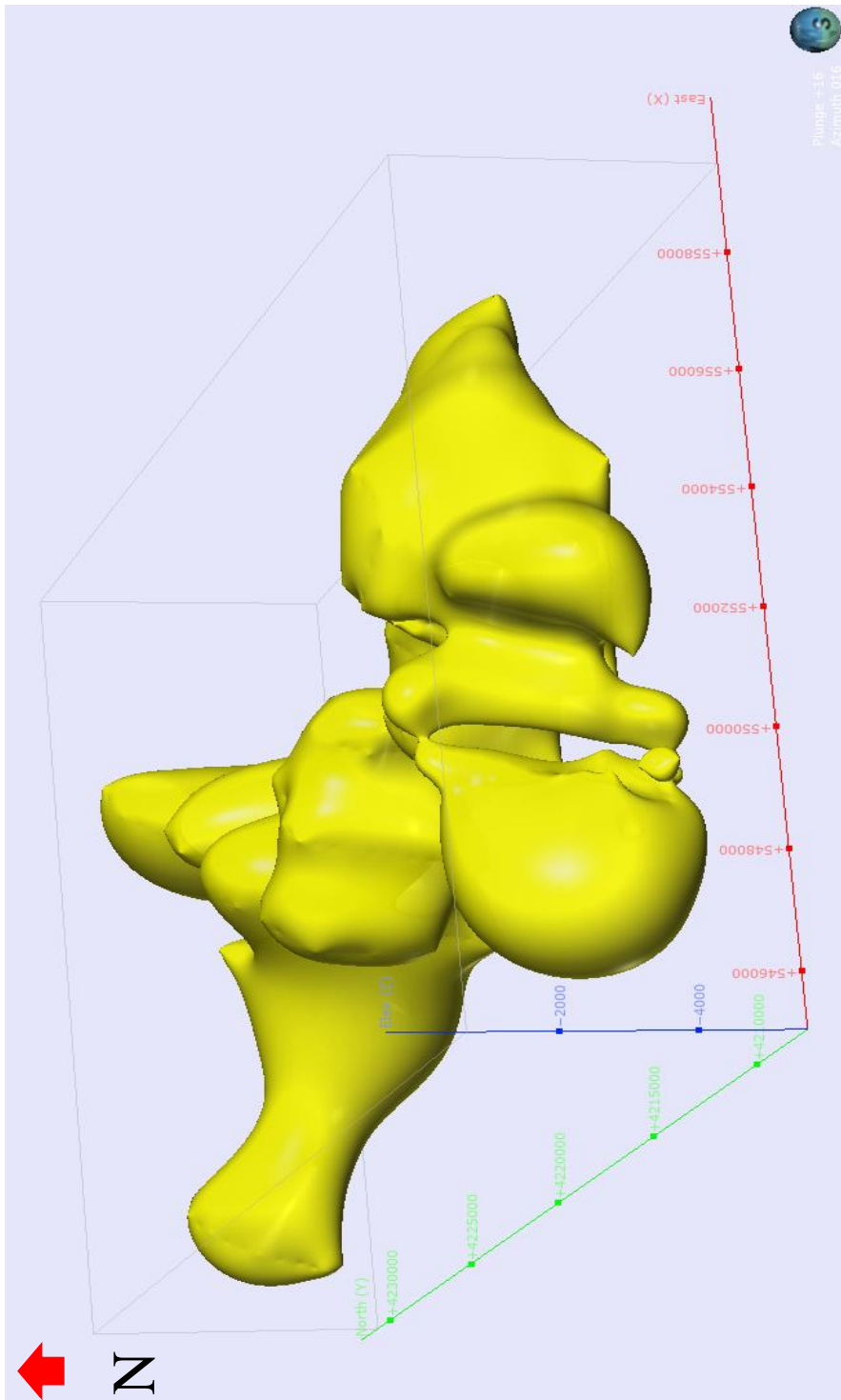


Figure 3. 13. 3D model of the Tuzgözü salt structure view to NE.

### 1.11.2. Çankırı Basin 3D Volume

The 3D solid volume of the Çankırı Basin is dominantly represented by the salt domes and elongated through the NNE-SSW direction, which encompasses approximately 70 km<sup>2</sup> area (Figure 3. 14). The total volume of the salt body is estimated at 443,050 bcm. In addition, the salt dome extends through the ages of the Eocene and the Oligocene. (Figure 3. 15).

The salt depth variant is noteworthy with a range of 400 -1450 meters for the top of the salt surface and a range of 2,200 -4,000 meters for the bottom of the salt structure. The substantial thickness of the 3D volume is discernible, having a variation between 1,800 - 2,550 meters (Table 3. 2).

The Sağpazar-1 borehole offers insight into the depth range of the 3D salt volume location when aligned with the borehole. This relationship reveals that the salt is observed at 1,450 meters and reaches a maximum of 3,455 meters. The partitioning of the salt body into three parts.

The three-dimensional salt volume is presented to explicitly display the dome shapes highlighted in Figure 3. 14, and the complete thickness in the z domain is visualized in Figure 3. 15.

Table 3. 2 The Çankırı Basin's Salt body information

	Min	Max
Salt Top	400m	1450m
Salt Bottom	2200m	4000m
The Bulk Thickness of Salt	1800m	2550m

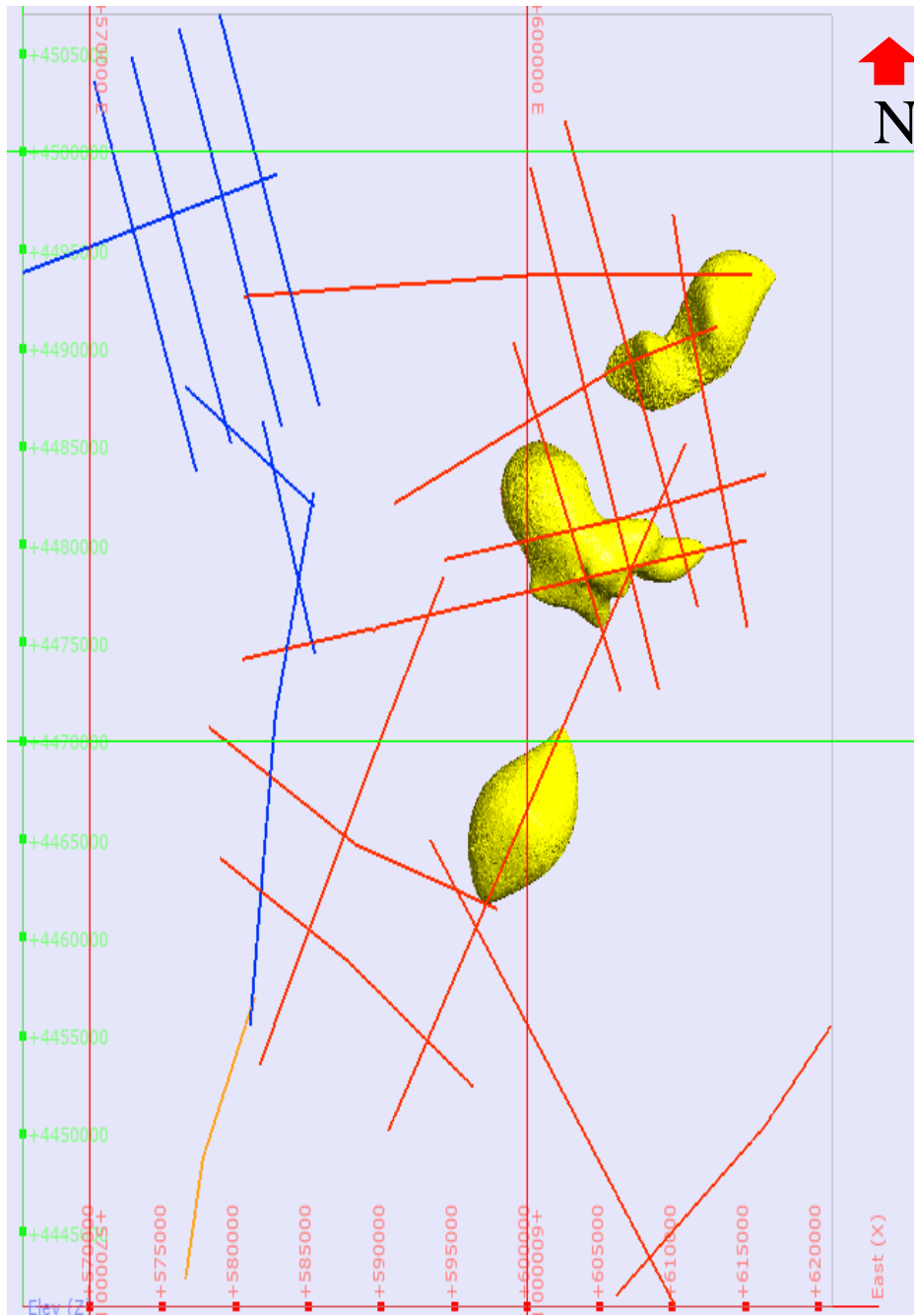


Figure 3. 14 Displaying the top view of the 3D salt body of the Çankırı Basin that is overlapping with the seismic database map. Three pieces of the salt body are seen clearly on the base map. (Blue and red color lines determine the seismic profile locations on the base map, the interpretation had been completed with the red color lines) (Generated by Leapfrog Geo).

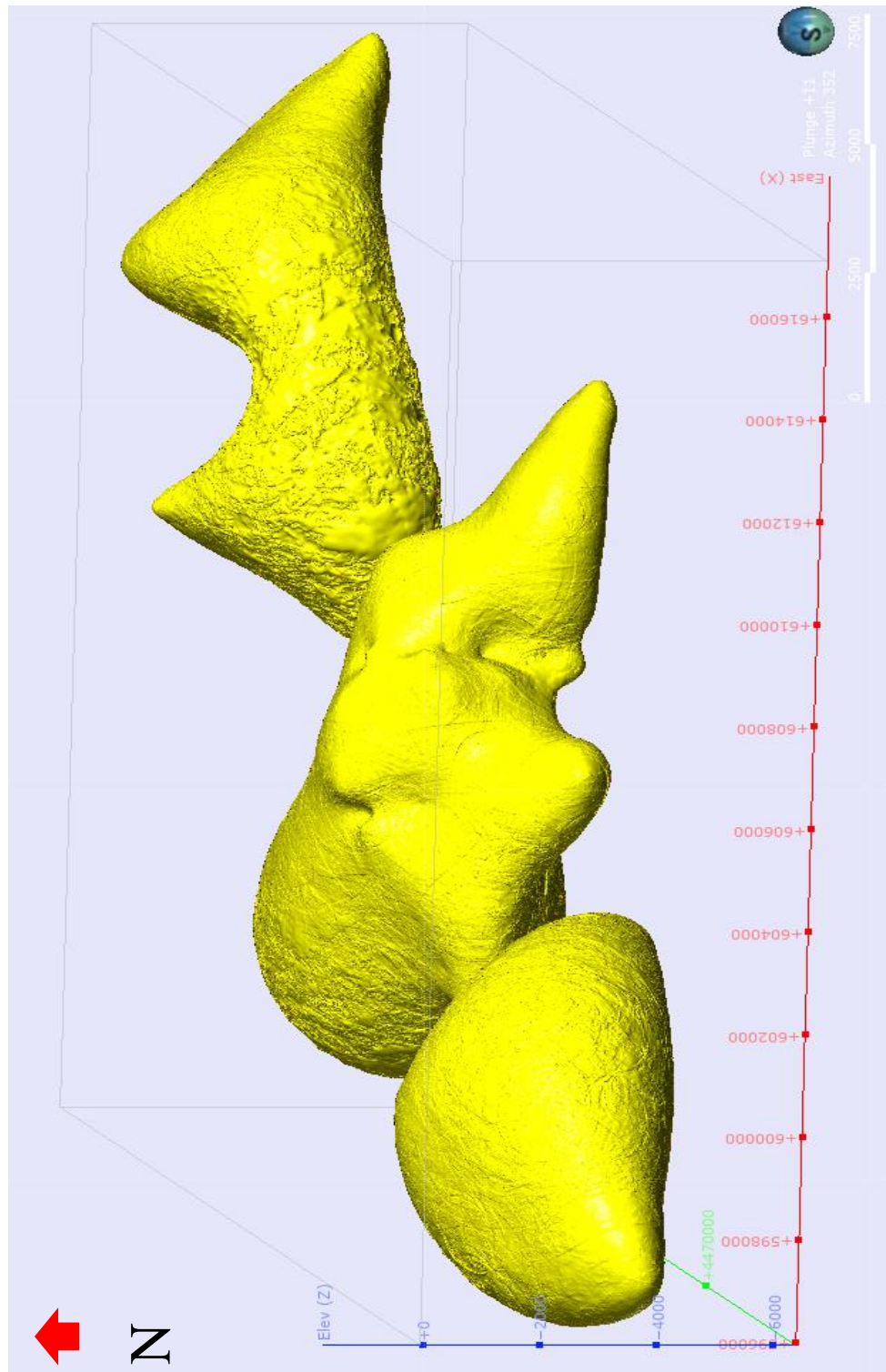


Figure 3. 15 The 3D volume of the Çankırı Basin salt structure view (Generated by Leapfrog Geo).

## **1.12. Designing of the Cavern**

Initially, the form of the cavern was crafted by utilizing the graphic design program as a mesh file with no geomechanical conditions. Subsequently, the volume is determined depending on the chosen geometric parameters of the cavern, which are diameter and height. The rock's medium is affected by different elements such as pressure, density, porosity, stability, subsidence rate, and volume convergence added into the system. This research is simplified as much as possible and squeezed into a three-step protocol for designing caverns, which involves assumptions, conjectural cavern scenarios, and parameters.

### **1.12.1. Assumptions**

The plan for the cavern takes into account a variety of presumptions, beginning with the salt content where the cavern is being constructed. It was assumed that the salt type was a comprehensive 100% Halite (NaCl) structure to generate an isotropic media.

The total stress ratio  $k$  is one of the most fundamental factors of the cavern, which is assumed to be one (1) by assuming vertical and horizontal stress is even. (Onal 2013).

Taking the estimated average temperature of 327 Kelvin as a constant, the temperature was assumed to be unchanging in the system. First, utilized the following function (14) to obtain the temperature for the beginning depths of both the salt and the cavern (Table 3. 3). And then took the average temperature value as the constant for the entire system under stable conditions with ignoring in terms of the temperature variation in depth.

Table 3. 3 The cavern design calculation with the temperature

The Temperature Chart				
Item	DEPTH(m)		H(m)	T(Kelvin)
	min	max		
Cavern	-1700	-1900	200	329,1
Salt	-1200	-5000	3800	317,6
Base gas	-1850	-1900	50	332,55
Roof salt	-1700	-1730	30	329,1
				<b>Average: 327,0875</b>

### 1.12.2. Cavern Scenarios

This research utilizes two cavern situations as its focus. To construct the first model, the parameters of the cavern were leveraged, along with features of the salt body and its background (Figure 3. 16 and Figure 3. 17). The chosen shape for the cavern was an ellipsoid and the mesh record influenced the parameters of guidance including volume, depth, and diameter. The second model demonstrates the connection between the two caverns using single-cavern features. (Figure 3. 18).

The most important factor during the construction of the cavern is the thickness of the salt. The depths are assumed to be 1,200 m for the top of the salt and 5,000 m for the bottom of the salt, respectively. Thereby the thickness of the salt is approximately 3,800 meters.

The topography of the salt structure influences the determination of the cavern's depth. In the Tuzgölü Basin, the salt top varies from 800m to 1,650m, and in the Çankırı Basin, it ranges from 400 meters to 1,450 meters. Furthermore, the depth range of the salt layer is between 3,500-4,500 meters in the Tuzgölü Basin and 2,200– 4,000 meters in the Çankırı Basin. Table 3. 4 reveals the depth of the salt within the Tuzgölü Basin is between 2,700 and 2,850 meters, and between 1,800 and 2,550 meters in the Çankırı Basin.

Ultimately, the minimum depth of the salt present is 1200 meters, with a maximum depth of 5,000 meters, constituting a total thickness of 3,800 meters (Table 3. 5).

Table 3. 5 details the volume, elevation, and depth specifics for the cavern, the salt, the bottom gas, and the top salt. The ellipsoidal cavern contains a volume of 1,302 mcm and measures 200 meters in height and 150 meters in diameter. To prevent the cavern stability from the convergence volume and creep the depth of the salt cavern was selected to start at 1,700 meters depth due to the transition zone approximation, which is known to initiate at 2,000 meters. It is imperative to sustain the pressure in the cavern as salt tends to be unmanageable below 2,000 meters. Subsequently, the height of the cavern stands at 200 meters, and the bottom of the cavern plunges to a depth of 1,900 meters before reaching 2000 meters. (Table 3. 5 and Figure 3. 16). It is predicted that the base gas area is 50 meters in height and encompasses 245,436 m<sup>3</sup> of volume while the roof cavern is 30m in height and encompasses 95,425 m<sup>3</sup> in area. The schematic diagram of the cavern mesh file is representing the base cavern and cavern roof thickness with the height information (Figure 3. 17).

Table 3. 4 Salt bulk depth information chart for study areas.

	The Tuzgölü Basin		The Çankırı Basin	
	Min	Max	Min	Max
Salt Top	800m	1650m	400m	1450
Salt Bottom	3500m	4500m	2200m	4000
The bulk Thickness	2700m	2850m	1800m	2550

Table 3. 5 The design parameter of the cavern

Item	DEPTH(m)		H(m)	Diameter (m)	VOLUME
	min	max			
Cavern	-1700	-1900	200	150	1.302 mcm
Salt	-1200	-5000	3800	-	443.840 bcm
Base gas	-1850	-1.900	50		245,436 m <sup>3</sup>
Roof salt	-1700	-1730	30		95,425 m <sup>3</sup>

Before generating a multi-cavern scenario, the width between the two caverns must be taken into account, which affects the cavern's stability and also the salt roof thickness, cavern height, and distance to the edge of the salt dome are also considered. This study creates a multi-cavern setup involving two similar caverns which are identically in the same material and checks it for general demands related to geomechanical design (Lux et al. 2009). In this case, the diameter of the caverns is 150 meters (d), and the height of the caverns is 200 meters (h) which are as the same as the single cavern scenario. Besides, the distance between the salt top and the cavern is assumed at 500 meters (z), and the pillow width, which is the distance of the caverns at 1,000 meters (b). The cavern distance from the edge of the salt body was selected as 1,000 meters (a) which is two times bigger than the distance of the cavern top and salt top value, 500 meters (Figure 3. 18).

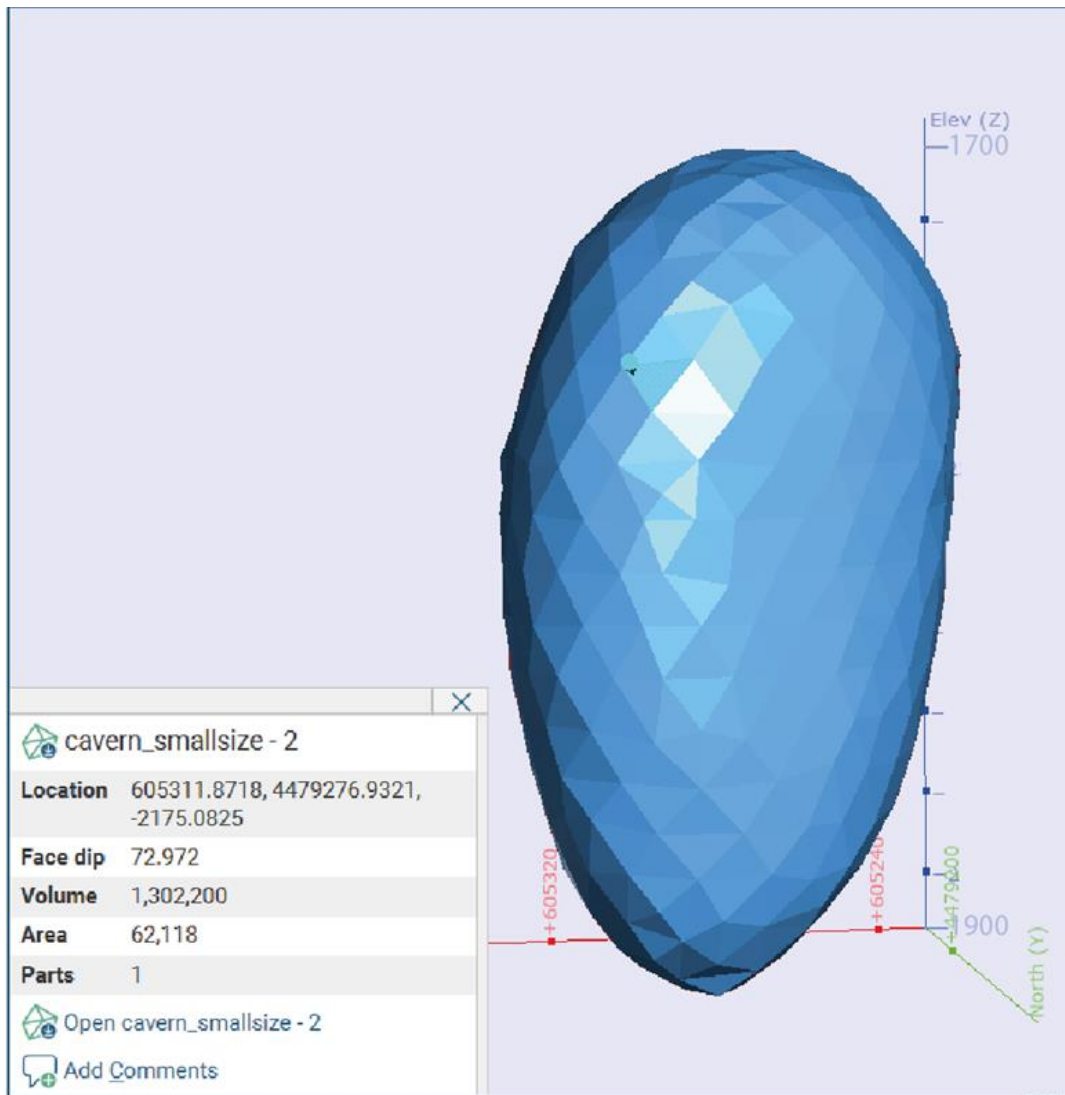


Figure 3. 16 The view of the ellipsoidal cavern mesh file and the information chart (Generated by Leapfrog Geo).

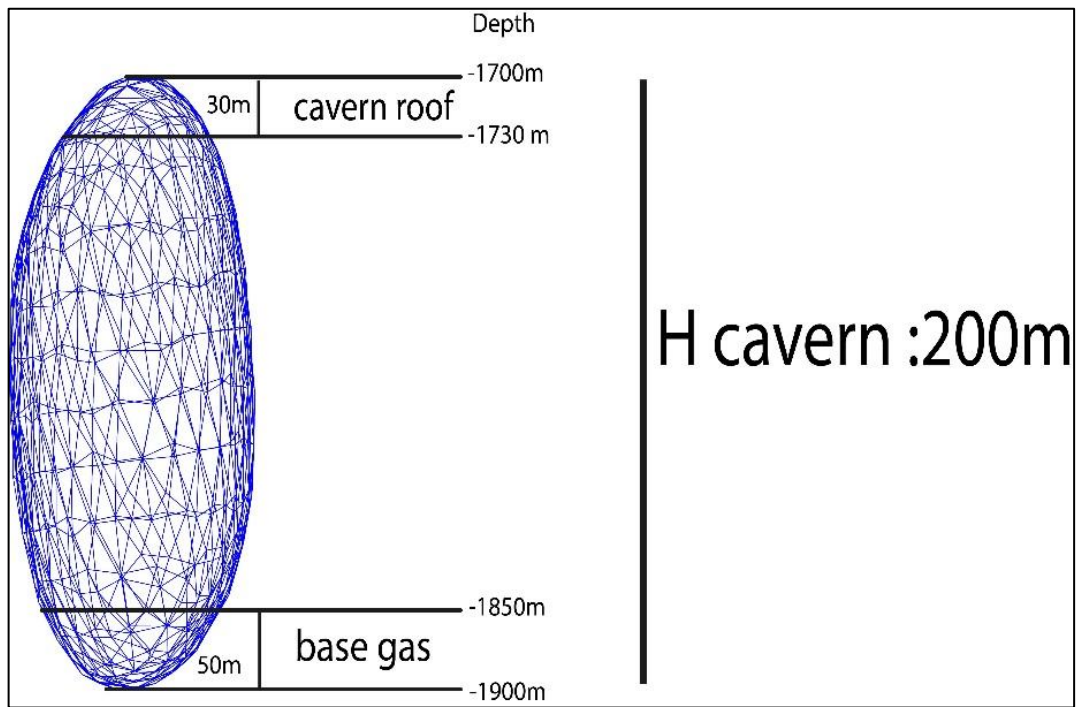


Figure 3. 17 The schematic view of the base gas and a rooftop view of the cavern.

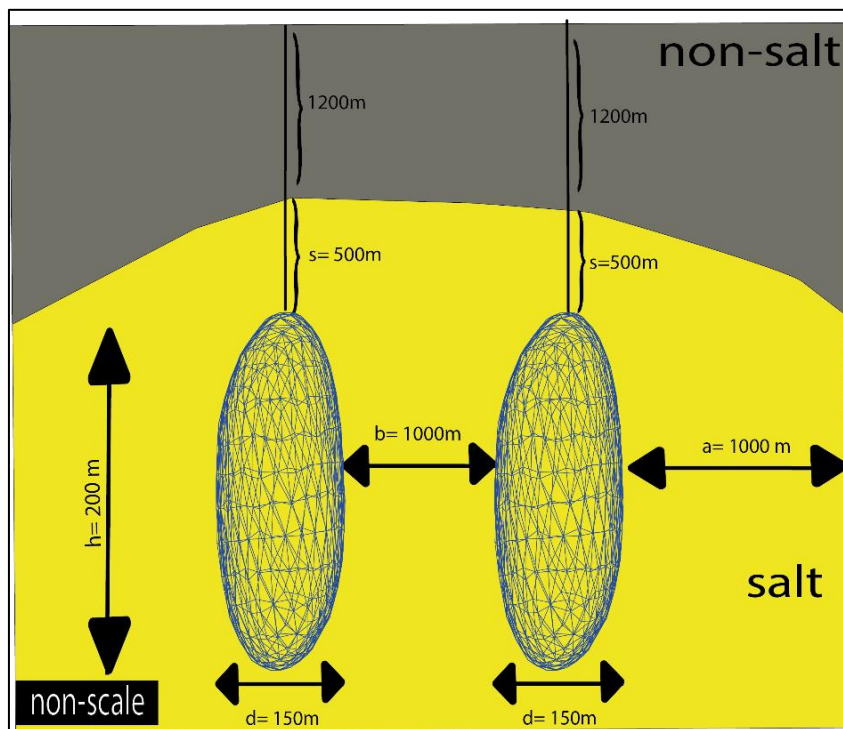


Figure 3. 18 The schematic view of the two-cavern scenario in the salt structure.

### 1.12.3. Parameters

Asses the cavern design, several parameters were assumed invariable. Nevertheless, numerous geomechanical parameters like density, porosity, young module, and Poisson rate had been obtained from former studies. Düzyol, (2004) and Özşen, (2009) had been studied in the Çankırı Basin, they were evaluated to get data on rock mechanics with the same samples. The laboratory results of these studies are depicted in Figure 3. 8.

The initial vertical stress was estimated through function (1), which multiplies the depth information with the coefficient number of  $0,022 \cdot H$ ; to provide the vertical initial pressure for minimum and maximum depth variants of the cavern, salt, base gas, and roof cavern.

Initial vertical stress ( $P_v$ ) and Vertical Total Stress gradient ( $S_v$ ) at the minimum and maximum depth of the Cavern, Salt, base (cushion) Gas, and Roof Cavern are individually depicted in Table 3. 6.

Vertical total stress gradient, ( $S_v$ ) is calculated for overburden strata, salt top, salt bottom, and inside of the cavern by the function (2) and the function (3), which is  $S_v(z) = \rho_{bulk} g z$ . Here, the overburden strata density is  $2,25 \text{ g/m}^3$ , the rock salt density of halite is  $2,17 \text{ g/m}^3$ , the gas density is  $0,225 \text{ g/m}^3$ , and the gravity acceleration ( $g$ )  $9,8 \text{ m/s}^2$  is taken. The results are outlined in Table 3. 6.

From the top to the bottom of the salt the increased vertical total stress graph is illustrated in Figure 3. 19. The salt rock Halite is under  $26,46 \text{ MPa}$  vertical stress, and the cavern structure is between  $37,09 \text{ MPa}$  and  $37,29 \text{ MPa}$  vertical stress rate. The cavern pressure rate is calculated under the natural gas injected into the system by taking the constant gas density as  $0,225 \text{ g/m}^3$ .

The geological tightness is the guarantee of the storage pressure and  $P_{max}$  should be 10% lower than the minimum pressure value ( $\sigma_{min} \geq 1.1 P_{max}$ ). On the other side, the technical tightness could be at most 15% of the maximum pressure rate that is given by compressive stress  $\sigma_{xx} = 0,85 P_{max}$  (Susan, 2019). The relationship with

the total vertical stress, the initial vertical stress, geological tightness, and technical tightness are listed in Table 3. 7.

This research regards the salt cavern to be in an even state, which is isotropic and maintains the pressure inside the cavern consistently. The geological tightness  $P_{max}$  is calculated by taking the total vertical horizontal stress value equal to the  $\sigma_{min}$  value ( $\sigma_{min} \geq 1.1 P_{max}$ ) within the cavern depth range and taking the average to get a constant parameter. Moreover, the technical tightness is determined in the same method, and the supposition is that compressive strength is equal to the inside pressure of the cavern. Ultimately, the average of the technical and geological tightness was set to facilitate the most effective stress level within the cavern. Therefore, the technical tightness  $P_{max} = 31,71$  Mpa, geological tightness  $P_{max} \leq 33,91$  Mpa, and so the optimum maximum cavern pressure is calculated as 32,81 Mpa, 4758 Psi.

The minimum pressure within the cavern is calculated by taking 30% of the initial vertical pressure which is at 11,85 MPa after taking the average of the  $P_v$  in the range of the 1700m and 1900 m depth (Ozarslan (2012)).

Table 3. 6 Initial vertical Stress ( $P_v$ ) and Vertical Total Stress gradient ( $S_v$ ) of the Cavern, Salt, base (cushion) Gas, and Roof Cavern individually.

Item	DEPTH(m)		$P_v = 0,022 H$ (MPa)		$S(v)$ (MPa)	
	min	max	min	max	min	max
Cavern	-1700	-1900	37,40	41,80	37,09	37,53
Salt	-1200	-5000	26,40	110,00	26,46	103,46
Base gas	-1850	-1900	40,70	41,80	37,42	37,53
Roof salt	-1700	-1730	37,40	38,06	37,09	37,16

Table 3. 7 The depth relationship with total vertical stress, with geological and technical tightness (Yellow columns are representing the salt strata, and grey columns are representing the cavern)

	$S_v(z) = \rho_{\text{bulk}} g z$	<b>Geological tightness</b>	<b>Technical tightness</b>
<b>Depth (m)</b>	<b>s(v)</b>	<b>Pmax Sv</b>	<b>Pmax Sv</b>
0	0,00	0,00	0,00
-1000	22,05	20,05	18,74
-1200	26,46	24,05	22,49
-1700	37,09	33,72	31,53
-1730	37,16	33,78	31,59
-1800	37,31	33,92	31,72
-1850	37,42	34,02	31,81
-1900	37,53	34,12	31,90
-2000	40,72	37,02	34,62
-2200	43,91	39,92	37,33
-3000	60,93	55,39	51,79
-4000	83,26	75,69	70,77
-5000	103,46	94,05	87,94
	37,30	33,91	31,71
		$P_{\text{max}} \leq 33,91 \text{ Mpa}$	$P_{\text{max}} = 31,71 \text{ Mpa}$

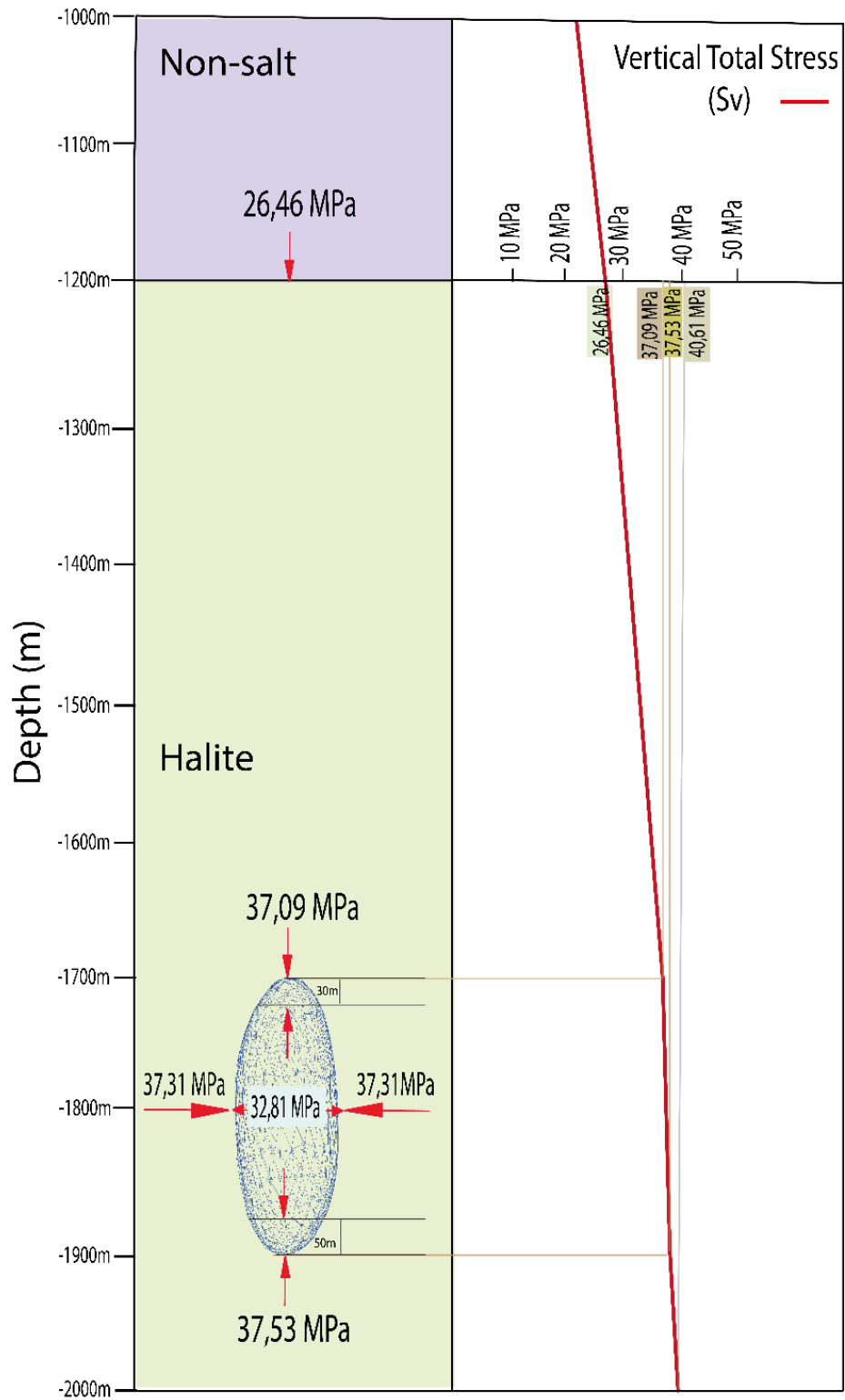


Figure 3. 19 Display the vertical total stress graph.

The elastic and creep properties of the Çankırı Basin and the Tuzgözü Basin were correlated with the geomechanical parameter and depicted in Table 3. 8. Ozarslan (2012) and Susan (2019) provided the values of the creep parameters. Table 3. 9 exhibits the value achieved from the relationship function with convergence velocity  $k$  ( $\text{day}^{-1}$ ) and the convergence volume ( $\text{m}^3$ ).

The pressure differences between cavern and lithostatic were calculated based on the surface subsidence topic in Chapter 2. Under these conditions, the average pressure value is assumed in a variety of 5 MPa, 10 MPa, 12.5 MPa, 14.5 MPa, 15 MPa, and 16.5 MPa, respectively and the convergence rate had been calculated via the function (13). Subsequently, the volume convergence values are computed for a single year, five years, and a decade. Those results are presented in Table 3. 9.

The calculation of the surface subsidence prediction could not be concluded appropriately as a consequence due to the missing components: the time coefficient  $\xi$ ,  $x$ , and  $y$  coordinate information of the cavern, and shape adjustment factor  $\delta$ .

Finally, the relationship between the average internal pressure and convergence rate is displayed as graphically for a year (Figure 3. 20).

Table 3. 8 Characteristic values used for the creep and elastic material properties of rock salt. (Modified from Ozarslan 2012 and Susan 2019)

Characteristic values used for the creep and elastic material properties of rock (Modified after Ozarslan 2012 and Susan 2019)		
Parameter definition	Symbol	Values
Steady-state creep rate	$\epsilon_{ss}$	5,39E-08
Creep stress value of the material model	A	5,79E-36
Activation energy	Q	12
Universal gas constant	R	0,008314
Temperature	T	338
Rock salt density (g/m <sup>3</sup> )	d	2,170
Creep strain rate stress dependency factor	n	5
Bulk modulus	K	20,7 GPa
Shear modulus	G	12,4 GPa
Elastic module	E	30 GPa
Top cavern		1700
Bottom cavern		1900
Average Depth		1700

Table 3. 9 Average Internal Pressure ( $V_i$ ) is listed with the Convergence Rate and Volume convergence calculation results of the Çankırı Basin

Çankırı Basin			
	Average Internal Pressure (MPa)	Convergence Rate % Day <sup>-1</sup>	Volume Convergence (m <sup>3</sup> )
	$V_p$	k	$V_k(t)$
1 year	5	1,5893	83440,9
	10	0,2531	82680,2
	12,5	0,0721	80410,3
	14,5	0,0197	71992,7
	15	0,0134	66675,5
	16,5	0,0034	35821,8
5 years	5	1,5893	417780,9
	10	0,2531	417020,2
	12,5	0,0721	414750,3
	14,5	0,0197	406324,1
	15	0,0134	26259,1
	16,5	0,0034	351038,1
10 years	5	1,5893	835705,9
	10	0,2531	834945,2
	12,5	0,0721	832675,3
	14,5	0,0197	824249,1
	15	0,0134	818814,5
	16,5	0,0034	768832,2

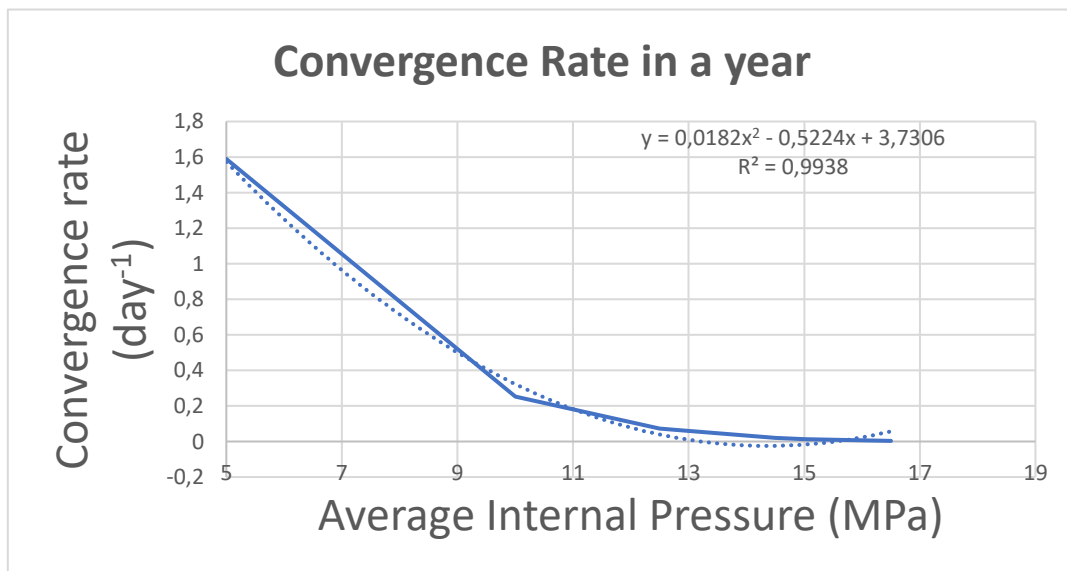


Figure 3. 20 Graphical display of the convergence rate versus average internal pressure in a year

## CHAPTER 4

### DISCUSSION

This chapter will assess the seismic interpretation, the 3D salt volume, and the salt cavern design as an underground storage.

#### 1.13. The Seismic Data Interpretation

During the interpretation of the Tuzgölü Basin, 15 seismic profiles were selected from among 28 total seismic profiles and are from the southern part. The interpretation of the salt was focused on the 15 total seismic profiles that are in the south and 12 of them parallel to each other and 3 of them crossing each other. During the interpretation, the salt was observed in the Paleocene strata and is getting narrower and deeper to the north and interpreted as becoming more expansive and shallower to the south in the parallel seismic profiles. Besides the salt, the associated strata were interpreted as well. Those are the Pliocene Cihanbeyli Formation and the Oligocene-Miocene Mezgit Formation to unravel the salt boundary. The salt observed in the Paleocene during the interpretation.

In the Çankırı Basin, interpretation concentrated on 9 of the total 15 seismic profiles due to the salt structure being in the target. In addition to the salt body, the strata associated with the salt are also interpreted. Those are the Late Eocene Incik formation and the Oligocene Bayındır Formation. The evaporite units were observed in the Late Eocene and the Oligocene strata in the study of Kaymakci 2003a. The salt interpreted within the 2,250 meters thickness in the Late Eocene - Oligocene Incik Formation is also stated by Kaymakçı et al. (2010) as the thickest formation in the Çankırı Basin with 2,000 meters in thickness.

In this research, the formation tops were correlated with the borehole reports of the previous studies for both study areas. The seismic velocity time-depth conversion sensitivity has caused a particularly noticeable divergence in thickness. For example, the report of the Sağpazar-1 borehole in the Çankırı Basin (Figure 1.13) explains the

Oligocene Bayındır Formation is about 480 meters thick, however, in the present study, the thickness calculated at 451 meters by the conversion of the seismic velocity information to the depth.

The interpretation of the seismic section of the study areas is also correlated with the gravity data for both study areas. The low gravity anomaly is taken as a reference for the salt boundary, which is concentrated in the eastern central part of the basin in the Çankırı Basin, while is concentrated in the southern part of the Tuzgölü Basin.

#### **1.14. 3D Salt Volume**

In the Tuzgölü Basin study, the 3D volume is displayed with several diapir structures which are observed through 2D seismic sections. Bağcı et al. (2007) constructed a 3D volume of the salt structure to be used with the 3D seismic data set. The salt body is elongated through the NNW- direction, covering 36 km<sup>2</sup> in total with an average width of 2,000-2,500 meters and 1,900 meters in thickness. On the contrary, Bağcı et al. (2007) constructed a 3D volume of the salt structure to be used with the 3D seismic data set. Bağcı et al. (2007) describe the salt structure as having no overhang, an elongated uniform shape with a steep flank on the edges concerning the 3D volume view of the salt body. While Bağcı et al. (2007), suggested that salt covers 36 km<sup>2</sup> area, in this study, it is calculated as 96 km<sup>2</sup>. Additionally, the Tuzgölü Basin has gained recognition in the commercial field due to the Botas facility since 2007. According to the report of the Botas, the salt layer of 15 km in length and 2.5 km in width, 37.5 km<sup>2</sup>. In this study, probably the 2D seismic data set contribution by interpolation during the creation of the salt structure is causing this difference in size. In the Çankırı Basin, Kaymakci et al. (2000) evaluated the same 2D seismic data set to construct a 3D fence diagram by digitizing the seismic sections in a computer analysis program. Even though the algorithm method is different while generating the salt body, the salt is discovered at the northeastern part of the basin and described as dome-type in both studies. The borehole report explains the salt located in the Late Eocene -Oligocene strata with the 2,000 meters bulk thickness. The obtained 3D salt volume of the Çankırı Basin is described as a dome type, which is aligned with the

Kaymakçı et al. (2010). These results show the salt is elongated through the NNE-SSW direction.

### **1.15. Salt cavern design**

The cavern was designed with a mesh file through Leapfrog Geo software in this study. The analytical model was applied to reach the optimum cavern parameter by assuming some fundamentals are constant. Besides, the lack of a laboratory test to analyze the medium of the rock salt forced getting them from previous studies. In literature, the cavern design does not have a standard way (Allen, 1982, Lux, 2009). Generally, it depends on the thickness and depth of the salt as the host.

The subsurface is not homogenous, and a complex salt structure limits the cavern design due to the thickness, strength properties, etc. Although the unique salt parameters give the protection naturally, solution mining causes some troubles, which are better to solve before construction.

The designing method plays an essential role here. In the history of cavern designing, the numerical approach method or even the analytical approach method do not exist in the 1970s (Habibi, 2019). Former construction design consisting of the empirical approach was extensively used without any consideration by regulating the parameter across varied conditions. Eminence cavern is a good example of an experimental methodology as it failed in two years. Conversely, the numerical method is a thorough process involving the simulation of the cavern in a variety of circumstances before construction. Those are important in all steps of the cavern design. If a problem occurs at any certain time, depth, and size, the simulation answers to how could solve the problems. To obtain a prediction answer in the simulation of the numerical approach method, the mechanical parameters for the salt and surrounding environment are required. Therefore, in-situ laboratory tests are a must for the construction of an underground storage facility.

Therefore, the salt rock is assumed as 100% of pure halite to design a regular shape cavern and to avoid the deformation of the media. Figure 1.5 is displaying the different depths, and different shapes of the caverns, and Figure 1.6 is illustrating the different depths and shapes caverns of worldwide examples. The salt depth is effective in the

selection of the cavern type as well as the salt type. The salt type is described as a dome in the Çankırı Basin, and as a diapir in the Tuzgözü Basin with bulk thicknesses over thousand meters for both study areas, so the salt cavern is suggested to design as an ellipsoidal shape to be more prevailing with the environment.

The Eminence salt cavern in Oklahoma was built in 1970 at 1,700 meters and 2,000 meters in depth range, with 300 meters in height, as a kind of ellipsoidal shape (Warren, 2006). The only challenge is with salt creep at that size and depth of the cavern because the cavern pressure and lithostatic pressure should be in an optimum value to protect the cavern from collapsing, convergence, or any damage. The Eminence cavern is squeezed in two years because the cavern pressure could have not been kept under control during the processing. That kind of unpredicted situation occurred, and the cavern was damaged in 1972. Such things happen if the design is not completed precisely before the construction of the underground storage facility.

The general demands of the salt cavern are shown in Figure 2. 5 (Lux 1984, 2009) based on the geomechanical parameters that consist of salt roof thickness ( $s$ ), cavern roof depth ( $z$ ), cavern height ( $h$ ), cavern diameter ( $d$ ), Pillar width ( $b$ ), and the distance to the edge of the salt dome ( $a$ ). The diameter of the cavern controls especially the distance between two adjacent salt caverns ( $b$ ) and the distance from the top of the salt to the cavern rooftop ( $z$ ).

The important criteria are the depth of the salt and the gap between the cavern and the salt to avoid surface subsidence. Here, the depth of the cavern is 1,700 meters, the depth of the salt top is 1,200 meters, the diameter is 150 meters, and the salt roof thickness is 500 meters. The cavern roof depth is selected as 1,000m, and the distance to the edge of the salt dome is 1,000 meters. The volume of the designed cavern is 1.302 mcm. The designed result of this study is displayed in Figure 3. 16.

It is essential to avoid caverns collapsing by stress on each other and potential damage in case of the multi-cavern scenario as well as single cavern scenario.

The primary concern is whether the desired cavern stability is provided during the injection/withdrawal period. Susan (2019) stated that the salt roof thickness is important to prevent any damage to the cavern during the construction and operation time and, it should be three times bigger than the diameter of the cavern. To provide long-term stability and daily production during the injection/withdrawal period cavern

size was preferred as smaller as possible. The designed ellipsoidal cavern geometry is 200 meters high, and 150 meters in diameter to get a small size of the cavern to provide the study aim.

On the other hand, Bağcı et al. (2007), preferred to design a cylindrical prism with a 500,000 m<sup>3</sup> volume. The Botas facility cavern shape is unknown though the cavern geometry is designed with 630,000 m<sup>3</sup> -750,000 m<sup>3</sup> volume capacity. Besides, the volume range is between 100,000 m<sup>3</sup> and 1.000,000 m<sup>3</sup> all around the world, which could be more in different conditions like technical or geological.

In this study, the shape of the cavern is ellipsoidal, which is quite different from the cylindrical cavern shape of Bağcı et al. (2007). The volume size of the salt cavern is nearly two times bigger when compared with the Botas facility and Bağcı et al. (2007) suggested cavern size. The volume of the 3D salt structure makes it possible to build a large cavern at present, but it might be different in the future if some circumstances alter.

Despite the assumption that the salt is present in an isotropic setting, the cavern pressure fluctuates depending on injection/withdrawal. For example, the cavern size should design in small size to complete the injection and withdrawal process in a short time. When the pressure of the cavern reaches the lithostatic pressure the process stopped therefore the cavern size is better to select a small size (Berest, 2001).

In this research, the size of the cavern is bigger than average in comparison to prior studies. This could result in circulation period increases, thereby considering reducing the cavern size as an option.

Gas pressure influences the volume shrinkage and so, limiting the maximum gas pressure and minimum gas pressure is the ultimate. Ozarslan (2012) stated that minimum gas pressure could be estimated at 30 % of the vertical initial stress ( $P_v$ ) to contribute to the design parameters. The cavern pressure cannot surpass the lithostatic pressure to avoid surface subsidence. This is also a necessity for the long-term stability of the cavern. The pressure range of the cavern is related to the subsidence rate and salt creep. If the internal pressure surpasses the lithostatic pressure surface subsidence occurs and salt creep squeezes the cavern. In this study, the  $P_{max}$  value is calculated in two ways, and getting the average value as an internal cavern pressure.

First, the total vertical stress is calculated from the surface to the bottom part of the cavern. The initial vertical stress in the cavern increases from 1,700 meters to 1,900 meters, in a range of 37,09 MPa and 37,53 MPa, respectively.

The scenarios of the cavern admitted the subsurface is isotropic so the vertical stress should be equal from the top to the bottom. Therefore, the changing stress in the vertical direction is ignored by taking the average cavern vertical stress constant after calculating within the cavern depth range. The average of the total vertical stress is 37,30 MPa, and also this value is assumed as the compressive stress value. The overburden pressure on the top of the cavern is 37,09 MPa/km which is the lithostatic pressure and should not be surpassed by the cavern pressure. The technical and geological tightness is also calculated in terms of the pressure inside the cavern by taking the generalized formulation from Susan (2019). The results of the average value of the technical and geological pressure in the depth range of the cavern are technical tightness  $P_{max}$  is 31,71 MPa, and geological tightness  $P_{max} \leq 33,91$  Mpa, respectively. These values are the guarantee in the cavern system that if one of them surpasses the lithostatic pressure the cavern is collapsed. Therefore, the technical and geological tightness pressures are taken as constant after calculating the average, which is the optimum cavern pressure with 32,81 MPa, 4758 Psi. As a result, the lithostatic pressure is higher than the technical tightness pressure. Therefore, the maximum cavern pressure is not surpassed the lithospheric pressure which means obtained the optimum pressure value was determined to avoid salt creeping.

Total vertical stress emphasizes the importance of the pressure of the overburdened strata in the system. The inside stress of the cavern was related to the overburden weight and the inside pressure is associated with the operating gas pressure.

The compressive strength of the rock strata is equalized to the center of the cavern vertical stress which is calculated as 37,31 MPa. The cavern stress value is not surpassed the compressive stress under these circumstances.

To calculate the creep value, the obtained results from the previous studies are enough though the surface subsidence calculation requires more information which is not able to obtain even from the previous studies. Therefore, the surface subsidence rate was not able to calculate due to the missing dataset. The previous studies concluded that

while keeping the subsidence rate as lower as possible to avoid convergence, the internal pressure should be selected as a high value.

The result of the daily convergence rate and volume convergence value relationship gives the same result, which is while the convergence rate decreases, volume convergence increases. The convergence rate and average internal pressure are compared via a graphical display during a year (Figure 3. 19). According to the produced graphic; as the average internal pressure increases the volume convergence gets smaller, which is one of the desired results for keeping the cavern pressure and lithospheric pressure in balance for long-term stability. On the other side, keeping the internal pressure as higher as possible causes to increase in the cost of the withdrawal period to provide long-term stability. Even if the cost is too much increased, the cushion (base) gas value necessarily should be increased to afford this much internal pressure increase.

That is required to avoid the caverns' pressure effect on each other and the possible damage from the collapsing based on the two-cavern scenario.

Since there is no numerical model calculation to obtain the optimum values for a cavern in different depths, thicknesses, and temperatures, all the assumptions are based on the constative laws while generating the cavern design. As a recommendation to build an underground storage facility in the future, it would be better to have a re-generated 3D volume of the salt structure that is a result of the 3D seismic survey. Additionally, it would be more appropriate having in-situ laboratory tests to evaluate the relationship between the cavern stability and the salt structure by the numerical model, based on changing geomechanical parameters. In other words, it would be better to have a numerical solution model instead of the analytical model.



## CHAPTER 5

### CONCLUSION

This thesis presented the following conclusions from the research conducted:

- Potential field methods have been utilized to uncover salt structure locations with special attention to the Tuzgölü and Çankırı Basin regions.
- Seismic interpretation is constrained by focusing on the salt structure in seismic sections. The salt type, depth, and orientation are described for both study areas individually.
- The 3D salt volume of the Tuzgölü Basin is determined as a diapir shape with a 443.050 bcm volume and an 800 meters-1,650 meters salt depth range. The salt covers roughly 70 km<sup>2</sup> area and elongated through NNE-SSW direction.
- The 3D salt volume of the Çankırı Basin is described as a salt dome that is extending in a 96 km<sup>2</sup> area with a volume of 219.03bcm, at a 400 meters-1,450 meters range salt depth range, and elongated through the NNE-SSW direction.
- The underground gas storage in salt structure is designed in an isotropic environment with several assumptions.
- The cavern design study revealed a future vision by assumptions based on an analytical model. Two different cavern scenarios were created as an ellipsoidal shape due to the thickness of the salt being over thousand meters.
  - The top of the cavern is 1,700 meters in depth, and the bottom of the cavern is 1,900 meters in depth, 200 meters in height, and 150m in diameter. The volume is 1,302 mcm. The single cavern and multi cavern have the same geometric information.
  - Moreover, the general demands for geomechanical design in two cavern scenarios are the diameter taken into consideration and the salt

roof thickness is 500 meters, the distance between caverns, and the distance to the edge part of the cavern is 1,000 meters.

- The lithostatic pressure and cavern max pressure are determined as 37,09 MPa and 32,81 MPa individually. Meanwhile, the compressive strength is calculated at 37,31 MPa.

## REFERENCES

- Allen, R. D., Doherty, T. J., and Thoms, R. L., 1982a. "Factors Affecting Storage of Compressed Air in Solution Mined Salt Cavities." *Proceedings of the Intersociety Energy Conversion Engineering Conference* 4:1992–99.
- Allen, R. D., Doherty, T. J., and Thoms., R. L., 1982b. "Factors Affecting Storage of Compressed Air in Solution Mined Salt Cavities." *Proceedings of the Intersociety Energy Conversion Engineering Conference* 4:1992–99.
- API, 2022. *Underground Natural Gas Storage*. Retrieved January 24, 2023 from <https://energyinfrastructure.org/energy-101/natural-gas-storage>.
- Bagci, A. Suat, and Ozturk, E., 2007. "Performance Prediction of Underground Gas Storage in Salt Caverns." *Energy Sources, Part B: Economics, Planning and Policy* 2(2):155–65. doi: 10.1080/15567240500402693.
- Barka, A.A. and Reilinger, R., 1997. Active tectonics of the Mediterranean region: deduced from GPS, neotectonic, and seismicity data. *Annali di Geophysica* XI, 587–610
- Bérest, P., Bergues, J., Brouard, B., Durup, J. G., and Guerber, B., 2001. A salt cavern abandonment test. *International Journal of Rock Mechanics and Mining Sciences*, 38(3), 357–368. [https://doi.org/10.1016/s1365-1609\(01\)00004-1](https://doi.org/10.1016/s1365-1609(01)00004-1)
- Bérest, P., B. Brouard, and Hévin, G., 2010. "A 12-Year Cavern Abandonment Test." *EPJ Web of Conferences* 6:357–68. doi: 10.1051/epjconf/20100622003.
- Berest P., Béraud J.B, Bourcier M., Dimanov A., and Gharbi H., et al., 2012 "Very slow creep tests on rock samples. *Mechanical Behavior of Salt VII*", Apr 2012, France. pp.81-88. fihal-00786923f
- Bérest, P. 2019. "Heat Transfer in Salt Caverns." *International Journal of Rock Mechanics and Mining Sciences* 120(June):82–95. doi: 10.1016/j.ijrmms.2019.06.009.
- Bertoni, C., Lofi, J., Micallef, A., and Moe, H., 2020. Seismic reflection methods in offshore groundwater research. *Geosciences*, 10(8), p.299.

- BGS, 2022 British Geological Survey. Retrieved July 01, 2022 from <https://www.bgs.ac.uk/research/energy/undergroundGasStorage.html>
- Botaş Turkish Petroleum Pipeline Corporation (BOTAS). Retrieved July 01, 2022 from <http://www.botas.gov.tr>
- Botaş (2017) Report, CON-0033, Turkish Petroleum Pipeline Corporation (BOTAS). Retrieved July 01, 2022 from <http://www.botas.gov.tr>; 2003
- Bozkurt, E. and Sözbilir, H., 2004. Tectonic evolution of the Gediz Graben: field evidence for an episodic, two-stage extension in western Türkiye. *Geological Magazine* 141, 63–79.
- Bozkurt, E., and Mittwede, S. K., 2001. “Introduction to the Geology of Türkiye - A Synthesis.” *International Geology Review* 43(7):578–94. doi: 10.1080/00206810109465034.
- Brouard, B., Bérest, P. and Couteau. J., 1997. “Influence of the Leaching Phase on the Mechanical Behavior of Salt Caverns.” *International Journal of Rock Mechanics and Mining Sciences* 34(3–4):26.e1-26.e15. doi: 10.1016/s1365-1609(97)00019-1.
- Bruno, M. S., 2005. “Geomechanical Analysis and Design Considerations for Thin-Bedded Salt Caverns (Final Report).” (626):142.
- CAES, 2022. Compressed air energy storage. Retrieved July 01, 2022 from [http://www.ridgeenergystorage.com/caes\\_underground-storage.htm](http://www.ridgeenergystorage.com/caes_underground-storage.htm)
- Çemen, I., Goncuoglu, M. C., and Dirik, K., 1999. “Structural Evolution of the Tuzgölü Basin in Central Anatolia, Türkiye.” *Journal of Geology* 107(6):693–706. doi: 10.1086/314379.
- Cristescu, N. D., and Paraschiv, I., 1995. “The Optimal Shape of Rectangular-like Caverns.” *International Journal of Rock Mechanics and Mining Sciences* 32(4):285–300. doi: 10.1016/0148-9062(95)00006-3.
- Dnicolasespinoza, 2022. Retrieved January 24, 2023 from <https://dnicolasespinoza.github.io/node8.html>
- Diñçer, B., and Işık, V., 2020. “Determination of Structural Characteristics of Tuzgölü Fault Zone Using Gravity and Magnetic Methods, Central Anatolia.”

Bulletin of the Mineral Research and Exploration 162(August):145–74. doi: 10.19111/bulletinofmre.661245.

Dirik, K. and Erol, O., 2000. “Tuzgölü ve Civarının Tektonomorfolojik Evrimi Orta Anadolu - Türkiye.” Haymana-Tuzgölü-Ulukışla Basenleri Uygulamalı Çalışma(WORKSHOP) (9-11 Ekim 2000) 27–46.

Düzyol, S. 2004. “Kaya Tuzuna Ait Mekanik Parametrelerin Belirlenmesi.” Selçuk University.

EIA, 2015. The Basics of Underground Natural Gas Storage. Retrieved July 01, 2022 from [https://www.eia.gov/naturalgas/storage/basics\(late\)](https://www.eia.gov/naturalgas/storage/basics(late)).

Fichler, C., H. Rueslåtten, C. Gram, A. Ingebrigtsen, and O. Olesen., 2007. “Salt Interpretation with Special Focus on Magnetic Data, Nordkapp Basin, Barents Sea.” (January). doi: 10.3997/2214-4609-pdb.166.c\_op\_06.

Fossum, A. F., and Fredrich, J. T., 2002. “Salt Mechanics Primer for Near-Salt and Sub-Salt Deepwater Gulf of Mexico Field Developments.” SANDIA Report, SANDIA 2063(July). doi: 10.2172/801384.

Gandhi, S. M., and B. C. Sarkar., 2016. “Geophysical Exploration.” Essentials of Mineral Exploration and Evaluation 97–123. doi: 10.1016/b978-0-12-805329-4.00012-0.

Gerling, P., Geluk, M.C., Kockel, F., Lokhorst, A., Lott, G.K. and Nicholson, R.A., 1999. January. ‘NW European Gas Atlas’–new implications for the Carboniferous gas plays in the western part of the Southern Permian Basin. In Geological Society, London, Petroleum Geology Conference series (Vol. 5, No. 1, pp. 799-808). Geological Society of London.

Görür, N., Oktay, F. Y., Seymen, I., and Şengör, A. M. C., 1984. “Palaeotectonic Evolution of the Tuzgölü Basin Complex, Central Türkiye: Sedimentary Record of a Neo-Tethyan Closure.” Geological Society Special Publication 17:467–82. doi: 10.1144/GSL.SP.1984.017.01.34.

Görür, N., Tüysüz, O., and Şengör, A. M. C., 1998. “Tectonic Evolution of the Central Anatolian Basins.” International Geology Review 40(9):831–50. doi: 10.1080/00206819809465241.

Gülyüz, E. 2020. “Late Cretaceous to Recent Kinematic History of the Tuzgölü

- Basin, Central Anatolia, Türkiye: A Paleostress Study.” *Yerbilimleri/ Earth Sciences* 41(2):114–46. doi: 10.17824/yerbilimleri.701207.
- Gürer, Ö. F., and Aldanmaz, E., 2002. “Origin of the Upper Cretaceous-Tertiary Sedimentary Basins within the Tauride-Anatolide Platform in Türkiye.” *Geological Magazine* 139(2):191–97. doi: 10.1017/S0016756802006295.
- Habibi, R., 2019. “An Investigation into Design Concepts, Design Methods and Stability Criteria of Salt Caverns.” *Oil and Gas Science and Technology* 74. doi: 10.2516/ogst/2018066.
- Haldar, S. K., 2018. “Exploration Geophysics.” *Mineral Exploration* 103–22. doi: 10.1016/b978-0-12-814022-2.00006-x.
- Han, J., Hu, C., and Zou, J., 2020. “Time Function Model of Surface Subsidence Based on Inversion Analysis in Deep Soil Strata.” doi: 10.1155/2020/4279401.
- Heinrich, F. C., Schmidt, V., Schramm M., and Mertineit, M., 2017. “Magnetic and Mineralogical Properties of Salt Rocks from the Zechstein of the Northern German Basin.” *Geophysical Journal International* 208(3):1811–31. doi: 10.1093/gji/ggw488.
- Heusermann, S., Rolfs, O., and Schmidt, U., 2003. “Nonlinear Finite-Element Analysis of Solution Mined Storage Caverns in Rock Salt Using the LUBBY2 Constitutive Model.” *Computers and Structures* 81(8–11):629–38. doi: 10.1016/S0045-7949(02)00415-7.
- Hudec, M. R., and Jackson, M. P. A., 2007. “Terra Infirma: Understanding Salt Tectonics.” *Earth-Science Reviews* 82(1–2):1–28. doi: 10.1016/j.earscirev.2007.01.001.
- Jackson, M. P. A., and Hudec M. R., 2017. *Salt tectonics: Principles and practice*. Cambridge University Press.
- Jackson, M. P. A., and Hudec M. R., 2017. *Seismic Interpretation of Salt Structures*. Cambridge University Press.
- Jeannin, L., Myagkiy, A., and Vuddamalay, A., 2022. Modeling the operation of gas storage in salt caverns: numerical approaches and applications. *Science and Technology for Energy Transition*, 77, 6. <https://doi.org/10.2516/stet/2022001>.

Kappa, 2022. Retrieved July 01, 2022 from <https://www.kappaeng.com/ugs/introduction>

Kaymakçı, N., White, S. H., and Van Dijk, P. M., 2000. Palaeostress inversion in a multiphase deformed area: Kinematic and structural evolution of the Cankiri Basin (central Türkiye), Part 1 - northern area. *Geological Society Special Publication*, 173, 295–323. <https://doi.org/10.1144/GSL.SP.2000.173.01.15>

Kaymakçı, N., and Dijk P, V., 2000. Palaeostress Inversion in a Multiphase Deformed Area Kinematic and Structural Evolution of the Cankiri Basin Central Turkey Part 1 Northern Area. *Geological Society, London, Special Publications*, 295–323. <https://hdl.handle.net/11511/39650>

Kaymakci, N., Özçelik, Y., White, S. H., and Dijk, P. M. V., 2009. Tectono-stratigraphy of the Çankırı Basin: Late Cretaceous to early Miocene evolution of the Neotethyan Suture Zone in Türkiye. *Geological Society Special Publication*, 311, 67–106. <https://doi.org/10.1144/SP311.3>

Kaymakci, N., Özmutlu, Ş., van Dijk, P. M., and Özçelik, Y., 2010. Çankırı havzası'nın yüzey ve yeraltı jeolojisi (orta anadolu, türkiye): Uzaktan algılama, sismik yorumlama ve gravite verilerinin entegrasyonu. *Turkish Journal of Earth Sciences*, 19(1), 79–100. <https://doi.org/10.3906/yer-0807-3>

Kergaravat, C., Ribes, C., Legeay, E., Callot, J.P., Kavak, K.S. and Ringenbach, J.C., 2016. Minibasins and salt canopy in foreland fold-and-thrust belts: The central Sivas Basin, Türkiye. *Tectonics*, 35(6), pp.1342-1366.

Ketin, İ., 1966. "Tectonic Units of Anatolia." *Maden Tetkik ve Arama Bulletin* 66:23–34.

Kılıçoğlu, A., Lenk, O., Diren., A., Simav, M., Yıldız, H., Aktuğ, B., Türkezer, A., Göçmen, C., Paslı, E., and Akçakaya, M., 2009. Türkiye İzostatik Gravite Anomali Haritası, *Harita Dergisi*, 144: 1-19

Li, H., Deng, J., Wanyan, Q., Feng, Y., Kamgue Lenwoue, A. R., Luo, C., and Hui, C., 2021. Numerical Investigation on Shape Optimization of Small-Spacing Twin-Well for Salt Cavern Gas Storage in Ultra-Deep Formation. *Energies*, 14(10). <https://doi.org/10.3390/en14102859>

Lichoro, C. M., 2016. Gravity and Magnetic methods: Presented at SDG Short Course I on Exploration and Development of Geothermal Resources, organized by UNU-GTP, GDC, and KenGen, at Lake Bogoria and Lake Naivasha, Kenya,

Nov. 10-31, 2016. Kenya. Figure 1.

- Liu, W., Zhang, Z., Fan, J., Jiang, D., and Daemen, J. J. K., 2020. Research on the Stability and Treatments of Natural Gas Storage Caverns with Different Shapes in Bedded Salt Rocks. *IEEE Access*, 8, 18995–19007. <https://doi.org/10.1109/ACCESS.2020.2967078>
- Lord, A. S., Kobos, P. H., and Borns, D. J., 2014. Geologic storage of hydrogen: Scaling up to meet city transportation demands. *International Journal of Hydrogen Energy*, 39(28), 15570–15582. <https://doi.org/10.1016/J.IJHYDENE.2014.07.121>
- Lux, K. H., 2009. “Design of Salt Caverns for the Storage of Natural Gas, Crude Oil, and Compressed Air: Geomechanical Aspects of Construction, Operation, and Abandonment.” *Geological Society Special Publication* 313:93–128. doi: 10.1144/SP313.7.
- Molíková, A., Vítězová, M., Vítěz, T., Buriánková, I., Huber, H., Dengler, L., Hanišáková, N., Onderka, V., and Urbanová, I., 2022. Underground gas storage as a promising natural methane bioreactor and reservoir? *Journal of Energy Storage*, 47. <https://doi.org/10.1016/j.est.2021.103631>
- Muhammed, N. S., Haq, B., Al Shehri, D., Al-Ahmed, A., Rahman, M. M., and Zaman, E., 2022. A review on underground hydrogen storage: Insight into geological sites, influencing factors and future outlook. *Energy Reports*, 8, 461–499.
- Xing, W., Zhao, J., Hou, Z., Were, P., Li, M., and Wang, G., 2015. Horizontal natural gas caverns in thin-bedded rock salt formations. *Environmental Earth Sciences*, 73(11), 6973–6985. <https://doi.org/10.1007/s12665-015-4410-y>
- Odé, H., 1968. Review of Mechanical Properties of Salt Relating to Salt-Dome Genesis.
- Okay, A., 2008. “Geology of Türkiye: A Synopsis Anatolian Metal IV.” *Small* (October 2008):19–42.
- Onal, E., 2013. “Stability Analyses of Differently Shaped Salt Caverns for Underground Natural Gas Storage.”
- Ozarslan, A., 2012. “Large-Scale Hydrogen Energy Storage in Salt Caverns.”

International Journal of Hydrogen Energy 37(19):14265–77. doi: 10.1016/j.ijhydene.2012.07.111.

Özsayın, E., Çiner, T. A., Rojay, F. B., Dirik, R. K., Melnick, D., Fernández-Blanco, D., and Sudo, M., 2013. Plio-quaternal extensional tectonics of the central Anatolian Plateau: A case study from the Tuz Gölü Basin, Turkey. *Turkish Journal of Earth Sciences*. doi:10.3906/yer-1210-5

Özşen, H., 2009. “Kaya Tuzuna Ait Kısa Ve Uzun Dönemli Mekanik Özelliklerin Belirlenmesi Ve Matematiksel Modellenmesi.” Selçuk University.

Richner, D.R., Arcy, S. D., J., Daryl, R.T., William, C.L., Millenacker, D.J., Robert Solution Mining: In Situ Techniques, SME Mining Engineering Handbook, Ed. Scott G. Britton, Vol. 2. Denver: Society for Mining, Metallurgy, and Exploration, 1992, 1479.

Robertson, A.H., Ustaömer, T., Pickett, E.A., Collins, A.S., Andrew, T. and Dixon, J.E., 2004. Testing models of Late Palaeozoic–Early Mesozoic orogeny in Western Türkiye: support for an evolving open-Tethys model. *Journal of the Geological Society*, 161(3), pp.501-511.

Rojay, F. B., and Süzen, M. L., 1997. Tectonostratigraphic evolution of the Cretaceous dynamic basins on accretionary ophiolitic mélange prism, SW of Ankara region: *Turkish Association of Petroleum Geologists Bulletin*, v. 9, p. 1-12

Sarris, A., 2008. “Remote Sensing Approaches | Geophysical.” *Encyclopedia of Archaeology* 1912–21. doi: 10.1016/B978-012373962-9.00270-3.

Schwab, F. L., 2003. “Sedimentary Petrology Sedimentary Rocks.” *Encyclopedia of Physical Science and Technology* 495–529.

Şenel, M., 2002. 1/500.000 Scale Geological map series of Türkiye, Kayseri Quadrangle. General Directorate of Mineral Research and exploration, Ankara, Türkiye.

Şengör, A.C. and Yılmaz, Y., 1981. Tethyan evolution of Türkiye: a plate tectonic approach. *Tectonophysics*, 75(3-4), pp.181-241.

Şengör, A.M.C., Yılmaz, Y. and Sungurlu, O., 1984. Tectonics of the Mediterranean Cimmerides: nature and evolution of the western termination of Palaeo-Tethys.

The Geological Evolution of the Eastern Mediterranean. Geological Society, London, Special Publications 17, 77–112.

Senseny, P. E., Hansen, F. D., Russell, J. E., Carter, N. L., and Handin, J. W., 1992. Mechanical behaviour of rock salt: Phenomenology and micromechanisms. *International Journal of Rock Mechanics and Mining Sciences* And, 29(4), 363–378. [https://doi.org/10.1016/0148-9062\(92\)90513-Y](https://doi.org/10.1016/0148-9062(92)90513-Y)

Stamfli, G.M., 2000. Tethyan oceans. In: Bozkurt, E. Winchester, J.A., Piper, J.D.A. (Eds.): *Tectonics and magmatism in Türkiye and surrounding area*. Geological Society London Special Publications, 173, 1-23.

Stampfli, G., Mosar, J., Fauri~, P., Pillevuit, A. and Vannay, J.-C., 2001. Permo-Mesozoic evolution of the Western Tethys realm: the Neotethys East Mediterranean basin connection. In: Ziegler, P., Cavazza, W., Robertson, A.H.F. and Crasquin- Soleau, S. (eds), *Peri-Tethyan Rift /Wrench Basins and Passive Margins, Peri-Tethys Mémoire 5, Mémoires du musée national d’histoire naturelle*, 51–108.

Susan, G. M., 2019. *Exploring the Energy Storage Capacity of Salt Caverns in the Netherlands (Doctoral dissertation) Groningen University, the Netherlands*, 89p.

Tajdus, K., Sroka A., Misa R., Tajdus A., and Meyer S., 2021. “Surface Deformations Caused by the Convergence of Large Underground Gas Storage Facilities.” *Energies* 14(2). doi: 10.3390/en14020402.

Tiab, D., and Donaldson, E. C., 2016. *Petrophysics: Theory and practice of measuring reservoir rock and Fluid Transport Properties*. Elsevier.

Tüysüz, O., and Dellaloğlu, A.A., 1992. Çankırı havzasının tektonik birlikleri ve jeolojik evrimi. *Türkiye 9. Petrol Kongresi, Bildiriler, Jeoloji*, 333-349.

Uğurtaş, G., 1975. Geophysical Interpretation of Part of the Tuz Gölü Basin. *Bulletin of the Mineral Research and Exploration*, 85(85).

Uğuz, M.F., Sevin, M. and Duru, M., 2002. 1/500.000 Scale Geological map series of Türkiye, Sinop Quadrangle. General Directorate of Mineral Research and exploration, Ankara, Türkiye.

Vaniček, P., Tenzer R., Sjöberg L. E., Martinec Z., and Featherstone W. E., 2004.

- “New Views of the Spherical Bouguer Gravity Anomaly.” *Geophysical Journal International* 159(2):460–72. doi: 10.1111/j.1365-246X.2004.02435. x.
- Verga, F., 2018. What’s conventional and what’s special in a reservoir study for Underground Gas Storage. *Energies*, 11(5), 1245. <https://doi.org/10.3390/en11051245>
- Wang, T., Xiangzhen Y., Henglin Y., Xiujuan Y., Tingting J., and Shuai Z., 2013. “A New Shape Design Method of Salt Cavern Used as Underground Gas Storage.” *Applied Energy* 104:50–61. doi: 10.1016/j.apenergy.2012.11.037.
- Wang, H. Y., and Samuel, R., 2016. 3D geomechanical modeling of salt-creep behavior on wellbore casing for Presalt Reservoirs. *SPE Drilling and Completion*, 31(04), 261–272. <https://doi.org/10.2118/166144-pa>
- Warren, J.K. *Solution Mining and Cavern Use, Evaporites: Sediments, Resources and Hydrocarbons, Germany*, 2006, pp. 893–943.
- Weijermars, R., Jackson, M. P. A. and Vendeville. B., 1993. “Rheological and Tectonic Modeling of Salt Provinces.” *Tectonophysics* 217(1–2):143–74. doi: 10.1016/0040-1951(93)90208-2.
- Wilcox, L. E., 1990. Gravity anomalies: Interpretation. *Encyclopedia of Earth Science*, 601–617. [https://doi.org/10.1007/0-387-30752-4\\_75](https://doi.org/10.1007/0-387-30752-4_75)
- World Bank. (n.d.). Retrieved February 7, 2023, from <https://documents1.worldbank.org/curated/en/450661496826169181/pdf/SFG3405-V1-REVISED-EA-P162727-PUBLIC-Disclosed-3-27-2018.pdf>
- Xing, W., Zhao, J., Hou, Z.M., Were, P., Li, M.Y., and Wang, G., 2015. Horizontal natural gas caverns in thin bedded rock salt formations. *Environ Earth Sci*. doi:10.1007/s12665-015-4410-y
- Zhang, G., Yuxuan L., Tao W., Hao Z., and Zhenshuo W., 2021. “Ground Subsidence Prediction Model and Parameter Analysis for Underground Gas Storage in Horizontal Salt Caverns.” *Mathematical Problems in Engineering* 2021. doi: 10.1155/2021/9504289.
- Zhang, Y., Niu, J., Wenqi Ke, G. C., and Zeng, H., 2021. Construction Progress of Deep Underground Salt Cavern Gas Storage and Challenges of its Drilling and Completion Technology. *E3S Web of Conferences*, 329, 01043.

<https://doi.org/10.1051/e3sconf/202132901043>

Zivar, D., Kumar, S., and Foroozesh, J., 2021. Underground hydrogen storage: A comprehensive review. *International Journal of Hydrogen Energy*, 46(45), 23436–23462. <https://doi.org/10.1016/J.IJHYDENE.2020.08.138>

## CURRICULUM VITAE

Surname, Name: Güngör Ayşe

### EDUCATION

Degree	Institution	Year of Graduation
MS	PNU Energy Resources Engineering, South Korea	2009
BS	DEU Geophysical Engineering, İzmir	2007
High School	TARAL (Foreign Language Intensive), İzmir	2002

### WORK EXPERIENCE

Year	Place	Enrollment
2018-Present	MTA	Seismic Data Geophysicist
2010-2017	Arar Oil and Gas Inc	Seismic Data Geophysicist

### FOREIGN LANGUAGES

Fluent English

### PUBLICATIONS

1. Gungor, A., Lee, G. H., Kim, H.-J., Han, H.-C., Kang, M.-H., Kim, J., et al. (2012). Structural Characteristics of the Northern Okinawa Trough and Adjacent Areas from Regional Seismic Reflection Data: Geologic and Tectonic Implications. *Tectonophysics* 522-523, 198–207.
2. Gungor, A., Yeralında Doğal Gaz Depolamaya Genel Bir Bakış. MTA Doğal Kaynaklar ve Ekonomi Bülteni (2019) 27: 39-43

Hobbies: Art, Sci-Fi Series, Sport Games, Designing, Photography, Coffee.